Yale University School of Medicine

DEPARTMENT OF THERAPEUTIC RADIOLOGY
Division of Radiological Physics

333 Cedar Street
New Haven, Connecticut 06510

(203) 785-2971
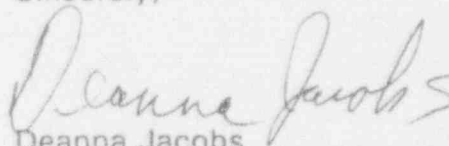FAX 203-737-4252
March 31, 1993

Dr. Hans Behling
263 Old Limekiln Road
Chalfont, PA   18914-1709

Dear Dr. Behling:

Here are some current iodine and palladium brachytherapy papers you requested written by Prof. Nath.

Most of his papers are printed in the *Medical Physics* journal. If you see any future publications by Prof. Nath that you want, please call and we'll send them to you.

Sincerely,

Deanna Jacobs
Administrative Assistant to
Ravinder Nath

dj

encs: CV 52, 56, 67, 69, 71, 72.

THERASEED™ - PALLADIUM 103
DOSIMETRY INFORMATION

Photon energy	20-23 keV
Half-life	16.97 days
Source strength available	0.3-2.7 $U^{a)}$
	0.4-2.1 mCi(App.)
Exposure to air kerma conversion factor	0.876 cGy R^{-1}
f-factor	0.886 cGy R^{-1}
Exposure rate constant	1.15 R cm^2 h^{-1} U^{-1}
	1.48 R cm^2 h^{-1} $mCi(App.)^{-1}$
Air kerma rate constant	1.00 cGy cm^2 h^{-1} U^{-1}
	1.29 cGy cm^2 h^{-1} $mCi(App.)^{-1}$
Specific dose rate constant[b]	0.735 cGy h^{-1} U^{-1}
	0.95 cGy h^{-1} $mCi(App.)^{-1}$
Average specific dose rate constant[c]	0.66 cGy h^{-1} U^{-1}
(Point source approximation)	0.86 cGy h^{-1} $mCi(App.)^{-1}$
Anisotropy factor[d]	0.90

Radial dose function[e] g(r) and Tissue-attenuation correction factor[f] α(r)

r (cm)	g (r)	α (r)	r (cm)	g (r)	α (r)
0.5	1.344	0.974	4.0	0.156	0.113
1.0	1.000	0.725	4.5	0.118	0.0856
1.5	0.737	0.534	5.0	0.0898	0.0651
2.0	0.539	0.391	5.5	0.0687	0.0498
2.5	0.393	0.285	6.0	0.0528	0.0383
3.0	0.288	0.209	6.5	0.0391	0.0283
3.5	0.211	0.153	7.0	0.0285	0.0207

a) 1U = Unit of air kerma strength = 1 μGy m^2 h^{-1} = 1 cGy cm^2 h^{-1}. A 1.293U source of ^{103}Pd is equivalent to a 1.0 mCi source.

b) Dose rate in water at a distance of 1 cm from the source center and perpendicular to the source axis for a unit strength source.

c) 4 - averaged specific dose rate constant which is applicable when point source approximation is used in dose calculations.

d) Ratio of 4 -averaged dose rate to the dose rate on the transverse axis at the same radial distance.

e) Defined following Dale, as the dose rate in water times distance squared divided by dose rate at 1 cm in water.

f) Ratio of dose to water in a water phantom and dose to a small mass of water in air at the same point.

SOURCE: Ali Meigooni, Sushil Sabnis, and Ravinder Nath, "Dosimetry of ^{103}Pd brachytherapy sources for permanent implants" (Endocurietherapy/Hyperthermia Oncology, 1989, In Press).

Dose Rate Times Distance Squared for ^{103}Pd, Model 200 Source

With an Air Kerma Strength of 1 U^* or Apparent Activity of 1 mCi

Distance Along the Transverse Axis of the Source (cm)	Dose Rate x r^2 (cGy h^{-1} cm^2)			
	1 U Source		1 mCi Source	
	Linear Source Approximation	Point Source Approximation	Linear Source Approximation	Point Source Approximation
0.5	1.001	0.901	1.294	1.165
1.0	0.735	0.662	0.950	0.855
1.5	0.539	0.485	0.697	0.627
2.0	0.395	0.356	0.511	0.460
2.5	0.290	0.261	0.375	0.337
3.0	0.213	0.192	0.275	0.248
3.5	0.157	0.141	0.203	0.183
4.0	0.116	0.104	0.150	0.135
4.5	0.086	0.077	0.111	0.100
5.0	0.064	0.058	0.083	0.074
5.5	0.048	0.043	0.062	0.056
6.0	0.036	0.032	0.046	0.042
6.5	0.028	0.025	0.036	0.033
7.0	0.021	0.019	0.027	0.024

* 1 U = unit of air kerma strength = 1 cGy cm^2 h^{-1}.

● *Technical Innovations and Notes*

SOME TREATMENT PLANNING CONSIDERATIONS FOR ^{103}Pd AND ^{125}I PERMANENT INTERSTITIAL IMPLANTS

RAVINDER NATH, PH.D., ALI S. MEIGOONI, PH.D. AND ANTHONY MELILLO, B.S.

Department of Therapeutic Radiology, Yale University School of Medicine, 333 Cedar St., New Haven, CT, 06510

Sealed sources of palladium-103 (^{103}Pd), which decay with a half life of 17 days and emit on average 21 keV photons, are now in clinical use for permanent implants. For seed implantation of prostatic cancer, ^{103}Pd implants are usually planned to deliver 115 Gy to full decay at an initial dose rate of 19.7 cGy/hr whereas ^{125}I implants are usually planned to deliver 160 Gy at an initial dose rate of 7.72 cGy/hr. Because of the lower energy of photons emitted by ^{103}Pd compared to the ^{125}I sources (27 keV average energy), the tissue attenuation is more severe for ^{103}Pd sources. The radial dose function drops more steeply with distance from the ^{103}Pd sources compared to the ^{125}I sources, raising a concern about the possibility of cold spots in the tumors implanted with ^{103}Pd sources. To investigate this issue, a detailed analysis of the dependence of dose uniformity as a function of seed spacing for ^{125}I and ^{103}Pd sources in various cubic and spherical configurations was carried out. Using the measured single source dosimetry data as input, dose distributions for a variety of cubic and spherical implants were generated on a computerized treatment planning system. This study indicates that relative dose distributions for ^{125}I and ^{103}Pd implants with the same geometric configuration and number of seeds are very similar inside the implanted volume for implants. Dose uniformity within a target volume implanted with ^{103}Pd seeds is also very similar to that for ^{125}I. To expedite clinical implementation of ^{103}Pd, an atlas of dose distributions for ^{103}Pd implants has been produced for various seed configurations, seed spacings, and target volumes. Using ^{125}I implants as a guideline, clinical procedures for planning of ^{103}Pd implants have been developed. It was found that the total source strength implanted divided by the dimension of the implant can be expressed as an exponential function of implant size, resulting in a simple method for estimating the strength of seeds necessary in an implant. Also, the air kerma strength of ^{103}Pd seeds is about 3.3 times that of ^{125}I sources in an implant with the same geometric configuration and number of seeds, provided treatment doses of 115 Gy and 160 Gy are chosen for ^{103}Pd and ^{125}I implants, respectively.

Palladium-103, Iodine-125, Brachytherapy, Interstitial implants, Permanent implants, Dosimetry, Dose calculations, Treatment planning.

INTRODUCTION

Permanent implantation of tumors by radioactive seeds is an established technique for treatment of several tumor sites such as the prostate (14). Recently, permanent implants of the prostate have become increasingly popular with the development of a transperineal percutaneous implantation technique under transrectal ultrasound and template guidance (2), which can be an outpatient procedure in a 1-day surgery unit. Because of the low energy of photons emitted by encapsulated sources of ^{125}I (27 keV, average), the ^{125}I sources are well-suited for permanent implants from the point of view of radiation exposure of persons around the patient during the procedure and after his or her release from the hospital. However, the half life of ^{125}I is long (60 days) for a permanent implant, resulting in highly protracted continuous low dose

rate irradiation. Typical ^{125}I implants are planned to deliver a dose of 160 Gy to full decay. The initial dose rate is 7.72 cGy/hr and 87.5% of the full dose is delivered over a period of 6 months (three half lives).

It is well known that the biological effectiveness of radiation decreases with decreasing dose rate because of repair of sublethal and potentially lethal damage, recruitment of relatively quiescent subpopulations of cells, and repopulation of target cell population itself (7). The only known exception to this overall trend is the inverse dose rate effect observed by Mitchell *et al.* (12) which occurs over a limited dose rate range near 50 cGy/hr in HeLa cells. In the dose rate range of permanent ^{125}I implants (7.72 cGy/hr and less), it has been argued by Freeman *et al.* (6) that for a 5-day cycle time, ^{125}I implants should be more effective than external beam. Using similar arguments, one can conclude that for ^{125}I permanent implants

---

the dose rate is so low that tumor cells that have cycle times of 2–5 days cannot be effectively killed by this low dose rate irradiation (see the review article by Eric Hall (7)). [103]Pd sources were developed to overcome this problem. [103]Pd sources emit on average 21 keV photons and have a half life of 17 days. Because of the low energy of photons emitted by ^{125}I and [103]Pd, both of these sources offer the considerable advantages of easy and effective radiation shielding of patient and personnel, compared to other sources used for permanent implants, such as [198]Au and [222]Rn. Because of its shorter half life, the [103]Pd implants offer initial dose rates of about 2.5 times larger than the ^{125}I implants, which may be beneficial in some tumors.

The energy of photons emitted by sealed sources of [103]Pd (21 keV, average) is lower than that for conventional sources of [125]I (27 keV, average). Because the attenuation coefficients increase rapidly with decreasing photon energy, approximately by the cube of photon energy in the range of 30 to 20 keV, there is a concern that the penetrating ability of [103]Pd photons may not be adequate for conventional seed configurations used in interstitial brachytherapy. In other words, one may obtain cold spots in the implanted volume if the geometric configuration of the seeds is identical to that for ^{125}I implants. Does one have to decrease the seed spacing to compensate for this effect? In this paper, we present an analysis of this issue for the planning of [103]Pd implants. Using the measured dosimetry data for [103]Pd sources such as the dose rate constant and radial dose function determined by Meigooni et al. (11), we have generated dose distributions produced by a wide variety of cubic and spherical volume implants. A detailed comparison of these dose distributions, and some clinical guidelines of planning [103]Pd interstitial implants, are presented.

METHODS AND MATERIALS

For the purpose of dose calculations in an implant, the seeds were assumed to be point, isotropic photon sources. This is a reasonable assumption for multiseed implants in which the seed orientations are randomly distributed (9). Using the point source approximation, the dose rate, $\dot{D}(r)$, in water at a distance r from a source, in units of cGy h^{-1}, is given by (8):

$$\dot{D}(r) = \frac{S_K \wedge}{r^2} g(r)\phi_{an} \tag{1}$$

where S_k is the air kerma strength of the seed, in units of U $(1U = 1\mu Gy\ m^2\ h^{-1})$, $\wedge$ is the dose rate constant in units of cGy h^{-1} U^{-1}, $g(r)$ is the radial dose function, and ϕ_{an} is the anisotropy factor, as defined in the following paragraphs. Equation 1 follows the recommendations of

the National Cancer Institute (NCI) sponsored Interstitial Collaborative Working Group (ICWG) as described in several recent publications (5, 8, 13, 15, 16). Briefly, the source strength of brachytherapy sources is expressed in terms of air kerma strength as recommended by the American Association of Physicists in Medicine (AAPM). The unit of air kerma strength is 1 μGy m^2 h^{-1}, which is numerically equal to 1 cGy cm^2 h^{-1}. This unit has been represented by the symbol U. The conversion factors between apparent activity and air kerma strength are (1, 17):

$$1.270\ U/mCi\ for\ ^{125}I$$
$$1.293\ U/mCi\ for\ ^{103}Pd. \tag{2}$$

The dose rate constant, $\wedge$, is defined as the dose rate at a distance of 1 cm in water along the transverse axis of a source with unit air kerma strength. For the [103]Pd Model 200 source,* the dose rate constant was taken from the work of Meigooni et al. (11), and for the [125]I Model 6711 source,[†] from the recommendations of the ICWG. The values adopted were:

$$\wedge = 0.84\ cGy\ h^{-1}\ U^{-1}$$
$$= 1.07\ cGy\ h^{-1}\ mCi^{-1}\ for\ ^{125}I\ Model\ 6711$$
$$\wedge = 0.73\ cGy\ h^{-1}\ U^{-1}$$
$$= 0.95\ cGy\ h^{-1}\ mCi^{-1}\ for\ ^{103}Pd\ Model\ 200. \tag{3}$$

The radial dose function, g(r), is defined as the ratio of the dose rate at r in water to that at a reference distance r_o, corrected for the inverse square falloff of dose. For point source approximation, it is given by:

$$g(r) = \frac{\dot{D}(r)}{\dot{D}(r_o)} \frac{r_o^2}{r^2} \tag{4}$$

where the reference distance, r_o, is usually taken to be at 1 cm. In this work, the radial dose function for [103]Pd seeds was taken from the published data of Meigooni et al. (11) and for [125]I Model 6711 from the ICWG recommendations (8).

The anisotropy factor, ϕ_{an}, is defined as the ratio of 4π-averaged dose rate at a given distance from the source and the dose rate at the same distance along the transverse axis. The values of ϕ_{an} were also taken from Meigooni et al. (11) for [103]Pd and the ICWG (8) for [125]I Model 6711 source and are:

$$\phi_{an} = 0.90\ for\ ^{103}Pd$$
$$\phi_{an} = 0.937\ for\ ^{125}I. \tag{5}$$

Using Eq. 1, the dose rate times distance squared along

---

the transverse axis of an actual source, and the same at a radius around an equivalent point source were calculated for both ^{125}I and [103]Pd. Since these data are not yet widely available, the actual values used in this work are presented in Table 1.

For a permanent implant, dose to full decay was obtained as the product of the Table 1 values and the average life (1.443 times the half life) for each radionuclide. For a multiseed implant, the dose rate and dose delivered to full decay was obtained by summing over all the seeds. It is implicit in this summation that there are no seed-to-seed shielding effects, such as those reported by Burns and Raeside (4) and Meigooni et al. (10).

Dose distribution around uniformly spaced cubic and spherical volume implants of ^{125}I and [103]Pd sources were calculated for implants with dimensions ranging from 1 to 6 cm. These dose computations were performed using a commercial computerized treatment planning system,[3] as well as a computer program specifically designed for these calculations on a MicroVAX II computer. The highest isodose curve which surrounds the target volume (tumor volume plus a margin) and the source strengths needed to deliver a specified dose to full decay were determined.

In this work, 115 Gy from [103]Pd is assumed to be equivalent to 160 Gy from [125]I. Of course, this equivalence of doses is merely a guideline, and only clinical trials can determine the equivalent dose for [103]Pd. If it turns out that a different dose is desired, one simply has to scale

linearly the source strength for 115 Gy presented in this paper. The choice of 115 Gy for [103]Pd implants can be rationalized using the time dose factor (TDF) formula for permanent implants developed by Orton (15). The TDF formula for permanent implantation in the notation of the original author is:

$$TDF = 4.76 \times 10^{-3} D t_{eq} \qquad (6)$$

where D is the dose delivered by full decay and t_{eq} is related to half life $t_{1/2}$ as follows:

$$t_{eq} = 1.069 t_{1/2}. \qquad (7)$$

Using Eqs. 6 and 7, the TDF for a 160 Gy implant using ^{125}I with an initial dose rate of 7.72 cGy/hr is 115.6. Therefore, an equivalent [103]Pd implant should deliver a TDF of 115.6. For this value of TDF, the total dose for a [103]Pd implant was calculated, using Eqs. 6 and 7, to be 115.5 Gy and initial dose rate was 19.7 cGy/hr. Thus, a 115 Gy [103]Pd implant has the same TDF as a 160 Gy ^{125}I implant. It is worth stressing again that the dosimetry analysis presented here can be easily modified for any value of total dose. We chose to use 115 Gy for [103]Pd because it is reasonable on the basis of the TDF formula and because it is the value being used in most [103]Pd clinical trials (3).

It is well known that dose distributions produced by interstitial implants are highly inhomogeneous in the immediate vicinity of seeds. To compare the inhomogeneity of dose distribution produced by [103]Pd with ^{125}I, dose uniformity was calculated as the ratio of maximum to minimum dose in a plane midway between the seed planes. This definition of dose uniformity is more meaningful for investigating cold spots in the implants and the minimum tumor doses, compared to the dose uniformity calculated in the entire implanted volume, including points in the immediate vicinity of seeds.

RESULTS

Figure 1 illustrates dose rate and dose delivered as a function of irradiation time for an ^{125}I implant delivering 160 Gy to full decay and a [103]Pd implant delivering 115 Gy to full decay. Under these conditions, the initial dose rate for [103]Pd is 19.7 cGy/hr, which is 2.55 times that for ^{125}I implants. As shown in Figure 1, the dose rates for [103]Pd and ^{125}I implants as a function of time crossover at about 4.5 weeks. By 4.5 weeks, [103]Pd would have delivered 83 Gy, which is 72% of dose to full decay, whereas ^{125}I implants would have delivered 50 Gy, which is only 43% of dose to full decay. Another way of comparing ^{125}I and [103]Pd dose rates is that [103]Pd implants deliver 87.5% of

Table 1. Dose rate times distance squared for [103]Pd model 200 and ^{125}I model 6711 sources using the point source approximation

Distance along the transverse axis of the source (cm)	Dose rate × r^2 (cGy h^{-1} cm^2)			
	1 U source*		1 mCi source	
	[103]Pd	[125]I	[103]Pd	[125]I
0.5	0.901	0.805	1.165	1.022
1.0	0.662	0.788	0.855	1.001
1.5	0.485	0.738	0.627	0.937
2.0	0.356	0.664	0.460	0.843
2.5	0.261	0.583	0.337	0.741
3.0	0.192	0.505	0.248	0.641
3.5	0.141	0.433	0.183	0.549
4.0	0.104	0.370	0.135	0.470
4.5	0.077	0.317	0.100	0.403
5.0	0.058	0.274	0.074	0.349
5.5	0.043	0.238	0.056	0.302
6.0	0.032	0.211	0.042	0.268
6.5	0.025	0.185	0.033	0.235
7.0	0.019	0.163	0.024	0.207

* 1 U = unit of air kerma strength = 1 μGy m^2 h^{-1} = 1 cGy cm^2 h^{-1}. For ^{125}I, 1.270 U is equivalent to 1 mCi apparent and for [103]Pd, 1.293 U is equivalent to 1 mCi apparent.
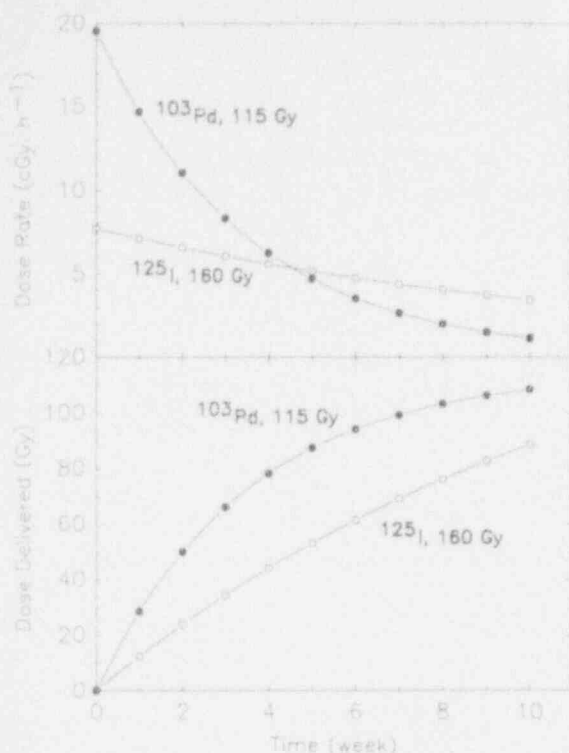
Fig. 1. Dose rate and dose delivered as a function of time for a [103]Pd implant delivering a total dose of 115 Gy to full decay and an ^{125}I implant delivering 160 Gy. Initial dose rates for [103]Pd and ^{125}I implants are 19.7 and 7.72 cGy/hr, respectively.

Fig. 2. Isodose curves for 5.0 cm cubic and 5.0 cm diameter spherical implants of ^{125}I and [103]Pd sources. The labels next to isodose curves represent dose in Gy. Seed spacing is 1.0 cm in all implants. The cubic implants contain 216 seeds of 0.48 and 1.61 U seeds of ^{125}I and [103]Pd, respectively. The spherical implants contain 160 seeds of 0.40 and 1.50 U seeds of ^{125}I and [103]Pd, respectively. Unit of source strength used here is U, which is the unit of air kerma strength; $1 U = 1 \mu Gy\ m^2\ h^{-1}$. For ^{125}I, 1.270 U is equivalent to 1.0 mCi apparent and for [103]Pd, 1.293 U is equivalent to 1.0 mCi apparent.

the dose to full decay in a shorter time course of about 51 days compared to 180 days for ^{125}I implants.

Dose distributions were calculated for cubic and volume implants of dimension 1, 2, 3, 4, 5, and 6 cm in a plane midway between the seed planes closest to the center of the implant. Figure 2 illustrates a typical dose distribution for a 5 cm cubic implant with 216 seeds of ^{125}I or [103]Pd seeds at a spacing of 1 cm. Also shown are dose distributions for two spherical implants with a diameter of 5 cm containing 160 seeds each. It is apparent from Figure 2 that dose distributions for [103]Pd implants in the target volume and at its periphery have the same overall pattern as those for ^{125}I implants. At larger distances from the implant, for example outside the patient, the radiation doses from [103]Pd implants are much smaller than those from ^{125}I implants, as can be estimated from the steeper falloff of radial dose function (Table 1); at a distance of 10 cm in tissue the radial dose function for [103]Pd is about 1/10th that for [125]I. In Figure 2, the isodose curves with highest values that completely surrounded the target volume were chosen to be 160 and 115 Gy for ^{125}I and [103]Pd, respectively. In this example, the target volume is a 5 cm cube for the cubic implant and a 5 cm diameter sphere for the spherical implants. The cubic seed configuration in this example was simply a cube of 5 cm length. The spherical seed configuration had principal diameters equal to 5 cm, and had a few seeds outside the 5 cm diameter sphere along the diagonals, as shown in Figure 2. This
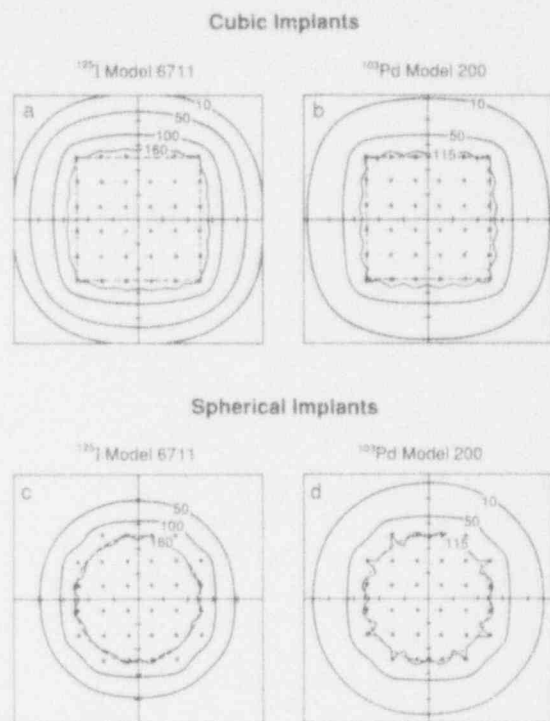
seed configuration provides isodose curves that conform to the target volume with minimum source strength per seed. Under these conditions an ^{125}I implant with 1 cm seed spacing requires seed strengths of 0.48 and 0.40 U/seed for the 5 cm cubic and spherical implants, respectively. On the other hand, [103]Pd implants require seed strengths of 1.62 and 1.50 U/seed for the 5 cm cubic and spherical implants, respectively.

Using the methodology described above, the source strength per seed necessary for cubic and spherical implants of ^{125}I and [103]Pd seeds at various seed spacings for average implant dimensions varying from 1 to 6 cm was determined (Fig. 3). For both isotopes, as the seed spacing increases, the source strength per seed increases. Also, as the average dimension of the implant increases, the source strength per seed is nearly independent of average dimension for implants with small seed spacing, and obviously the number of seeds increases rapidly with increasing size. However, for larger seed spacings, the source strength per seed decreases slightly with increasing average dimension (Fig. 3), as a result of smoother peripheral dose contours associated with larger seed arrays.

The Figure 3 data for a seed spacing of 1 cm are listed in Table 2 for cubic implants and in Table 3 for spherical
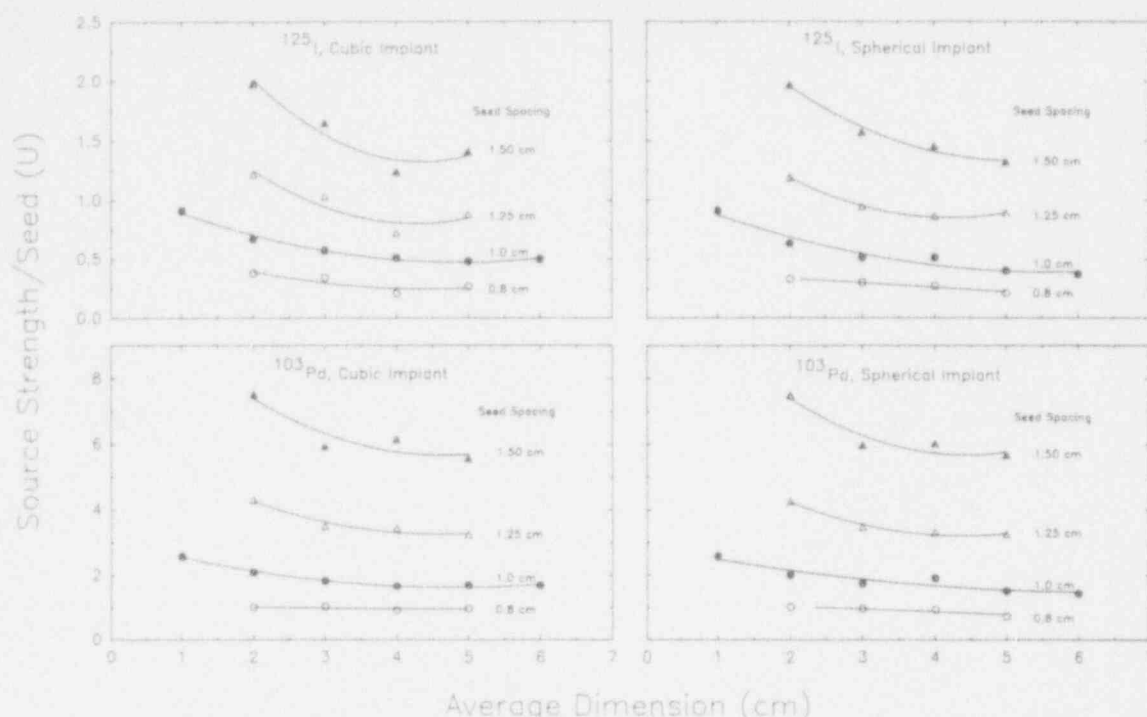
Fig. 3. Source strength per seed required for delivering 160 Gy and 115 Gy using ^{125}I and ^{103}Pd implants of different sizes and seed spacings. Unit of source strength used here is U, which is the unit of air kerma strength; $1\ U = 1$ $\mu Gy\ m^2\ h^{-1}$. For ^{125}I, $1.270\ U$ is equivalent to 1.0 mCi apparent and for ^{103}Pd, $1.293\ U$ is equivalent to 1.0 mCi apparent.

implants. For cubic implants, as the implant dimension increases from 1 cm to 6 cm, the number of seeds in the implant increase from 8 to 343: the total source strength implanted increases from 7.28 to 165 U for ^{125}I and from 20.6 to 580 U for ^{103}Pd. This is a 23-fold increase from ^{125}I compared to a 28-fold increase for ^{103}Pd. The source

strength per seed in cubic implants over this range of implant dimensions of 1 to 6 cm varied from 0.91 to 0.48 U for ^{125}I implants and from 2.58 to 1.69 U for ^{103}Pd (Table 2). Similarly, for spherical implants, the source strength per seed decreased from 0.91 to 0.37 U for ^{125}I and from 2.58 to 1.42 U for ^{103}Pd, as the implant dimension increased from 1 cm to 6 cm (Table 3). At the same

Table 2. Dosimetry parameters for cubic implants of ^{125}I and ^{103}Pd with a 1.0 cm seed spacing

Length of cube, d (cm)	Source	Number of seeds	Total source strength, $S_k\ (U)$*	Source strength per seed (U)*	$\dfrac{S_k}{d}$ $(U\ cm^{-1})$*
1	^{125}I	8	7.28	0.91	7.28
1	^{103}Pd	8	20.6	2.58	20.6
2	^{125}I	27	18.1	0.67	9.05
2	^{103}Pd	27	56.2	2.08	28.1
3	^{125}I	64	36.5	0.57	12.2
3	^{103}Pd	64	116.	1.82	38.8
4	^{125}I	125	63.8	0.51	15.9
4	^{103}Pd	125	211.	1.69	52.8
5	^{125}I	216	104.	0.48	20.7
5	^{103}Pd	216	350.	1.62	70.0
6	^{125}I	343	165.	0.48	27.4
6	^{103}Pd	343	580.	1.69	96.6

Note: Total doses to full decay are 160 and 115 Gy for ^{125}I and ^{103}Pd, respectively.

* $1\ U$ = unit of air kerma strength = $1\ \mu Gy\ m^2\ h^{-1}$ = $1\ cGy\ cm^2\ h^{-1}$. For ^{125}I, $1.270\ U$ is equivalent to 1 mCi apparent and for ^{103}Pd, 1.293 U is equivalent to 1 mCi apparent.

Table 3. Dosimetry parameters for spherical implants of ^{125}I and ^{103}Pd with a 1.0 cm seed spacing

Diameter of sphere, d (cm)	Source	Number of seeds	Total source strength, $S_k\ (U)$*	Source strength per seed (U)*	$\dfrac{S_k}{d}$ $(U\ cm^{-1})$*
1	^{125}I	8	7.28	0.91	7.28
1	^{103}Pd	8	20.6	2.58	20.6
2	^{125}I	27	17.3	0.64	8.6
2	^{103}Pd	27	54.0	2.0	27.0
3	^{125}I	56	28.6	0.51	9.5
3	^{103}Pd	56	96.9	1.73	32.3
4	^{125}I	81	41.3	0.51	10.3
4	^{103}Pd	81	154.	1.90	38.5
5	^{125}I	160	64.0	0.40	12.8
5	^{103}Pd	160	240.	1.50	48.0
6	^{125}I	275	102.	0.37	17.0
6	^{103}Pd	275	391.	1.42	65.1

Note: Total doses to full decay are 160 and 115 Gy for ^{125}I and ^{103}Pd, respectively.

* $1\ U$ = unit of air kerma strength = $1\ \mu Gy\ m^2\ h^{-1}$ = $1\ cGy\ cm^2\ h^{-1}$. For ^{125}I, $1.270\ U$ is equivalent to 1 mCi apparent and for ^{103}Pd, 1.293 U is equivalent to 1 mCi apparent.
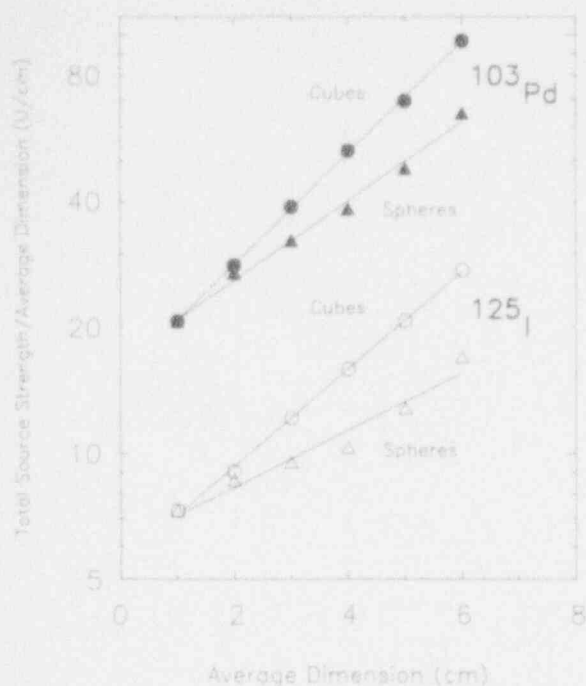
Fig. 4. Total source strength divided by average dimension as a function of average dimension for spherical and cubic implants of ^{125}I and ^{103}Pd. Unit of source strength used here is U, which is the unit of air kerma strength; $1\ U = 1\ \mu Gy\ m^2\ h^{-1}$. For ^{125}I, 1.270 U is equivalent to 1.0 mCi apparent and for ^{103}Pd, 1.293 U is equivalent to 1.0 mCi apparent.
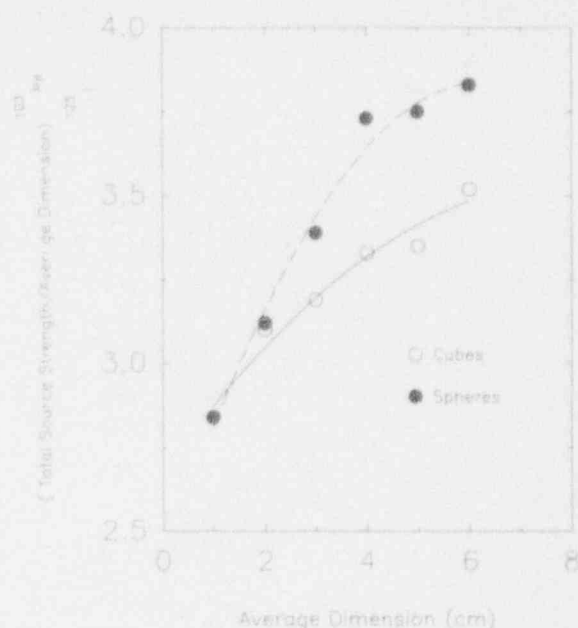

Fig. 5. The ratio of total source strength per average dimension for ^{103}Pd to that for ^{125}I, as a function of average dimension. Unit of source strength used here is U, which is the unit of air kerma strength; $1\ U = 1\ \mu Gy\ m^2\ h^{-1}$. For ^{125}I, 1.270 U is equivalent to 1.0 mCi apparent and for ^{103}Pd, 1.293 U is equivalent to 1.0 mCi apparent.

time, the total source strength increased 14-fold from 7.28 to 102 U for ^{125}I and 19-fold from 20.6 to 391 U for ^{103}Pd, for spherical implants, as the diameter of the implant increased from 1 cm to 6 cm (Table 3).

The total source strength divided by the average dimension was observed to increase exponentially with average dimension of the implant. This results in a linear relationship on a semi-logarithmic plot, as shown in Figure 4. The lines for ^{103}Pd are nearly parallel to those for ^{125}I for both spherical and cubic implants; the ^{103}Pd line being higher by a factor of about 3. Also, we note that for a given isotope, the cubic implant line has a larger slope than the spherical implant, indicating that the cubic implants require higher strength sources than spherical implants as the average dimension increases. The data shown in Figure 4 were fitted to a straight line using the following simple equation:

$$S_K/d = \alpha e^{\beta d} \qquad (8)$$

Table 4. Coefficients from the linear regression of data shown in Tables 2 and 3 using Eq. 10, valid for average dimensions ranging from 1 to 6 cm

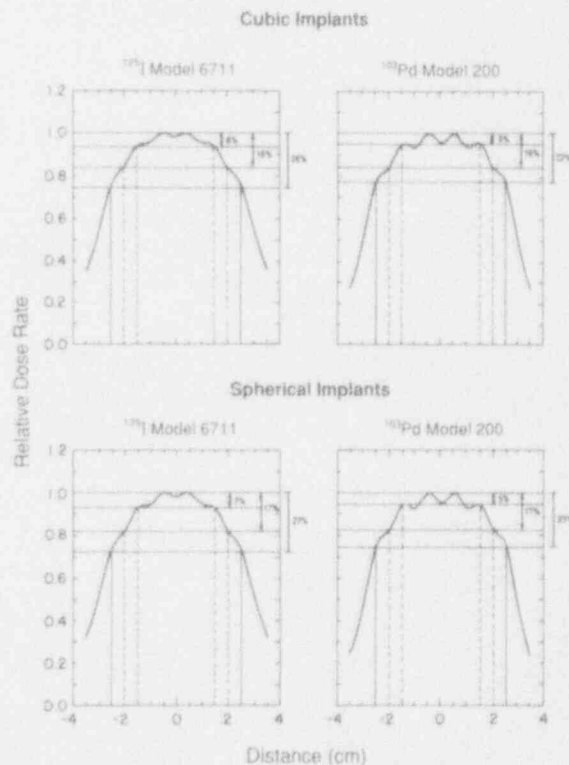| Source	Implant type	α	β
^{125}I	Cubic	5.348	0.278
	Spherical	6.059	0.157
^{103}Pd	Cubic	15.248	0.307
	Spherical	16.746	0.218

Fig. 6. Dose profiles in the central planes of 5 cm cubic and 5 cm diameter spherical implants of ^{125}I and ^{103}Pd. The seed spacing is 1.0 cm in all implants. The profiles are normalized to 1.0 on the center. The implanted volume is shown by the solid vertical lines at ± 2.5 cm. The broken vertical lines at ± 2.0 cm and ± 1.5 cm represent the target volume, if margins of 0.5 and 1.0 cm, respectively, are used around the tumor or the implanted volume.

Table 5. Dose uniformity for a 5 × 5 × 5 cm cubic volume implant

Seed spacing (cm)	Margin (cm)	Dose uniformity (%)	
		[125]I	[103]Pd
0.83	0.0	27.5	25.0
	0.5	18.0	17.0
	1.0	8.4	7.0
1.0	0.0	26.0	22.0
	0.5	16.0	16.0
	1.0	6.0	5.0
1.25	0.0	23.0	20.0
	0.5	15.0	16.0
	1.0	7.6	7.0
1.67	0.0	18.3	16.0
	0.5	13.0	13.7
	1.0	8.4	11.4
2.5	0.0	13.6	12.0
	0.5	10.6	12.0
	1.0	10.6	16.0

where α and β are coefficients which were determined from linear regression. Their values are given in Table 4.

As noted above, the straight lines exhibiting relationships of total source strength implanted, per unit average dimension as a function of the average dimension of the implant (Fig. 4) for the same geometry, are about a factor of 3 higher for [103]Pd compared to [125]I. Figure 5 exhibits this trend in more detail by plotting the ratio of the S_k/d for [103]Pd and ^{125}I implants as a function of average dimension. This ratio ranges from 2.8 to 3.5 for cubic implants and from 2.8 to 3.8 for spherical implants, as the average dimension increases from 1 to 6 cm (Fig. 5). The average value of this ratio is 3.3.

Next, the effect of seed spacing on dose uniformity was investigated. Figure 6 illustrates dose profiles in the central plane through a 5 × 5 × 5 cm cubic and a 5 cm diameter spherical implants. In both, the seed spacing was 1 cm. If the target volume is taken to be coincident with implant volume, then the edges of the target volume are at distance of ±2.5 cm from center in both cases. For this case of no margin, the dose uniformity in the target volume was 26 and 22% for ^{125}I and [103]Pd cubic implants, respectively (Fig. 6). If the target volume was assumed to be 0.5 cm inside the implant volume, that is, the edges of the target were ±2.0 cm from the center, then the dose uniformity was 16% for both isotopes; for a margin of 1.0 cm, it was 6 and 5%, for ^{125}I and [103]Pd cubic implants, respectively (Fig. 6). As shown here, the dose uniformity inside the target volume for 1 cm seed spacing implants with [103]Pd and ^{125}I was essentially the same.

To investigate the effect of seed spacing, dose uniformity was calculated for a variety of seed spacings and margins around a 5 cm cubic implant. Results of this calculation are shown in Table 5. As shown in Table 5, the dose

uniformity improves as margin between the implanted volume and target volume increases (target volume being progressively smaller) for a given seed spacing with the exception of the largest spacing of 2.5 cm. And for a given value of margin, the dose uniformity is a complicated function of seed spacing. For the margins of 0.0 and 0.5 cm, the uniformity improves somewhat as the seed spacing increases up to 2.5 cm. For the case of a 1.0 cm margin, the uniformity first improves with increasing spacing and then deteriorates as spacing increases further.

DISCUSSION AND CONCLUSIONS

[103]Pd is currently being investigated as a potential alternative to ^{125}I for permanent implants of prostate carcinoma with a higher Gleason pattern score by Blasko et al. in Seattle (3). Although no clinical data with long term follow up are available yet, the higher dose rate of [103]Pd is believed to offer a potential advantage over ^{125}I implants, which have had somewhat disappointing results for more aggressive and rapidly proliferating tumors (14). Also, the lower energy of photons emitted from [103]Pd compared to ^{125}I also reduces the risk of complications arising from irradiation of normal tissues outside the tumor volume, because the dose rate outside the [103]Pd implants falls off more rapidly than outside ^{125}I implants.

In this work we have presented a detailed dosimetric comparison of ^{125}I and [103]Pd implants with special attention paid to dose uniformity within the tumor volume, as well as guidelines for determination of source strength per seed and seed spacing to deliver 160 Gy for ^{125}I implants and 115 Gy for [103]Pd implants.

Note that we have used the new dosimetry data for the [125]I Model 6711 seed, as recommended by the ICWG (8). The dose rate constant recommended by this group is about 20% lower than the currently used values. Also note that data for both ^{125}I and [103]Pd, as reported by the ICWG (8) and Meigooni et al. (11), are for a Solid Water[s] phantom. Although Solid Water is nearly equivalent to water, it is not identical to it and a revision of the basic dosimetry of single sources of ^{125}I and [103]Pd may be necessary in the future. The AAPM has formed a task group (AAPM Task Group No. 43) to investigate this problem.

In this work we chose 115 Gy and 160 Gy [103]Pd and ^{125}I implants, respectively, because these are the commonly used dosages. If it is necessary to determine source strengths for a different total dose, it can be easily determined from the values provided in this paper by linearly adjusting the source strength for the dosage required.

In this work we assume point source approximation for calculation of dose distribution around the ^{125}I and [103]Pd sources, which are known to have anisotropic emission of radiation (9, 11). As is common practice in interstitial brachytherapy calculation, we simply apply an an-

isotropy correction which results in dose rate averaged over all orientations around the actual seed. This approximation is strictly valid only for large multiseed implants that have randomly distributed seed orientations (9). Therefore, the use of our data for small implants or those with uniformly aligned seeds is not warranted.

For both ^{125}I and ^{103}Pd, we assume that there is no interseed effect, that is, no source-to-source shielding effect. It is possible that this effect is larger for ^{103}Pd implants compared to ^{125}I. Therefore, a further study along these lines is warranted.

Despite these limitations, which are common to all interstitial brachytherapy dosimetry today, we conclude the following:

● Within the tumor volume, the isodose distributions produced by ^{103}Pd are very similar to those by ^{125}I, and outside the tumor volume those for ^{103}Pd fall off more rapidly.

● Dose uniformity (as defined here) in the tumor volume is essentially the same for ^{103}Pd and ^{125}I implants of same geometry.

● As a rule of thumb, source strength for a ^{103}Pd implant delivering 115 Gy should be about 3.3 times that for an ^{125}I implant delivering 160 Gy. The ratio of source strengths is greater for larger implants, and the ratio would be higher if relative to the currently used ^{125}I dose rate constant.

To expedite the clinical implementation of ^{103}Pd sources in brachytherapy, an atlas of dose distributions produced by various cubic and spherical implants has been developed and can be obtained from the authors. This atlas can be used in a manner similar to a nomograph.

Similar work dealing with other implant shapes, such as ellipsoids, single and double plane, will also be helpful in a quantitative comparison of the dosimetric characteristics of ^{103}Pd implants versus those of ^{125}I, and is currently in progress.

REFERENCES

1. American Association of Physicists in Medicine (AAPM). AAPM Report No. 21. Specification of brachytherapy sources. Report of AAPM Task Group No. 32. New York, NY: American Institute of Physics; 1987.
2. Blasko, J. C.; Radge, H.; Schumacher, D. Transperineal percutaneous iodine-125 implantation for prostatic carcinoma using transrectal ultrasound and template guidance. Endocuriether. Hyperther. Oncol. 3: 131–139; 1987.
3. Blasko, J. C. Early results with ^{125}I and ^{103}Pd. Prostate cancer, the role of interstitial implantation. Seattle: Pacific Northwest Cancer Foundation; 1991.
4. Burns, G. S.; Raeside, D. E. The accuracy of single-seed dose superposition for ^{125}I implants. Med. Phys. 16: 627–631; 1989.
5. Chiu-Tsao S.; Anderson, L. L.; O'Brien, K.; Sanna, R. Dose rate determination for ^{125}I seeds. Med. Phys. 17: 815–825; 1990.
6. Freeman, M. L.; Goldhagen, P.; Sierra E.; Hall E. J. Studies with encapsulated ^{125}I sources. II. Determination of the relative biological effectiveness using cultured mammalian cells. Int. J. Radiat. Oncol. Biol. Phys. 8: 1355–1361; 1982.
7. Hall, E. J. The biological basis of endocurietherapy. Endocuriether. Hyperther. Oncol. 1: 141–152; 1985.
8. Interstitial Collaborative Working Group (ICWG). In: Anderson, L. L., Nath, R., Weaver, K. A., et al., eds. Interstitial brachytherapy. New York, NY: Raven Press; 1990.
9. Ling, C. C.; Anderson, L. L.; Shipley, W. U. Dose inho-

mogeneity in interstitial implants using ^{125}I seeds. Int. J. Radiat. Oncol. Biol. Phys. 5: 419–425; 1979.
10. Meigooni, A. S.; Meli, J. A.; Nath, R. Interseed effects on dose for ^{125}I brachytherapy implants. Med. Phys. (in press).
11. Meigooni, A. S.; Sabnis, S.; Nath, R. Dosimetry of ^{103}Pd brachytherapy sources for permanent implants. Endocuriether. Hyperther. Oncol. 6: 107–117; 1990.
12. Mitchell, J. B.; Bedford, J. S.; Bailey, S. M. Dose-rate effects on the cell cycle and survival of S3 HeLa and V79 cells. Radiat. Res. 79: 520–536; 1979.
13. Nath, R.; Meigooni, A. S.; Meli, J. A. Dosimetry on the transverse axes of ^{125}I and ^{192}Ir interstitial brachytherapy sources. Med. Phys. 17: 1032–1040; 1990.
14. Nori, D.; Hilaris, B. S.; Peschel, R. E.; Phillips, T. L.; Leibel, S. A. Prostate cancer. In: Anderson, L. L., Nath, R., Weaver, K. A., et al., eds. Interstitial brachytherapy. New York, NY: Raven Press; 1990: 199–212.
15. Orton, C. G. Time-dose factor analysis of dose rate effects in permanent implant dosimetry. Int. J. Radiat. Oncol. Biol. Phys. 2: 55–60; 1977.
16. Weaver, K. A.; Smith, V.; Huang, D.; Barnett, C.; Schell, M. C.; Ling, C. C. Dose parameters of ^{125}I and ^{192}Ir sources. Med. Phys. 16: 636–643; 1989.
17. Williamson, J. F.; Nath, R. Clinical implementation of AAPM Task Group 32 recommendations on brachytherapy source strength specification. Med. Phys. 18: 439–448; 1991.

● *Technical Innovations and Notes*

A COMPARISON OF RADIAL DOSE FUNCTIONS FOR ^{103}Pd, ^{125}I, ^{145}Sm, ^{241}Am, ^{169}Yb, ^{192}Ir, AND ^{137}Cs BRACHYTHERAPY SOURCES

ALI S. MEIGOONI, PH.D. AND RAVINDER NATH, PH.D.

Department of Therapeutic Radiology, Yale University School of Medicine, 333 Cedar Street, New Haven, CT 06510

Recently, encapsulated sources of ^{103}Pd (21 keV average), ^{145}Sm (41 keV average), ^{241}Am (60 keV), and ^{169}Yb (93 keV average) have been introduced as alternatives to conventional brachytherapy sources of ^{125}I Model 6711 (27 keV average), ^{125}I Model 6702 (28 keV average), ^{192}Ir (369 keV average), and ^{137}Cs (662 keV). To illustrate the dependence of the penetrating ability of photons from brachytherapy sources as a function of photon energy, a comparison of their radial dose functions is presented. Using the ITS Monte Carlo simulation code for photon-electron transport, the radial dose functions were calculated for monoenergetic photon sources with energies in the range of 30 keV to 1 MeV. Also, similar calculations were performed using the photon spectra emitted by the encapsulated brachytherapy sources. To verify the accuracy of Monte Carlo calculations, comparisons are made with our new measured data for ^{241}Am and existing experimental and theoretical data from other investigators. A comparison of radial dose functions indicates that for ^{241}Am, ^{169}Yb, ^{192}Ir and ^{137}Cs sources radial dose functions are close to unity for distances up to 10 cm, for ^{145}Sm the radial dose function drops to about 0.4 at 10 cm, and for ^{125}I and ^{103}Pd it drops precipitously to less than 0.20 at 7 cm. At 5 cm, the measured radial dose functions for ^{103}Pd, ^{125}I Model 6711, ^{125}I Model 6702, ^{145}Sm, ^{241}Am, and ^{192}Ir have values of 0.09, 0.34, 0.38, 0.86, 1.12, and 0.97, respectively. While all of these radioisotopes provide adequate penetrating power for interstitial brachytherapy, only the radioisotopes emitting photons with energies greater than about 40 keV can provide adequate depth dose (that is, small or no tissue attenuation) for intracavitary irradiation. Our criterion for choice of minimum photon energy suitable for intracavitary irradiation is that the radial dose function at 5 cm should not be less than 0.90. Also, note that photons with energies around 80 keV exhibit maximum penetrating ability in solid water for distances up to 5 cm.

Brachytherapy, Radial dose function, Penetrating ability, ^{103}Pd, ^{125}I, ^{145}Sm, ^{241}Am, ^{169}Yb, ^{192}Ir, ^{137}Cs.

INTRODUCTION

There is considerable interest in the development of brachytherapy sources emitting low energy photons (14) because they offer advantages over higher energy photon emitters in terms of ease of radiation shielding within the patient and radiation protection of medical personnel. However, the effects of photon absorption in tissue are also more pronounced for lower energy photon emitters such as ^{125}I and ^{103}Pd, compared to ^{192}Ir or ^{137}Cs (8). Because the penetrating ability of photons, quantified here with the radial dose function (defined in the next section), varies with photon energy, it is important to evaluate carefully the effects of photon absorption and scattering in tissue as a function of photon energy. These considerations regarding the penetrating ability of photons are more important for intracavitary brachytherapy than interstitial brachytherapy because a better depth dose is

necessary to irradiate tumors adequately using intracavitary irradiation.

It is generally accepted that effects of photon absorption and scattering in tissue compensate each other (within 5–10% for distances up to 5 cm) for brachytherapy sources such as ^{192}Ir and ^{137}Cs that emit photons with energies greater than 100 keV (17). Although data for tissue attenuation factors and radial dose functions of various isotopes exist in the literature (4, 5, 7, 8, 9, 10, 11, 12, 13, 16, 17), these data are scattered in publications spanning a time period of many years. In this work, we have pooled together the relevant previous data and generated new data to investigate systematically the tissue attenuation effects for brachytherapy sources as a function of photon energy. We have calculated the radial dose functions for photons in a water-equivalent phantom with energy in the range of 30 keV to 1 MeV using Monte Carlo simulations. These theoretical results are compared with those from previous

theoretical and experimental investigations. From an examination of radial dose functions for different isotopes studied, we investigate the penetrating ability of photons from brachytherapy sources as a function of photon energy, and address the question of suitability of particular sources for interstitial and/or intracavitary irradiation.

METHODS AND MATERIALS

Radial dose function

The Interstitial Collaborative Working Group (ICWG) defines the radial dose function as (7):

$$g(r) = \frac{\dot{D}(r) \cdot G\left(r_0, \frac{\pi}{2}\right)}{\dot{D}(r_0) \cdot G\left(r, \frac{\pi}{2}\right)} \qquad (1)$$

where $\dot{D}(r)$ is the dose rate at a distance of r and $\dot{D}(r_0)$ is the dose rate at a reference distance r_0 from the source center, along the transverse axis of the sources. $G(r, \pi/2)$ and $G(r_0, \pi/2)$ are the geometry factors at the same points of r and r_0, respectively. The angle $\pi/2$ refers to the angle between the source axis and the line segment connecting the point of interest and source center. Using the notation of the ICWG, the geometry factors, which take into account the distribution of radioactive material in the source, are defined by:

$$G(r, \pi/2)$$
$$= \begin{cases} 1/r^2 & \text{for point source approximation} \\ \dfrac{2 \tan^{-1}(L/2y)}{Ly} & \text{for line source approximation} \end{cases} \qquad (2)$$

where L is the active length of the source and y is the coordinate of the calculation point along the transverse axis of the seed. For a point source, the geometry factor is simply the inverse square factor. At distances greater than $2L$ the geometry factor of a linear source in Eq. 2 converges to the same values as with point source approximation. The geometry factors for ^{125}I and ^{192}Ir with about 3 mm active length are calculated to be 3.886, 0.993, and 0.250 at distances of 0.5, 1.0, and 2 cm from the source. These values are different by about 3.1%, 0.7%, and 0% compared to the inverse square law values at the same distances from the source. These differences are more pronounced for larger sources such as [241]Am with a 1.6 cm active length (2 Ci source).

The radial dose function, defined in Eq. 1, is the ratio of dose rate at a point along the transverse axis relative to the dose rate at a reference point, r_0, with the effects

of inverse square law and the distribution of the radioactive material in the source taken out. The reference distance is taken to be 1 cm in agreement with the original definition by Dale (4). Assuming point source approximation, Eq. 1 simplifies to

$$g(r) = \frac{\dot{D}(r) \, r_0^2}{\dot{D}(r_0) \, r^2} \qquad (3)$$

Monte Carlo calculations

Monte Carlo simulations were performed using the Integrated Tiger Series (ITS) (6), version 2.1. The ITS code is an expansion of the ETRAN code (1) allowing simulations in a multidimensional and multimedia phantom. It is a combination of three codes: (a) TIGER, for 1-dimensional calculations; (b) CYLTRAN, for calculations in cylindrically symmetric geometry; and (c) ACCEPT, for any complex geometry. These codes incorporate photon and electron transport in the energy range of 1.0 keV to 1.0 GeV and use the library of photon cross-section generated from the analytical approximation of Biggs and Lighthill (2, 3). In this work calculations were performed in spherical geometry, using the ACCEPT section of the ITS series. All the calculations were done on the MicroVax II, operating under the VMS system, version 5.1, or the VAXstation 3100, operating under VMS, version 5.3.

Monte Carlo simulations in Solid Water* were performed for isotropic point sources emitting monoenergetic photons with energies of 30, 40, 50, 60, 80, 100, 200, 400, 600, and 1,000 keV. No encapsulation was assumed for these calculations. A spherical Solid Water phantom of 20 cm radius was considered around the source. This simulates full scattering conditions for all distances up to 10 cm. Dose rates and hence, radial dose functions and also photon energy spectra, were calculated at distances of 1 cm to 10 cm at 1 cm intervals. Energy deposition in spherical shells of 2 mm thickness, with their average radii at distances of 1 cm to 10 cm at 1 cm intervals, were calculated using 1 keV cutoff energies for photons and electrons. Variances of less than 2% were obtained by simulating 20–200 batches with 10,000 histories per batch, in the energy range of 1 MeV to 30 keV, respectively with typical computation times of 4–30 hrs (CPU), respectively.

For simulation of brachytherapy sources, photon energy spectra emitted by the radioisotopes were obtained from the literature (5, 9, 10, 11, 12, 13, 16) and are shown in Table 1. It was assumed that a point source emitting this spectrum is encapsulated in a small spherical shell of the same thickness and material of the encapsulation as the actual source around the source. Shells of 0.05 mm thick titanium for ^{125}I and [103]Pd, 0.2 mm thick stainless steel of ^{192}Ir, 0.076 mm thick titanium for [169]Yb, and 1 mm thick titanium for [241]Am sources were assumed.

Table 1. Photon energy spectra used in the calculations*

Source	Half life	Photo-energy spectrum (keV)	Percent yield (%)
[103]Pd	17 d	20.07	28.66
		20.22	54.43
		22.72	16.90
		352.4	0.003
		397.5	0.009
		497.1	0.0005
		21 keV average	
[125]I Model 6711	60 d	35.4	3.60
		31.8	2.30
		30.9	11.10
		27.4	41.12
		27.2	21.09
		25.2	4.59
		22.1	16.20
		27 keV average	
[125]I Model 6702	60 d	35.4	4.54
		31.8	2.70
		30.9	14.02
		27.4	51.91
		27.2	26.63
		28 keV average	
[145]Sm	340 d	38.2	25.33
		38.7	48.75
		43.8	14.64
		44.9	2.90
		61.4	8.38
		41 keV average	
[241]Am	432 y	59.54	100.00
[169]Yb	32 d	49.8	15.99
		50.7	28.36
		57.5	11.61
		63.1	13.18
		93.6	0.802
		109.8	5.25
		118.2	0.567
		130.5	3.35
		177.2	6.45
		198.0	10.54
		240.3	0.039
		261.1	0.572
		307.7	3.258
		93 keV average	
[192]Ir	74.2 d	884.0	0.138
		612.0	2.445
		604.0	3.782
		589.0	2.030
		489.0	0.138
		484.0	0.134
		468.0	21.68
		416.0	0.276
		374.0	0.323
		316.0	38.158
		308.0	14.16
		296.0	13.65
		283.0	0.138
		206.0	1.568
		201.0	0.184
		369 keV average	
[137]Cs	30 y	662.0	100.00

* Not included in this table are very low energy photons or those with very low percent yield.

Dose measurement techniques

Dose rates were measured in Solid Water phantom at distances of 1 cm to 10 cm at 1 cm intervals along the transverse axis of the sources, using $3.1 \times 3.1 \times 0.89$ mm^3 LiF TLD chips.[†] A slab of Solid Water was carefully machined to accommodate the source and TLD chips, as described in a previous publication (11). The TLD chips were staggered to minimize the dose perturbation experienced by each TLD chip due to the presence of the other chips. This slab of Solid Water phantom was then surrounded by several other slabs of Solid Water of various thicknesses (0.5 cm, 1.0 cm, and 2.0 cm) to have an approximately 7 cm phantom at each direction from the TLD's and sources, for a full scattering condition. The outside dimension of the whole phantom became about $30 \times 25 \times 20$ cm^3. For protection from irradiation, the whole setup was placed within a lead cubic box of 5 cm thick walls and had inner dimensions of about 60 cm. A 4 mm lead equivalent leaded acrylic sheet was used for the top to facilitate visual observation of the setup. We have verified that this lead box does not perturb dose measurements inside the Solid Water phantom by repeating some of the measurements in a large treatment room used for external beam radiotherapy where shielding walls were not so close to the phantom material. To achieve good statistical quality of experimental data ($\pm 3\%$), each measurement was repeated at least twice (four times for distances of 1 and 2 cm from the source). Typically, each measurement was repeated three times.

In our protocol, the TLD chips are read after at least a 24 hr waiting period, using a precision TLD reader.[‡] Responses of the TLD chips were converted to dose rates by calibrating at least 10 chips, divided into two sets exposed to two different doses, with a calibrated 4 MV X ray beam to get TLD response per unit dose. Since sensitivity of TLD chips is energy dependent, the measured TLD response was corrected using the relative sensitivity of LiF TLD chips as a function of photon energy (11, 12).

RESULTS

Figure 1 illustrates a comparison of measured radial dose functions of the [103]Pd Model 200 source from Meigooni et al. (13), [125]I Model 6702 source from Nath et al. (16), [125]I Model 6711 source from Nath et al. (16), [145]Sm source from Fairchild et al. (5), [241]Am 2 Ci cylindrical source, (15) and [192]Ir 0.2 mm stainless steel source from Nath et al. (16). The [145]Sm data from Fairchild et al. (5) were measured in A150 tissue-equivalent plastic phantom. However, the [125]I Models 6702 and 6711, ^{192}Ir data from Nath et al. (16), and also the [103]Pd data from Meigooni et al. (13) were measured in Solid Water phantoms. For [241]Am source, new data were generated in the present work using the same methodology as that used in our measurements for ^{125}I, ^{192}Ir, and [103]Pd sources (13, 16). These results, shown in Figure 1, indicate considerable differences in penetration ability of these sources. For [192]Ir
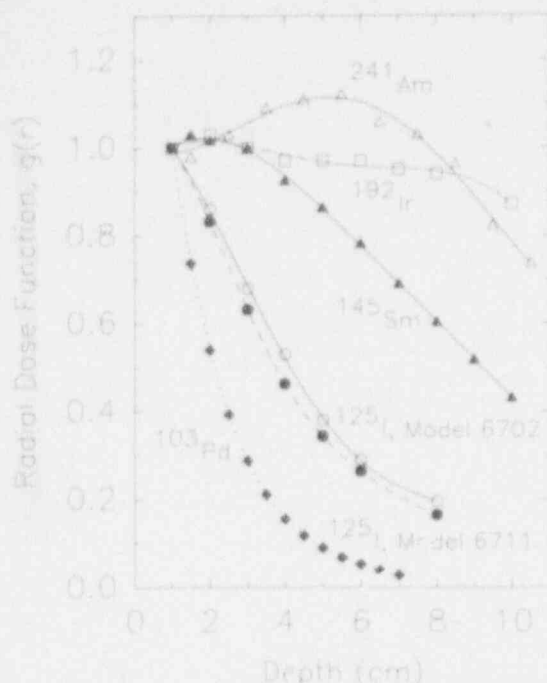
Fig. 1. A comparison of measured radial dose functions of [103]Pd Model 200 (solid diamonds) from Meigooni et al. (11), [125]I Model 6711 (solid circles) from Nath et al. (16), and Model 6702 (open circles) from Nath et al. (16), [241]Am (open triangles) from present work, and [192]Ir 0.2 mm stainless steel (open squares) from Nath et al. (16) brachytherapy sources in Solid Water. Also shown is the radial dose function for [145]Sm (solid triangles) in an A150 phantom, extracted from Fairchild et al. (5). The lines connecting the measured data are obtained from least square polynomial fit just to guide the eye.

the radial dose function gradually decreases from unity at 1 cm to 0.87 at 10 cm; for [241]Am it first increases to 1.12 at a distance of 5 cm and then drops to 0.80 at 10 cm; for [145]Sm it drops to 0.40 at 10 cm; and for ^{125}I and [103]Pd, it drops precipitously to less than 0.2 at 7 cm. At a 5 cm distance from the source the measured radial dose functions for [103]Pd, [125]I (Model 6711 and 6702), [145]Sm, [241]Am, and ^{192}Ir have values of 0.09, 0.34, 0.38, 0.86, 1.12, and 0.97, respectively.

As shown in Figure 1, the measured radial dose functions from different brachytherapy sources vary considerably from each other and depend upon photon energy in a very complex fashion. At a depth of 5 cm, the radial dose function first increases with increasing photon energy as evident from the trends in the measured data from [103]Pd (21 keV average energy), [125]I Model 6711 (27 keV average energy), [125]I Model 6702 (28 keV average energy), [145]Sm (41 keV average energy), and [241]Am (60 keV). However, as the photon energy increases further from that of [241]Am, the radial dose function at 5 cm decreases slightly as is evident from the data for ^{192}Ir sources, which have an average energy of 369 keV. At present, no measured data for the radial dose function of [169]Yb (93 keV average energy) are available although preliminary data

were reported by Mason et al. (9, 10), but the results are not published yet.

To understand the dependence of radial dose function on photon energy, we undertook the present study using Monte Carlo simulations of monoenergetic photons in a wide range of photon energies. Figure 2 shows the Monte Carlo calculated radial dose functions of isotropic monoenergetic point sources of 30 keV to 1 MeV, as a function of distance in Solid Water from the source. This result can be explained as follows: for photons with energy of less than 30 keV, dose deposition is mainly through the photoelectric process. However, at higher energies the Compton scattering makes a larger contribution to energy deposition. For higher energy photons (with energies greater than 100 keV), the direction of scattered photons becomes more forward and hence they deposit energies at larger depth. Also, higher energy photons loose a considerable fraction of their initial energy upon Compton scattering. Thus, for intermediate photon energies in the range of 50–100 keV, there is considerable multiple photon scattering which leads to buildup of dose in a medium.

A steep change in radial dose function between 30 keV to 100 keV is observed, as shown in Figure 3. Note that the radial dose functions at 5 and 10 cm from the source increase with increasing energy up to 80 keV and then decrease to about unity for higher energy photons (Fig. 3). The radial dose function at 5 cm has a maximum value for photon energies around 80 keV, which is close to those for [241]Am and [169]Yb. Also, it is observed that for photons with energies greater than about 40 keV, the radial dose function at 5 cm is equal to or greater than unity.
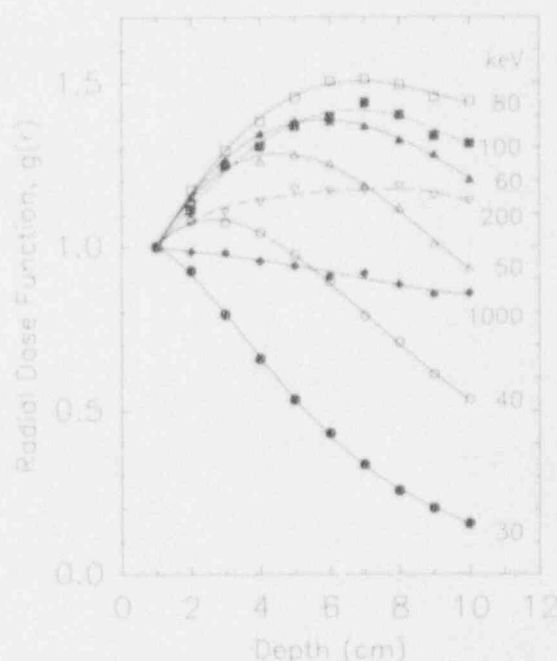

Fig. 2. Monte Carlo calculated radial dose function of isotropic monoenergetic point sources of 30 keV to 1 MeV in Solid Water, as a function of distance from the source in Solid Water.
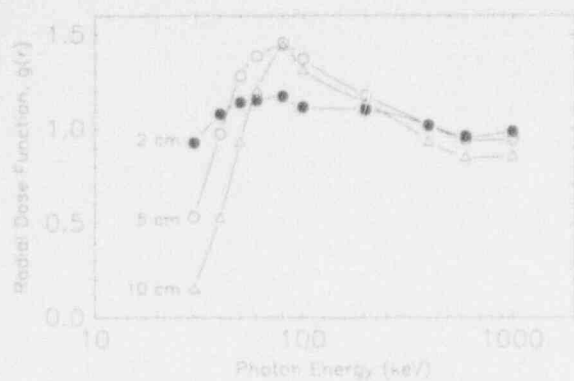
Fig. 3. Variation of radial dose functions in Solid Water at 2, 5, and 10 cm from isotropic monoenergetic point sources with photon energies from 30 keV to 1 MeV.

Therefore, their photon energies are likely to have penetrating abilities that are adequate for intracavitary irradiation.

To test the validity of our Monte Carlo simulations, we compared our results against theoretical and experimental data from other investigators. A comparison of measured and calculated radial dose functions at 2, 4, and 8 cm for brachytherapy sources of ^{103}Pd, ^{125}I, ^{145}Sm, ^{241}Am, ^{169}Yb, ^{192}Ir and ^{137}Cs is presented in Figure 4. The Monte Carlo data shown in Figure 4 were generated by using methods described in the earlier sections, with exception of those for ^{169}Yb. For ^{169}Yb, Monte Carlo data of Mason *et al.* (9, 10) are shown, and as mentioned above no measured data for ^{169}Yb are available yet. For ^{145}Sm the measured data from Fairchild *et al.* (5) are shown. Overall, good agreement between the measured data and results of our Monte Carlo simulation is observed, supporting the validity of our Monte Carlo simulation technique for the determination of radial dose functions of brachytherapy sources.

DISCUSSION

From an evaluation of the measured and calculated radial dose functions we have investigated the penetrating ability of the photons emitted by ^{103}Pd, ^{125}I, ^{145}Sm, ^{241}Am, ^{169}Yb, ^{192}Ir, and ^{137}Cs brachytherapy sources. Also, we have studied the penetrating ability of photons as a function of energy using the Monte Carlo simulation of radial dose functions for isotropic monoenergetic point sources emitting photons with energies ranging from 30 keV to 1 MeV. These simulations were conducted in Solid Water because we needed to test the validity of these calculations by a direct measurement of radial dose functions, which were performed in Solid Water phantoms. Note that Solid Water has been shown to be nearly equivalent to water for photons with energies as low as those from ^{125}I (11). Therefore, reasonable conclusions regarding penetrating ability in water, which is the medium of primary interest
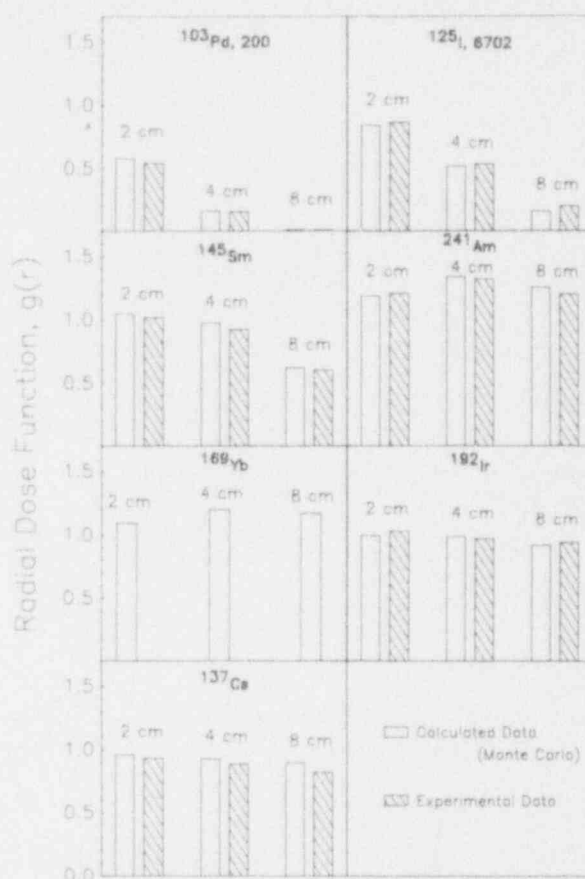

Fig. 4. A comparison of Monte Carlo calculated and measured radial dose functions at distances of 2, 4, and 8 cm from ^{103}Pd, ^{125}I Model 6702, ^{145}Sm, ^{241}Am, ^{169}Yb, ^{192}Ir, and ^{137}Cs brachytherapy sources. The ^{145}Sm data are from Fairchild *et al.* (5), the ^{169}Yb data from Mason *et al.* (9, 10), the ^{125}I and ^{192}Ir data from Nath *et al.* (16), the ^{103}Pd data from Meigooni *et al.* (13), and the ^{137}Cs data from Shalek *et al.* (17).

in radiation oncology, can be derived from the data for Solid Water.

The dose rate from brachytherapy sources falls rapidly as the distance increases. The inverse square law has a dominating effect on the shape of dose distributions produced by most brachytherapy sources, especially those emitting high energy photons. However, for lower energy photons, the tissue attenuation can also have considerable influence on the depth dose characteristics of a brachytherapy source. Because the radial dose function removes the inverse square effects, it is an appropriate choice to study photon energy dependence of tissue attenuation effects in brachytherapy.

The radial dose function, as defined by Eq. 1, takes out the effects of inverse square law as well as the distribution of radioactive material in the source, that is, the source geometry. Therefore, it is reasonable to compare radial dose function extracted from measured data for actual sources with results of Monte Carlo simulations using a point source in a spherical geometry. To the extent that

the focus of our work is to investigate trends in radial dose functions as a function of photon energy, our approach to this problem is valid for drawing conclusions about the relative penetrating ability of different radioisotopes in tissue.

For intracavitary irradiation, especially in gynecological applications, it is necessary to deliver an adequate dose to point B, which is about 5 cm away from the sources in the uterine tandem. It would be difficult to achieve this goal with brachytherapy sources emitting photons with energy of less than 30 keV, because the tissue attenuation would reduce the dose at 5 cm by a factor of more than two. This dose reduction due to tissue attenuation is on top of the rapid falloff of dose due to inverse square law. Therefore, we conclude that while all of the radioactive sources studied in this work can provide adequate penetration for interstitial brachytherapy, only those emitting photons with energies greater than 40 keV can provide adequate depth dose for intracavitary irradiation. Also, we observe that photons with energies around 80 keV exhibit maximum penetrating ability for distances up to 5 cm in a water-equivalent medium.

REFERENCES

1. Berger, M. J.; Seltzer, S. M. ETRAN Monte Carlo code system for electron and photon transport through extended media. CCC-107, Radiation Shielding Information Center, computer code collection. Oak Ridge National Laboratory; May, 1973.
2. Biggs, F.; Lighthill, R. Analytical approximations for x-ray cross-sections II. SC-RR-71 0507. Sandia National Laboratories, December 1971.
3. Biggs, F.; Lighthill, R. Analytical approximations for total pair-production cross-sections. SC-RR-68-619, Sandia National Laboratories, September, 1968.
4. Dale, R. G. A Monte Carlo derivation of parameters for use in the tissue dosimetry of medium and low energy nuclides. Brit. J. Radiol. 55: 748–757; 1982.
5. Fairchild, R. G.; Kalef-Ezra, J.; Packer, S.; Wielopolski, L.; Laster, B. H.; Robertson, J. S.; Mausner, L.; Kanellitsas, C. Samarium-145: a new brachytherapy source. Phys. Med. Biol. 32: 847–858; 1987.
6. Halbleib, J. A.; Mehlhorn, T. A.; Kensek, R. P. ITS: The Intergrated Tiger Series of coupled electron/photon Monte Carlo code system, version 2.1. Sandia National Laboratories; CCC-467, Radiation Shielding Information Center, Computer Code Collection, Oak Ridge National Laboratory, 1987.
7. Interstitial Collaborative Working Group (ICWG). Interstitial brachytherapy: physical, biological and clinical considerations. Anderson, L. L., et al., eds. New York, NY: Raven Press; 1990.
8. Loevinger, R. Absorbed dose from interstitial and intracavitary sources. In: DHEW Publication FDA-72-8024. Afterloading in radiotherapy. Rockville, MD: Dept. of Health, Education and Welfare; 1972: 192–203.
9. Battista, J. J.; Porter, A. T.; Mason, D. L. D.; Barnett, R. Ytterbium-169: A novel brachytherapy source (Abstract). Int. J. Radiat. Oncol. Biol. Phys. 19(Suppl. 1): 152; 1990.
10. Mason, D. L. D.; Barnett, R.; Battista, J. J.; Porter, A. T. Preliminary dosimetric studies of prototype ytterbium-169 seeds for brachytherapy (Abstract). Med. Phys. 16: 458; 1989.
11. Meigooni, A. S.; Meli, J. A.; Nath, R. A comparison of solid phantoms with water for dosimetry of 125I brachytherapy sources. Med. Phys. 15: 695–701; 1988.
12. Meigooni, A. S.; Meli, J. A.; Nath, R. Influence of the variation of energy spectra with depth in the dosimetry of 192Ir using LiF TLD. Phys. Med. Biol. 33: 1159–1170; 1988.
13. Meigooni, A. S.; Sabnis, S.; Nath, R. Dosimetry of palladium-103 brachytherapy sources for permanent implants. Endocuriether. Hyperther. Oncol. 6: 107–117; 1990.
14. Nath, R. New radioactive sources for brachytherapy. Phys. Today 42(1): 50–51; 1989.
15. Nath, R.; Gray, L.; Park, C. H. Dose distribution around cylindrical 241Am sources for a clinical intracavitary applicator. Med. Phys. 14: 809–817; 1987.
16. Nath, R.; Meigooni, A. S.; Meli, J. A. Dosimetry on the transverse axis of 125I and 192Ir interstitial brachytherapy sources. Med. Phys. 17: 1032–1040; 1990.
17. Shalek, R. J.; Stovall, M. Dosimetry in implant therapy. In: Attix, F. H., Tochlin, E., eds. Radiation dosimetry, Vol. III New York, NY: Academy Press; 1969.

Dosimetry of Palladium-103 Brachytherapy Sources for Permanent Implants

ALI S. MEIGOONI, PhD, SUSHIL SABNIS, BS, RAVINDER NATH, PhD

Department of Therapeutic Radiology, Yale University School of Medicine,
New Haven, Connecticut

A new design of encapsulated sources of palladium-103, model 200 Theraseed, is now available for interstitial brachytherapy. ^{103}Pd emits 20 to 23 keV photons and decays with a half-life of 17 days. Compared with iodine-125, the ^{103}Pd implants could deliver approximately four times higher initial dose rate, which could be clinically significant in treatment of certain tumors. For the earlier ^{103}Pd source design, model 100, about 30% of the dose at a distance of 5 cm was from high-energy and longer-lived isotopes, created by activation of trace elements in the source materials and their encapsulation when the source assembly was irradiated in a nuclear reactor. To address this problem, the model 200 source is fabricated by irradiating ^{102}Pd with thermal neutrons, followed by chemical purification and coating of the ^{103}Pd on graphite cylinders, which are then hot-loaded into titanium cylinders for encapsulation. This new design essentially eliminates the contribution of trace elements to the absorbed dose. Dose distribution around a ^{103}Pd model 200 source has been measured using LiF TLD in solid water. The measured data have been fitted to an analytical expression, and a two-dimensional table of dose rates around the ^{103}Pd source has been generated. Dose rate at a distance of 1 cm along the transverse axis of the ^{103}Pd model 200 source, with unit air kerma strength, is 0.735 ± 0.03 cGy h^{-1}, which is equivalent to 0.95 ± 0.04 cGy h^{-1} from a 1-mCi (apparent) source. The exposure rate constant for ^{103}Pd was calculated to be 1.48 R cm^2 h^{-1} mCi^{-1}. The anisotropy correction factor for ^{103}Pd was determined to be 0.90. Using the two-dimensional dose rate data, the radial dose function and the tissue attenuation factors for ^{103}Pd have also been determined.

Key Words: Palladium-103, Brachytherapy, Dosimetry, Permanent Implants

Interstitial brachytherapy continues to play an important role in the management of cancers of several sites such as the head and neck, brain, and prostate. The physical advantages of interstitial brachytherapy result from a better localization of dose to the tumor volume. In an interstitial implant, as radiation is continuously delivered over a period of time, repair of sublethal and potentially lethal damage, proliferation, and other cell kinetic effects modify the response of tumor and normal tissues, resulting in complex dose rate effects.[1-3] In general, as the dose rate is decreased from acute dose rate, the cell survival curves become less steep, primarily because of the repair of sublethal damage. At intermediate dose rates (10 to 100 cGy h^{-1}) where cell

cycle redistribution may accumulate more cells in a more radiosensitive phase, the reverse dose rate effect may occur, ie, the cell survival curves become steeper with decreasing dose rates.[4] As the dose rate is further reduced, the cell proliferation effects begin to dominate and the slopes of cell survival curves become progressively shallower. In fact, it has been argued that if the dose rate is decreased below a critical dose rate, cell division will continue and cell population will continue to grow, though at a slower rate than normal because of cell death and radiation-induced mitotic delays.[5] Most temporary interstitial implants employ dose rates above 30 cGy h^{-1}. However, permanent implants, especially those with iodine-125, deliver initial dose rates on the order of 5 to 10 cGy h^{-1}, delivering 10,000 to 20,000 cGy to total decay, most of the dose being delivered over three half-lives, which is approximately six months for ^{125}I implants. For some tumors, these dose rates, obtained in ^{125}I permanant implants, may not be adequate for tumor control. Recently introduced palladium-103 sources offer the possibility of irradiating tumors by permanent implants at higher dose rates.

^{103}Pd emits photons in the range of 20 to 23 keV with a half-life of 17 days. With a shorter half-life, ^{103}Pd sources deliver most of the radiation dose to the tumor in a much shorter time than ^{125}I implants, which have a half-life of 60 days. In this report, we present dosimetry data for ^{103}Pd sources.

Materials and Methods

^{103}Pd Sources

^{103}Pd decays primarily by electron capture to a metastable state of ^{103m}Rh, primarily emitting characteristic x-rays with photon energies of 20.07, 20.22, and 22.70 keV with relative intensities of 19.8%, 37.7%, and 11.7%, respectively. The ^{103m}Rh, in turn, makes internal transition (internal conversion) to its ground state emitting 20.07, 20.22, and 22.70 keV photons at relative intensities of 2.20, 4.18, and 1.30 per 100 decays of ^{103}Pd, respectively. In addition, there are several very low yield gamma rays emitted in the decay of ^{103}Pd. Some of these photons have energies up to 497 keV, but their total yield is less than 0.04% (Table 1).

Measurements reported here were performed using two different models of ^{103}Pd seeds, namely, model 100 and model 200, manufactured by Theragenics Corporation (Atlanta, Georgia). In the fabrication of model 100 seeds, stable ^{102}Pd was uniformly distributed throughout two aluminum cylinders (0.6 mm diameter × 0.9 mm length)

Table 1. Spectrum of the Major Photons Emitted by Decay of ^{103}Pd (Unencapsulated)

Energy, keV	No. of Photons per Decay
20.07	0.2205
20.22	0.4188
22.72	0.1300
357.4	0.0000221
397.5	0.0000699
497.1	0.00000398

separated by a lead x-ray marker (0.25 mm diameter × 1.4 mm length) and encapsulated in a 0.05 mm thick titanium tube. The two ends of the tube were then sealed with two titanium cups using a laser welding technique. The assembled seed was then irradiated in a neutron reactor for activation of ^{102}Pd to ^{103}Pd. The outside dimensions of the ^{103}Pd were 0.81 mm diameter × 4.5 mm length, which are identical to those of ^{125}I sources manufactured by 3M Company (Medical Products Division, St. Paul, Minnesota).

For the fabrication of model 200 seeds, the stable ^{102}Pd element was first irradiated in a nuclear reactor to produce ^{103}Pd. Then, pure ^{103}Pd was obtained by a chemical separation procedure. The purified ^{103}Pd was then electroplated onto the surface of two graphite cylinders, which were then "hot" loaded into titanium tubes. Titanium cups were welded to the tubes using the same procedure as for the earlier design. The outside dimensions of model 200 were identical to those of model 100 ^{103}Pd, or ^{125}I sources (Figure 1).

Dose Measurement Technique

The low energy of x-rays from ^{103}Pd and high dose gradients, especially at distances close to the source, requires a precise determination of source-to-detector distance for dose measurements. Experiments were performed using 20 × 20-cm slabs of solid water (electron and photon water equivalent, model 457, Radiation Measurement, Inc., Middleton, Wisconsin) with thicknesses of 0.5, 1.0, and 2.0 cm. Because of the low dose rate of the brachytherapy seeds, the ratio of signal to noise would be very small for a typical ionization chamber. Therefore, LiF TLDs (TLD-100, Teflon chips, Harshaw/Filtrol Partnership, Solon, Ohio)
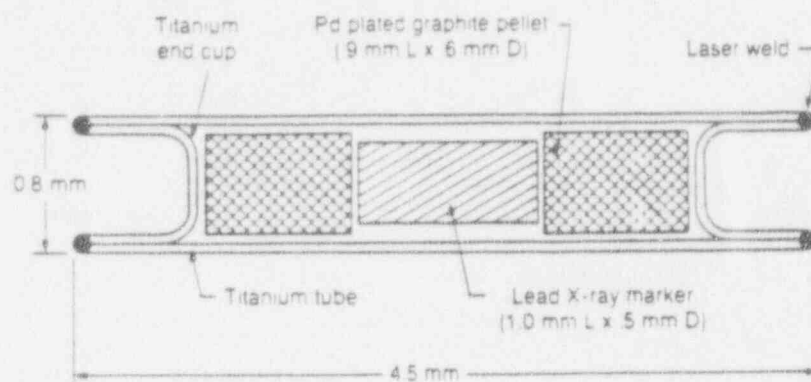
Figure 1 Schematic diagram of the ^{103}Pd, model 200 source

with dimensions of $1 \times 1 \times 1$ mm and $3.1 \times 3.1 \times 0.89$ mm were employed as dosimeters.

A solid water phantom was carefully machined to accommodate the source and TLD chips. For the measurement of dose along the transverse axis of the source, three different irradiation geometries were used (Figures 2A, 2B, and 2C). The arrangement shown in Figure 2A was used with a single source positioned perpendicular to the surface of the phantom and TLD chips were distributed along the transverse axis of the seed. In an experiment for ^{125}I, Meigooni et al[6] have found about a 6% interchip effect, ie, interference of one TLD by the other TLD chips if they are aligned along one line. To avoid this effect, TLDs were staggered around the seed. The phantom holding the source and TLD was sandwiched between several slabs of solid water (about 10 cm on each side) to provide full scattering conditions. With this arrangement, measurements were performed at five radial distances from 1 to 5 cm at a 1-cm interval. There were two TLDs at each source-detector distance,

and the entire experiment was repeated twice for a better statistical quality of the data. Each experiment lasted about 24 hours to obtain sufficient response from the TLDs and the measured responses were corrected for the decay of the source during the 24-hour experiment period, to give the response at the beginning of this period.

After approximately one month, the sources had decayed to about one quarter of their initial activity. With this reduced activity it was very difficult to get a reasonable response from the TLD chips. Therefore, the arrangement shown in Figure 2B was used. In this arrangement, eight sources with the same activity were positioned in holes made on a circle around a single TLD chip, except for the 1-cm radius around the TLD, which has only four sources. For each source-to-detector distance, the holes on one of the circle was used to accommodate the sources and the unoccupied holes were filled with liquid water to eliminate any air cavity effects. The entire experiment was repeated several times to get data with good statistical quality. In this situa-
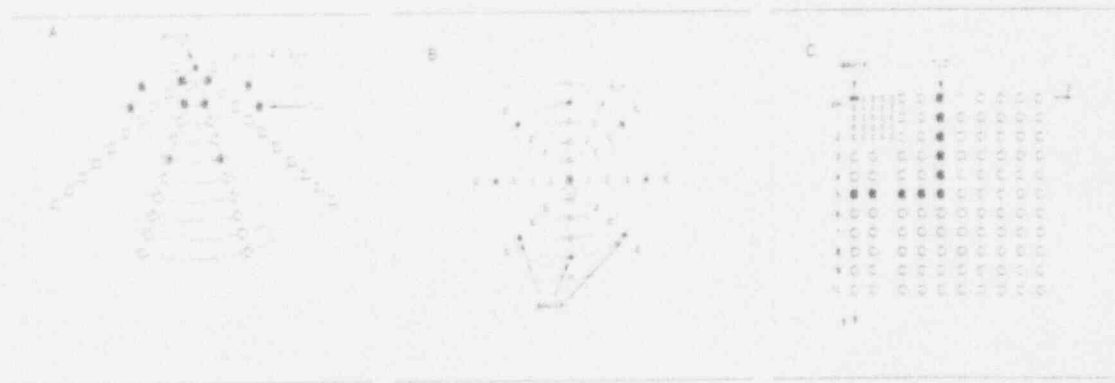

Figure 2 Schematic diagram of the experimental setup. Figures 2A and 2B show the arrangement of the TLD relative to the source for the measurement of dose rates along the transverse axis of the source, and Figure 2C shows the experimental setup for two-dimensional dose distribution measurements around the ^{103}Pd, model 200 source.

tion also, the phantom holding the sources and TLD were sandwiched between several slabs of solid water to provide full scattering conditions.

Dose distribution around a [103]Pd seed in a two-dimensional plane was measured with the arrangement shown in Figure 2C. For this arrangement, a solid water phantom was machined to accommodate $1 \times 1 \times 1$-mm TLD chips at short distances from the seeds, namely, points with z (along the longitudinal axis of the seed) and y (along the transverse axis of the seed) coordinates of up to 2.0 cm at 0.5-cm intervals. At larger distances with z and y coordinates up to 7.5 cm, the $3.1 \times 3.1 \times 0.89$-mm TLD chips were used. To minimize the interchip effect, the measurements were performed by arranging the TLD chips parallel to the z and y axis, as shown in Figure 2C. Each experiment was repeated at least twice to improve the statistical quality of the data. In these experiments the empty holes were filled with solid water plugs to eliminate any air gap effects. Moreover, the depth of the holes for the TLD chips and the source was carefully selected to have the longitudinal axis of the seed in the same plane as the center of the TLD chips.

TLD responses obtained during each experiment, with any of the three configurations, were converted to absorbed dose by calibrating them with a 4 MV x-ray beam, which was calibrated using an exposure-calibrated ionization chamber (0.6 cm³ Farmer chamber) as prescribed by the AAPM dosimetry protocol.[7] Because of the energy dependence of the sensitivity of TLDs, a correction factor for the photon energies of [103]Pd was determined. This energy correction factor was obtained by measuring the relative sensitivity of LiF TLDs for a variety of photon beams, namely, 60, 80, 100, and 250 kV, 4 MV x-rays, and iridium-192 photons.[6] From these measurements, the energy dependence of the relative sensitivity of LiF was determined. Since the relative sensitivity of TLDs was nearly constant (1.41 ± 0.04) for photons in the energy range of 20 to 30 keV, we have employed an energy correction factor of 1.41 for [103]Pd. It is the same as that for ^{125}I photons as determined by us[6] and is in good agreement with the results reported by a number of other investigators for ^{125}I photons.[8,9]

Source Strength Determination

The manufacturer has determined the strength of [103]Pd seeds using the following procedure.[10] The photon spectrum emitted in air at a large distance along the perpendicular bisector of the source axis

is measured using a calibrated NaI detector. The total number of photons in the energy range of 20 to 23 keV is obtained by integrating this spectrum. This result is corrected for detector efficiency, and knowing that only 74% of the [103]Pd disintegrations lead to photon emission, the number of [103]Pd disintegrations per second, and hence the apparent activity of the [103]Pd seed, is determined.

An accurately calibrated source was obtained from the manufacturer in order to calibrate a reentrant well-type ionization chamber,[11] which has been calibrated for a variety of other radioactive sources including cesium-137, ^{125}I, and ^{192}Ir by the Radiological Physics Center (RPC) at M. D. Anderson Hospital and Tumor Institute.

The apparent activity of the seeds used in these experiments was up to 74 MBq (2 mCi), which corresponds to an air kerma strength of 2.586 U ($1U = 1$ μGy m² h⁻¹ = 1 cGy cm² h⁻¹ is the unit of air kerma strength, as defined by AAPM Report No. 21.[12] For [103]Pd, a $1.23U$ source is equivalent to a 1 mCi [apparent] source.)

Results

Figure 3 illustrates the measured dose rates along the perpendicular bisector of the model 100 and model 200 [103]Pd sources. The dose rates multiplied by distance squared along the transverse axis of these two sources are found to be in good agreement with each other at short distances (Figure 3 and Table 2); however, at larger distances the model 200 sources produces a smaller dose rate. For example, at a distance of 5 cm, the dose rates multiplied by distance squared produced by a unit air kerma strength source are 0.079 ± 0.003 cGy cm² h⁻¹ and 0.064 ± 0.003 cGy cm² h⁻¹ for model 100 and model 200 sources, respectively. The dose rate constants, Λ, defined as the dose rate at a distance of 1 cm along the perpendicular bisector of a unit strength source, are 0.71 ± 0.03 cGy h⁻¹ U^{-1} and 0.735 ± 0.03 cGy h⁻¹ U^{-1} for model 100 and model 200 sources, respectively. The same quantities for a source with apparent activity of 1 mCi are 0.91 ± 0.04 and 0.95 ± 0.04 cGy h⁻¹ mCi⁻¹.

Since [103]Pd model 100 sources were made from the "cold" seeds placed in the nuclear reactor, some chemical impurities also become activated. The contribution of these trace elements to the total dose rate for a fresh seed for which only 0.3% of the seed activity was from the trace elements[10] was measured at different distances from the source by shielding the low-energy photons using a 1.0 mm thick lead sleeve around the seed. This amount of
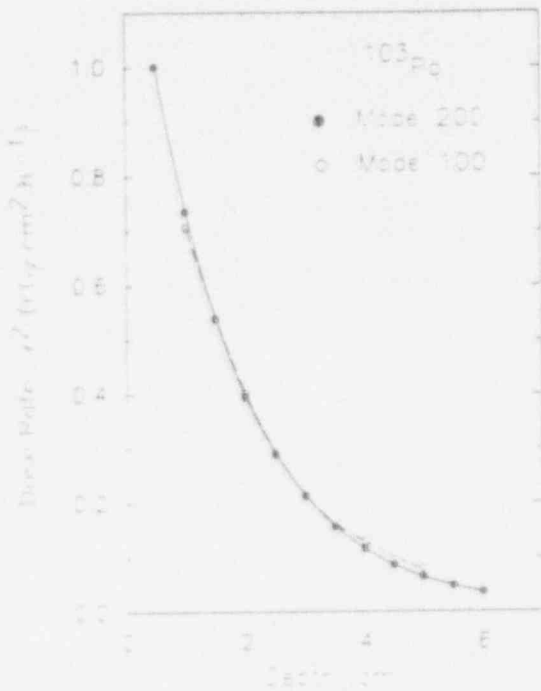
Figure 3. Dose rate multiplied by distance squared for ^{103}Pd, model 100 (open symbols) and model 200 (filled symbols) sources. Distance are along the transverse axis of the seed.

Table 2. Measured Dose Rates Times Distance Squared for ^{103}Pd, Model 200 and Model 100 Sources With Unit Air Kerma Strength ($1.293U = 1$ mCi [Apparent])

Distance Along the Transverse Axis, cm	Dose Rate × Distance Squared (cGy cm^2 h^{-1})	
	Model 200	Model 100
0.5	1.001	
1.0	0.735	0.706
1.5	0.539	
2.0	0.395	0.402
2.5	0.290	
3.0	0.213	0.214
3.5	0.157	
4.0	0.116	0.129
4.5	0.086	
5.0	0.064	0.0792
5.5	0.048	
6.0	0.036	

lead shielding is about 100 HVLs for 21 keV photons from ^{103}Pd, hence it will absorb all the 21 to 23 keV photons from the ^{103}Pd, but will only slightly attenuate the higher energy photons from

^{103}Pd and trace elements. Figure 4 shows the dose rates due to these high-energy photons with the total dose rates from the model 100 and model 200 seeds with no shielding. These measurements show that
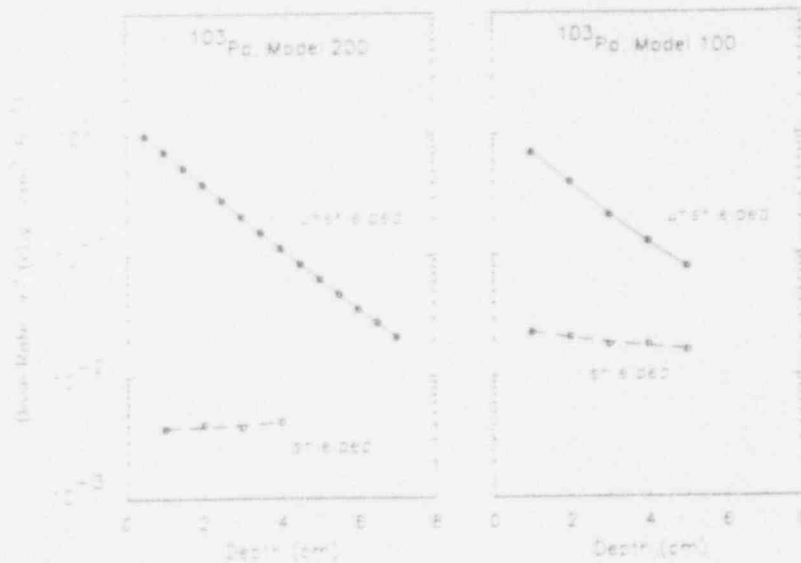

Figure 4. Dose rate multiplied by distance squared of model 200 (left side) and model 100 (right side) ^{103}Pd sources. The dashed curve in each graph represents the measured contribution of the dose rates from the trace elements and higher energy photons from ^{103}Pd, by shielding the low energy photons emitted by ^{103}Pd, using a 1 mm thick lead sleeve.

for [103]Pd model 100, about 5% and 35% of the dose rate at 1 and 5 cm, respectively, were due to the high-energy photons from [103]Pd and trace elements. However, for model 200 sources, this effect of higher energy photons from [103]Pd and trace elements is reduced by an order of magnitude compared with the model 100 source, as shown in Figure 4.

These experiments for the model 200 source were repeated after a few months, and it was observed from GeLi spectrometer measurements that all of the higher energy photons for the model 200 source had decayed with the same half-life as [103]Pd. Thus, the contribution to dose from trace elements is essentially negligible for the model 200 source. Although some very low yield, high-energy photons from the decay of [103]Pd are present, their contribution to dose is also very small (less than 5%).

Considering the relatively high contribution of dose from trace elements in model 100 seeds, their use for permanent implants is less desirable. Since the model 200 sources have essentially eliminated this problem, the more detailed dosimetry data were obtained for model 200 seeds only.

Two-dimensional dose rates around a model 200 source in a cartesian grid, as shown in Figure 2C, were measured using LiF TLDs in a solid water phantom. To improve the statistical quality of the data, dose rates at each point were measured at least twice, and four times for distances less than 2 cm. With an overall uncertainty of ±4%, these data were reproducible. Dose measurements were made

at 36 carefully selected points in the z-y plane (Figure 2C) for distances less than 2.0 cm at 0.5-cm intervals, and then at z values of 2.5 cm, 3.5 cm, 4.5 cm, 5.5 cm, and 7.5 cm and y values of 3.0 cm, 4.0 cm, 5.0 cm, and 7.0 cm. To generate dose rate data at points other than these locations, the measured data for given z or y values were fitted to the following expressions using the least-square regression technique:

$$D(z,y)\, r^2 = \exp\left\{ \sum_{i=0}^{N} a_i(z)\, y^i \right\} \text{ for each z value, and} \quad (1)$$

$$D(z,y)\, r^2 = \exp\left\{ \sum_{i=0}^{N} b_i(y)\, z^i \right\} \text{ for each y value.} \quad (2)$$

where $r = \sqrt{(z^2 + y^2)}$. Figure 5 shows two samples of this least-square fit, for the data along the z and y axes. Using the parameters a's and b's, a two-dimensional table of dose rates at a 0.5-cm interval in cartesian coordinates with dimensions up to 7.5 cm was generated (Table 3).

Since some of the treatment planning systems require a two-dimensional dose table in polar coordinates, such a table was generated (Table 4). The polar coordinate table was obtained for polar angle θ, from 0° to 90° at 2.5° to 10° intervals using the values of parameters a's and b's to calculate dose rates along different radii. The dose rates shown in Table 4 were fitted to the following expression:

$$D(r,\theta)\, r^2 = \exp\left\{ \sum_{i=0}^{N} c_i(\theta)\, r^i \right\} \text{ for each } \theta \text{ value} \quad (3)$$
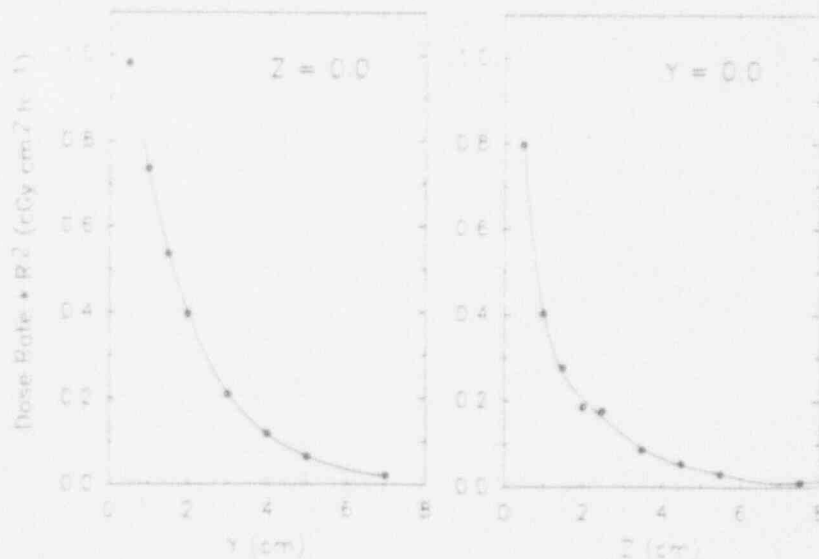

Figure 5. A sample of least-square fit to the measured dose rate data along the y axis (left) and along the z axis (right).

Table 3. Dose Rate Multiplied by Distance Squared (cGy cm² h⁻¹) for a ¹⁰³Pd, Model 200 Source With a Unit Air Kerma Source Strength* in Cartesian Coordinates With z Along the Source Axis

z (cm) y(cm)	0.000	0.500	1.000	1.500	2.000	2.500	3.000	3.500	4.000	4.500	5.000	5.500	6.000	6.500	7.000	7.500
0.00		0.789	0.409	0.270	0.201	0.157	0.123	0.094	0.071	0.053	0.040	0.030	0.024	0.019	0.015	0.011
0.50	1.001	0.765	0.456	0.285	0.207	0.157	0.119	0.090	0.067	0.050	0.037	0.028	0.022	0.018	0.014	0.011
1.00	0.735	0.663	0.472	0.302	0.203	0.146	0.110	0.083	0.062	0.047	0.036	0.028	0.022	0.017	0.013	0.010
1.50	0.539	0.507	0.409	0.292	0.201	0.142	0.106	0.080	0.061	0.046	0.035	0.028	0.022	0.017	0.013	0.010
2.00	0.395	0.373	0.325	0.254	0.185	0.135	0.100	0.077	0.059	0.045	0.035	0.027	0.022	0.017	0.013	0.010
2.50	0.290	0.274	0.249	0.208	0.160	0.121	0.092	0.071	0.056	0.044	0.034	0.027	0.021	0.017	0.013	0.010
3.00	0.213	0.203	0.187	0.162	0.132	0.104	0.082	0.065	0.052	0.041	0.033	0.027	0.021	0.017	0.013	0.010
3.50	0.157	0.151	0.140	0.124	0.106	0.087	0.070	0.057	0.047	0.038	0.031	0.025	0.020	0.016	0.013	0.009
4.00	0.116	0.113	0.106	0.095	0.083	0.070	0.059	0.049	0.041	0.034	0.028	0.023	0.019	0.015	0.012	0.009
4.50	0.086	0.085	0.080	0.072	0.064	0.056	0.048	0.041	0.035	0.030	0.025	0.021	0.018	0.014	0.011	0.009
5.00	0.064	0.064	0.061	0.055	0.050	0.044	0.038	0.034	0.029	0.025	0.022	0.019	0.016	0.013	0.011	0.008
5.50	0.048	0.048	0.047	0.043	0.038	0.034	0.030	0.027	0.024	0.021	0.019	0.016	0.014	0.013	0.010	0.008
6.00	0.036	0.036	0.035	0.033	0.030	0.027	0.024	0.022	0.020	0.017	0.015	0.014	0.012	0.011	0.010	0.008
6.50	0.028	0.028	0.027	0.026	0.024	0.022	0.020	0.018	0.016	0.014	0.013	0.011	0.010	0.009	0.008	0.008
7.00	0.021	0.021	0.021	0.020	0.019	0.017	0.016	0.014	0.013	0.012	0.010	0.009	0.008	0.007	0.007	0.007

*Unit air kerma strength = 1 μGy m² h⁻¹ = 1 cGy cm² h⁻¹.

Table 4. Dose Rate Multiplied by Distance Squared (cGy cm² h⁻¹) for ¹⁰³Pd, Model 200 Source With a Unit Air Kerma Source Strength* in Polar Coordinates With the Polar Axis Along the Source Axis

θ (deg) r (cm)	0.0	5.0	10.0	12.5	15.0	17.5	20.0	30.0	40.0	50.0	60.0	70.0	80.0	90.0
0.50	0.789	0.793	0.820	0.823	0.832	0.816	0.819	0.835	0.854	0.902	0.971	1.012	1.037	1.001
1.00	0.409	0.412	0.423	0.415	0.424	0.457	0.469	0.527	0.597	0.660	0.705	0.735	0.740	0.735
1.50	0.270	0.271	0.282	0.280	0.287	0.299	0.306	0.353	0.417	0.475	0.512	0.534	0.533	0.539
2.00	0.201	0.201	0.209	0.212	0.215	0.214	0.217	0.248	0.295	0.341	0.372	0.388	0.387	0.395
2.50	0.157	0.156	0.160	0.162	0.163	0.160	0.160	0.180	0.212	0.246	0.272	0.283	0.283	0.290
3.00	0.123	0.121	0.122	0.122	0.122	0.120	0.121	0.134	0.155	0.179	0.199	0.206	0.208	0.213
3.50	0.094	0.093	0.091	0.090	0.090	0.091	0.092	0.101	0.116	0.132	0.146	0.151	0.154	0.157
4.00	0.071	0.069	0.067	0.066	0.066	0.068	0.070	0.078	0.088	0.099	0.108	0.112	0.115	0.116
4.50	0.053	0.051	0.050	0.050	0.050	0.052	0.054	0.061	0.068	0.075	0.081	0.083	0.086	0.086
5.00	0.040	0.038	0.038	0.038	0.039	0.039	0.041	0.048	0.054	0.058	0.061	0.062	0.065	0.064
5.50	0.030	0.029	0.029	0.030	0.031	0.031	0.032	0.038	0.043	0.045	0.046	0.047	0.049	0.048
6.00	0.024	0.022	0.022	0.024	0.024	0.025	0.025	0.031	0.034	0.036	0.035	0.035	0.037	0.036
6.50	0.019	0.018	0.018	0.019	0.019	0.020	0.020	0.025	0.028	0.028	0.027	0.027	0.028	0.028
7.00	0.015	0.014	0.014	0.014	0.014	0.016	0.016	0.020	0.023	0.022	0.021	0.021	0.022	0.021
7.50	0.011	0.011	0.011	0.011	0.011	0.013	0.013	0.016	0.018	0.018	0.017	0.017	0.017	0.016
8.00	0.007	0.007	0.008	0.009	0.010	0.009	0.010	0.013	0.015	0.014	0.013	0.013	0.013	0.013
8.50	0.003	0.003	0.006	0.008	0.011	0.005	0.007	0.010	0.013	0.011	0.011	0.011	0.010	0.010
9.00	0.001	0.001	0.005	0.012	0.023	0.002	0.004	0.007	0.011	0.009	0.009	0.009	0.007	0.008
9.50	0.000	0.000	0.006	0.038	0.144	0.001	0.002	0.005	0.009	0.007	0.007	0.008	0.006	0.007
10.00	0.000	0.000	0.009	0.449	5.428	0.000	0.001	0.003	0.009	0.005	0.006	0.007	0.004	0.006

*Unit air kerma strength = 1 μGy m² h⁻¹ = 1 cGy cm² h⁻¹.

Table 5. Parameters Resulting From Least-Square Fit to the Doss Rate Time Distance
Squared Data in Polar Coordinates Using Equation 3.

θ (deg)	c_0	c_1	c_2	c_3	c_4	c_5	c_6
0.0	3.58650E-01	-1.15830E+00	5.37180E-01	-1.42800E-01	1.75480E-02	-8.05400E-04	0.00000E+00
5.0	3.56280E-01	-1.14370E+00	5.24540E-01	-1.38600E-01	1.68720E-02	-7.65700E-04	0.00000E+00
10.0	4.08890E-01	-1.28500E+00	6.93440E-01	2.25540E-01	3.79780E-02	-3.17310E-03	1.04130E-04
12.5	4.75290E-01	-1.50450E+00	9.19320E-01	-3.27570E-01	6.04000E-02	-5.52050E-03	1.97910E-04
15.0	4.71690E-01	-1.48710E+00	9.21840E-01	-3.37710E-01	6.43080E-02	-6.07860E-03	2.25440E-04
17.5	2.75890E-01	-8.75980E-01	3.35360E-01	-8.57840E-02	1.04590E-02	-4.79260E-04	0.00000E+00
20.0	2.42130E-01	-7.69100E-01	2.49670E-01	-5.77370E-03	6.51460E-03	-2.81090E-04	0.00000E+00
30.0	1.57000E-01	-5.13150E-01	9.26560E-02	-1.64590E-02	1.69300E-03	-7.28500E-05	0.00000E+00
40.0	8.33200E-02	-2.94660E-01	-2.19450E-02	1.01550E-02	-1.21170E-03	4.95860E-05	0.00000E+00
50.0	7.86000E-02	-2.29650E-01	-3.93730E-02	1.07720E-02	-1.00520E-03	3.14800E-05	0.00000E+00
60.0	1.26350E-01	-2.78110E-01	-8.21490E-04	5.34130E-04	0.00000E+00	0.00000E+00	0.00000E+00
70.0	1.42860E-01	-2.74490E-01	-2.54300E-03	6.75180E-04	0.00000E+00	0.00000E+00	0.00000E+00
80.0	1.65990E-01	-3.04610E-01	8.32000E-03	-3.12130E-04	0.00000E+00	0.00000E+00	0.00000E+00
90.0	1.33270E-01	-2.64700E-01	-2.88580E-03	5.43800E-04	0.00000E+00	0.00000E+00	0.00000E+00

The parameters c_i are given in Table 5 for θ between $0°$ to $90°$.

This result indicates that the dose rates at a distance of 3 cm along the transverse axis of the ^{103}Pd source is about 1.73 times the dose rate at the same distance along the axis of the source. Although
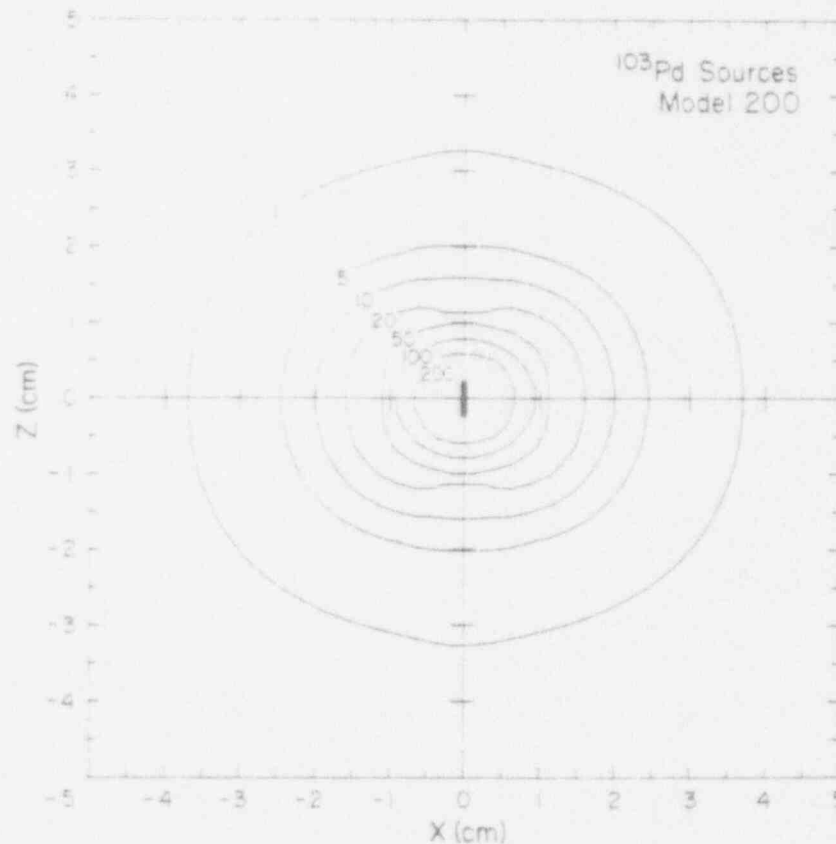

Figure 6. Isodose distribution produced a ^{103}Pd model 200 source with an air kerma strength of 129.3 U (= 100 mCi [apparent]). The dose values are in units of centigray.

this dose distribution is quite anisotropic, it should be kept in mind that the dose distribution for the ^{125}I, model 6711, is even more anisotropic; for example, dose rate at 3 cm along the transverse axis of a ^{125}I source is 2.10 times the dose rate at the same distance along the source axis.[13] Figure 6 illustrates the isodose rate curves around a [103]Pd model 200 source, generated by interpolating between the dosimetry data shown in Table 3. The two-dimensional interpolation and searching of isodose rates was performed on MicroVAX II computer using the NCAR graphics software package developed by the National Center for Atmospheric Research.

It is customary to use the point source approximation in the calculation of dose distributions produced by clinical implants with a large number of seeds implanted in a random orientation. In this case, the average dose at a given radius from the source can be easily calculated from the two-dimensional dose table in polar coordinates (Table 4). The ratio of the 4π averaged dose rate to the dose rate at the same distance along the transverse axis was calculated for distances ranging from 0.5 to 6.5 cm. This ratio, sometimes called the anisotropy factor, was found to be relatively independent of distance from the source and has an average value of 0.90. Thus, for dose calculations using the point source approximation, the dose rate
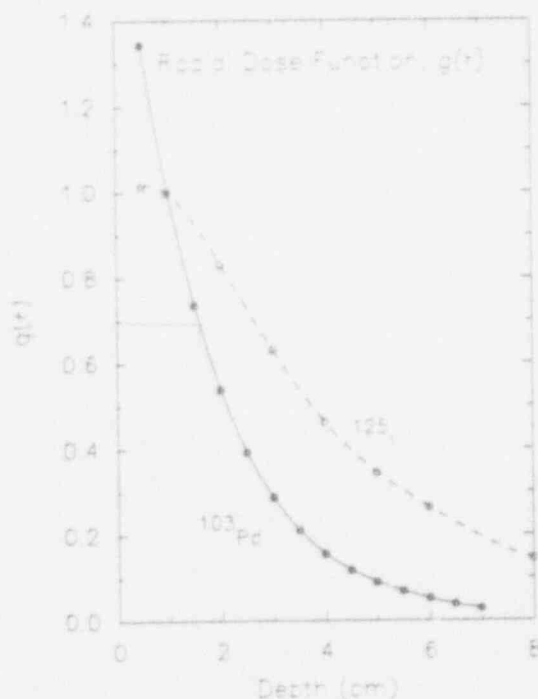
Table 6. Radial Dose Function, g(r), and Tissue Attenuation Correction Factors, σ(r), for [103]Pd, Model 200 Source

Distance, cm	g(r)	σ(r)
0.5	1.344	0.974
1.0	1.000	0.725
1.5	0.737	0.534
2.0	0.539	0.391
2.5	0.393	0.285
3.0	0.288	0.209
3.5	0.211	0.153
4.0	0.156	0.113
4.5	0.118	0.0856
5.0	0.0898	0.0651
5.5	0.0687	0.0498
6.0	0.0528	0.0383
6.5	0.0391	0.0283
7.0	0.0285	0.0207

at a distance of 1 cm from a unit air-kerma strength [103]Pd model 200 source is $0.735 \times 0.90 = 0.66$ cGy h^{-1}. The same quantity for a 1-mCi apparent activity source is 0.86 cGy h^{-1}.

Radial dose function, g(r), for a point source approximation is defined by the following expression[14]:

$$g(r) = \frac{\dot{D}(r)}{\dot{D}(1\,cm)} \cdot r^2 \qquad (4)$$

Using this definition, the radial dose function was calculated for a [103]Pd model 200 source and is shown in Figure 7 and Table 6. Also shown in Figure 7 is the radial dose function for ^{125}I model 6711 (3M Company/Medical Products Division, St. Paul, Minnesota) source for comparison.

Dose rate at a point along the transverse axis can be calculated using equation (4), g(r) in Table 6 and the dose rate at 1 cm. Dose rate at 1 cm is the product of the dose rate constant i.e. 0.66 cGy h^{-1}U^{-1} and the source strength. It should be noted that the 4π-averaged value of the dose rate constant should be used, if the sources are treated as a point source. Alternatively, the dose rate at any point can be calculated using the traditional approach, as

Figure 7. Radial dose function, g(r), of the [103]Pd model 200 source as compared with that of a ^{125}I model 6711 source.

$$D(r) = \frac{\Gamma \cdot S \cdot f}{r^2} \cdot \sigma(r) \qquad (5)$$

where Γ is the exposure rate constant, which was calculated to be 1.15 R cm^2 h^{-1} U^{-1} (1.48 R cm^2 h^{-1} mCi^{-1}) using the photon spectrum given in Table 1; f is the exposure-to-dose conversion factor, equal to 0.866 cGy/R for the ^{103}Pd spectrum in water; and $\sigma(r)$ is the tissue attenuation factor, as defined in the review article by Shalek and Stovall.[15] Tissue attenuation factors are related dose function by the expression[16]:

$$\sigma(r) \quad = \quad g(r) \quad \sigma(1) \tag{6}$$

Using equation (5), $\sigma(1)$ was determined to be 0.724, and values of $\sigma(r)$ for distances between 0.5 to 7.0 cm were calculated. Results of these calculations are given in Table 6.

Discussion

We have presented some of the physical and dosimetric aspects of ^{103}Pd sources. The exposure rate constant, dose rate constant, radial dose function, tissue attenuation factors, and angular dependence of dose around the ^{103}Pd source, model 200, have been determined. The dose rate data in a two-dimensional grid around the source have been fitted to a polynomial series and the coefficients of this fit are presented so that the dosimetry data can be easily incorporated into computerized treatment planning systems.

The model 200 sources appear to be free of any photons from contaminant trace elements. Most of the photons emitted are in the energy range of 20 to 23 keV, but a very low yield of high-energy photons from the decay of ^{103}Pd itself is present. Since the total yield of these high-energy photons is less than 0.0004 per decay of ^{103}Pd, it does not present a problem in radiation shielding. Also, the contribution to dose in water from the higher energy photons is negligibly small; less than 5% of the dose due to the 20 to 23 keV photons from ^{103}Pd.

The dose rate constant, dose rate at 1 cm along the transverse bisector of the source per unit source strength, for ^{103}Pd has a magnitude similar to that of ^{125}I sources and the outside dimensions of the ^{103}Pd sources are identical to those of the ^{125}I sources. Thus, the clinical instrumentation such as applicator guns used for ^{125}I can also be used for the implantation of ^{103}Pd sources. The general configuration of implants, ie, the number and geometrical arrangement of seeds, is likely to be very similar to that for ^{125}I implants. However, the radial dose function for ^{103}Pd falls more rapidly than

that for ^{125}I sources, and anisotropy of dose distribution around the ^{103}Pd sources is slightly less pronounced than that of the ^{125}I sources. These differences must be taken into account in the development of exact planning techniques for ^{103}Pd implants, and further research in this area is warranted.

The shape of relative dose distributions in the patient with a ^{103}Pd implant is likely to be similar to that produced by a similar configuration of ^{125}I sources. The principal advantage of ^{103}Pd, if any, lies in the delivery of radiation at a higher dose rate than ^{125}I implants. For the same biological endpoint, the clinically equivalent dose to full decay for ^{103}Pd implant would be expected to be less than that for ^{125}I implants. The optimum dose to fully decay for specific tumor sites using ^{103}Pd remains to be explored by carefully planned clinical investigations and radiobiological studies.

Acknowledgment

References

1. Hall EJ: Radiobiology for the Radiologist, ed 3. New York, New York, Harper & Row, 1988

2. Steel GG, Down JD, Peacock JH, Stephens TC: Dose rate effects and the repair of radiation damage. Radiother Oncol 1986;5:321-331

3. Steel GG, Deacon JM, Duchesne GM, Horwich A, Kelland LR, Peacock JH: The dose-rate effect in human tumor cells. Radiother Oncol 1987;9:299-310

4. Mitchell JB, Bedford JS, Bailey SM: Dose rate effects in mammalian cells in culture III. Comparison of cell killing and cell proliferation during continuous irradiation for six different cell lines. Radiat Res 1979;79:537-551

5. Hall EJ: The biological basis for endocurietherapy. Endocurietherapy/Hyperthermia Oncol 1985;1:141-152

6. Meigooni AS, Meli JA, Nath R: A comparison of solid phantoms with water for dosimetry of ^{125}I brachytherapy sources. Med Phys 1988;15:695-701

7. Task Group 21 Radiation Therapy Committee, American Association of Physicists in Medicine: A protocol for the determination of absorbed dose from high-energy photons and electron beams. Med Phys 1983;10:741-771

8. Weaver KA: Response of LiF powder to ^{125}I photons. Med Phys 1984;11:850-854

9. Hartmann GH, Schlegel W, Scharfenberg H: The three-dimensional dose distribution of ^{125}I seeds in tissue. Phys Med Biol 1983;28:693-699

10. Russell J: Product insert for ^{103}Pd Theraseeds and private communication. Theragenics Corporation, 1988

11. Berkley LW, Hanson WF, Shalek RJ: Discussion of the characteristics and results of measurements with a portable well-

type ionization chamber for calibration of brachytherapy sources, in Shearer DR (ed): Recent Advances in Brachytherapy Physics. American Association of Physicists in Medicine, Medical Physics Monograph No. 7, pp 38-48, American Institute of Physics, 1981.

12. Task Group 32 Radiation Therapy Committee, American Association of Physicists in Medicine: Specification of Brachytherapy Source Strength. AAPM Report No. 21. Published for the American Association of Physicists in Medicine by the American Institute of Physics, 1987.

13. Ling CC, Schell MC, Yorke ED: Two-dimensional dose distribution of ^{125}I seeds. Med Phys 1985;12:652-655.

14. Dale RG: A Monte Carlo derivation of parameters for use in the tissue dosimetry of medium and low energy nuclides. Br J Radiol 1982;55:748-757.

15. Shalek RJ, Stovall M: Dosimetry in Implant Therapy. New York, New York, Academic Press, 1969, pp 743-807.

16. Meli JA, Meigooni AS, Nath R: On the choice of phantom material for dosimetry of ^{192}Ir sources. Int J Radiat Oncol 1988; 14:587-594.

September 17, 1991

ERRATA FOR:

"Dosimetry of Palladium-103 Brachytherapy Sources for Permanent Implants," Ali S. Meigooni and Ravinder Nath, authors. *Endocurietherapy/Hyperthermia Oncol.* 6(2), 107-117, 1990.

Page 110; Col. 2, 21st line from the top: "...a 1.23U source..." should read, "...a 1.293U source...".

Page 114; Fig. 6 caption: "...129.3 U (= 100 mCi..." should be, "...100 U (= 77.33 mCi...". Also in that figure, the legend of longitudinal axis, "X (cm)" should be, "Y (cm)".

Page 114; Eq. (3): The exponent contained by the curly brackets in Eq. (3) should be multiplied by 2.3026.

Page 116; Col. 1, 5th line from the top: "...0.866 cGy/R..." should read, "...0.886 cGy/R...".

Page 116; Col. 1, 8th line from the top: "Tissue attenuation factors are related dose function..." should read, "Tissue attenuation factors are related to radial dose function...".

#

Tissue inhomogeneity correction for brachytherapy sources in a heterogeneous phantom with cylindrical symmetry

Ali S. Meigooni and Ravinder Nath
Yale University School of Medicine, Department of Therapeutic Radiology, 333 Cedar Street, New Haven, Connecticut 06510

In brachytherapy it is customary to perform dose calculations for an implant assuming that the tumor and surrounding tissues constitute a uniform, homogeneous medium equivalent to water. In this work, the validity of the above assumption is studied quantitatively for points along the transverse axis of ^{103}Pd, ^{125}I, and ^{241}Am brachytherapy sources, using measured and Monte Carlo calculated dose rates in homogeneous and heterogeneous media with cylindrical symmetry. The irradiation geometry chosen was a single source implanted in a Solid Water phantom which had a 1- or 2-cm-thick cylindrical Solid Water shell replaced by a polystyrene shell. The Monte Carlo simulations were performed using the integrated tiger series CYLTRAN Code. Experimental data were obtained for the same geometry to test the validity of the Monte Carlo calculations for a heterogeneous phantom. Measured dose rates just beyond a 2-cm-thick polystyrene heterogeneity were observed to be greater than those in a homogeneous Solid Water phantom by about 130%, 55%, and 10% for ^{103}Pd, ^{125}I, and ^{241}Am, respectively. Thus the effect of a relatively small polystyrene heterogeneity in Solid Water can be substantial for lower energy photons. This perturbation of dose was found to increase steeply with decreasing energy and increasing size (thickness) of inhomogeneity. A simple dose calculation formalism has been developed to predict dose rate in a heterogeneous phantom with cylindrical symmetry, which uses as input the radial dose functions of the uniform media comprising the heterogeneous phantom. Dose rate predictions using this formalism are in reasonable agreement with the experimental data and the Monte Carlo calculated values. Also, this formalism predicts no inhomogeneity effect for ^{192}Ir sources in the geometrical configuration studied in this work.

I. INTRODUCTION

The most abundant types of tissues in the human body have radiation absorption characteristics similar to those of water. Therefore, for radiation dosimetry it is reasonable to assume as a first approximation that the tumor and surrounding tissues constitute a uniform homogeneous medium equivalent to water. This is a good assumption particularly for higher energy photons because they interact with water primarily via Compton scattering which is almost independent of the atomic number of the medium. However, this assumption may not be valid for low-energy photon emitters that are becoming increasingly popular in brachytherapy.[1] The relative probability of photoelectric effect (as compared to the competing Compton process) increases rapidly as photon energy decreases below about 30 keV for water and about 50 keV for bone.[2] Because the probability of photoelectric effect depends strongly on the atomic numbers of the materials involved, the penetrating ability of low-energy photons can vary considerably from one type of tissue to another.[3] However, experimental studies using brachytherapy sources in heterogeneous phantoms are extremely sparse and little quantitative information on dose perturbations caused by tissue heterogeneities in brachytherapy is available in the literature.[4,5]

In this work, we study quantitatively dose perturbations caused by the presence of tissue heterogeneities in a Solid Water phantom containing a single ^{103}Pd, ^{125}I, and ^{241}Am brachytherapy source using measured and/or

Monte Carlo calculated dose rates. Our approach is to develop a dose calculation formalism that has been tested by comparisons with measured data. Measurements were performed in a specially designed heterogeneous phantom. We selected cylindrical symmetry because: (i) Monte Carlo simulations of photon-electron transport with high computational efficiency can be performed in this geometry and (ii) this geometry allows multiple measurements at different radial distances in a single experimental determination, thus improving the statistical quality of the measured data. Using this formalism, the inhomogeneity effect for ^{192}Ir was also investigated.

II. MATERIAL AND METHODS

A. Brachytherapy sources and phantom materials

Dose rates were measured along the transverse axes of ^{241}Am (Gulf Nuclear Industries), ^{125}I, model 6702 (3M Medical Division), and ^{103}Pd, model 200 (Theragenics Corporation) sources with air kerma strengths of 44, 33.3, and 2.27 U, respectively. (U is the unit of air kerma strength, defined by AAPM.[6] It is equal to 1 μGy m^2 h^{-1} or equivalently, 1 cGy cm^2 h^{-1}.) In terms of conventional, but now obsolete quantities, the source strengths were 2 Ci, 26.2 mCi, and 1.76 mCi, respectively. The outside dimensions of the ^{125}I and ^{103}Pd sources were 4.5 mm long $\times$ 0.8 mm diameter and the ^{241}Am source was 16 mm long $\times$ 10 mm diameter. Details of the ^{241}Am source have been described earlier.[7]
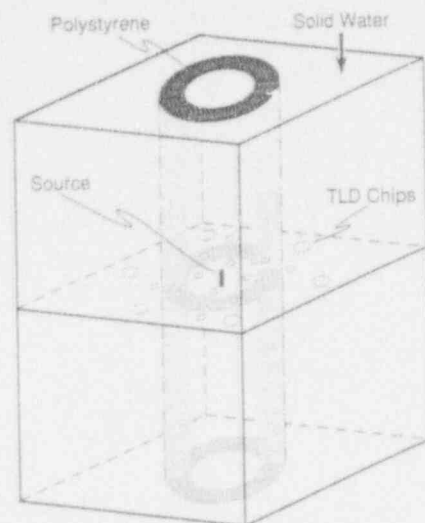
FIG. 1. Schematic diagram of experimental setup for measurement of dose rate along the transverse axis of the brachytherapy sources in a heterogeneous phantom. The phantom made of Solid Water, is represented by the cubic outline (not to scale, actual dimensions are $20 \times 20 \times 8$ cm). The shaded area represents a cylindrical shell (8 cm high $\times 2.1$ cm thick) of polystyrene.

Measurements were performed in homogeneous and heterogeneous media. For these measurements two slabs of $20 \times 20 \times 4$ cm of Solid Water phantom (RMI, model 457) were carefully machined such that in each slab, one of the two cylindrical polystyrene shells, with 2.1- and 1.0-cm thickness and 4-cm height, could be placed as shown in Fig. 1. The inner and outer radii of one shell were 1.9 and 4.0 cm, respectively; and 3.0 and 4.0 cm for the other one. Most of the experiments were performed with the 2.1-cm-thick shell. These polystyrene shells could be exchanged with Solid Water cylindrical shells of the same dimensions (Fig. 1). Holes were machined in the Solid Water slabs and cylindrical shells to accommodate $1 \times 1 \times 1$ mm^3 and $3.1 \times 3.1 \times 0.89$ mm^3 LiF TLD chips with their centers located at distances of 1.0, 1.5, 1.8, 2.15, 2.40, 2.65, 2.75, 3.10, 3.40, 3.60, 3.80, 4.15, 4.50, 5.0, 6.0, 7.0, and 8.0 cm from the source center. TLDs were distributed in a plane containing the transverse bisector of the source (Fig. 2)
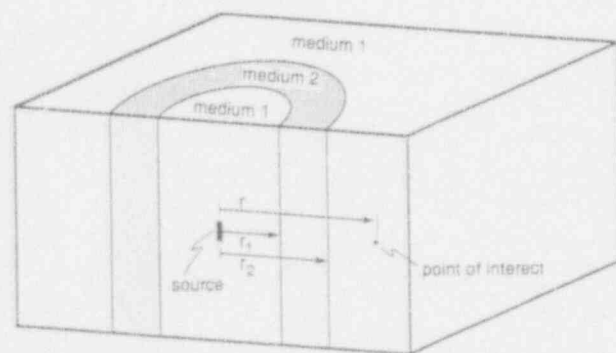

FIG. 2. Geometry of the heterogeneous phantom for the calculation of dose rates. A cylindrical shell of medium 2 is placed in medium 1. The inner and outer radii of the shell are r_1 and r_2, respectively.

with the smaller TLDs placed at distances up to 5 cm, and larger TLDs placed at distances greater than 5 cm from the source. The TLD positions were selected such that the "interchip" effect would be negligible.[8] Care was taken to ensure that there would be at least 7 cm of phantom material around the source and each TLD. To provide full scattering conditions, the TLDs at 7.0 and 8.0 cm from the center were placed along the diagonal of the square sheet containing the TLDs.

For personnel protection, the whole setup was arranged within a cage made of 5-cm-thick lead bricks (bottom and four vertical sides) and a leaded acrylic slab (Nuclear Associates) with a 4-mm lead equivalent thickness. The inner dimensions of the cubic cage of lead were about $60 \times 60 \times 60$ cm. We observed that there was no measurable effect of the lead cage on the dosimetry of the sources.

Dose rates were measured with and without the polystyrene inhomogeneity. From these data, relative dose rates at each source-to-detector distance were calculated as the ratio of dose rate in the heterogeneous phantom to that in the homogeneous phantom. The relative dose rates are presented here as the inhomogeneity correction factors.

Details of our protocol for the TLD dosimetry have been described earlier.[8] Dose rates at each source-to-TLD distance were extracted from four to eight TLD measurements. To check the reproducibility of measured data, measurements were repeated at least twice, typically three times. For each distance, our phantom with cylindrical symmetry allows four simultaneous TLD measurements resulting in about 12 measurements for each point. The standard error (due to random errors) in the determination of mean value of TLD measurements was within $\pm$ 3% for all points. To achieve similar levels of uncertainties at all points, the TLDs at larger distances were irradiated for longer times because the dose rate falls off rapidly with increasing distance from the source. Measurements of dose rates at large distances (greater than 5 cm) from the ^{103}Pd sources required about seven days of irradiation. Typical irradiation times were about 1–2 days. Corrections for source decay during irradiation experiments were made.

B. Monte Carlo simulations

Dose rates from brachytherapy sources of ^{103}Pd, ^{125}I, ^{241}Am, and ^{192}Ir in homogeneous and heterogeneous phantoms were calculated using the CYLTRAN code from the ITS (integrated tiger series) code[9] which has its roots in the Berger–Seltzer electron transport code ETRAN.[10] The CYLTRAN code incorporates the photon and electron transport in the energy range of 1.0 keV to 1.0 GeV and uses the photon cross-section library generated from the analytical approximation of Biggs and Lighthill.[11,12] These calculations were performed using the point source approximation with the source located at the midpoint of a 20-cm long $\times$30-cm diameter cylinder of Solid Water. Multiple scattering step lengths were obtained using the logarithmic grid spacing option that results in energy loss by a factor of 0.917 ($2^{-1/8}$) in a path increment. This path length was further subdivided by the code into 1–10 step lengths, de-

pending upon atomic number and density of the medium. Energy depositions by the secondary electrons were calculated for 2-mm-thick cylindrical shells with average radii of 1.06, 1.48, 1.9, 2.1, 2.3, 2.5, 2.7, 2.9, 3.1, 3.3, 3.5, 3.7, 3.9, 4.1, 4.3, 4.9, 5.9, 6.9, and 7.9 cm. Height of the cylindrical shell at 1 cm was selected to be 4 mm and it was increased gradually to 1.6 cm at 8.0 cm to maintain the same solid angle and to improve statistical quality of the data at distances greater than 1 cm. Beyond 8 cm from the source center, calculations were performed using a 40-cm diameter phantom; i.e., an additional 10 cm of medium was included to provide the full scattering conditions. The effect of the encapsulation for each source type was incorporated by introducing a small cylinder of the encapsulation material around the source with its radius equal to the encapsulation thickness of that source (e.g., 0.05-mm Ti for ^{125}I and ^{103}Pd). Energy depositions were converted to dose rates for both homogeneous and heterogeneous media and inhomogeneity correction factors were calculated.

To obtain good statistical quality data ($\pm 3\%$) it was necessary to use 200 batches with 10 000 histories per batch. Calculations were performed on a Micro VAX II, running on a VMS operating system, version 5.1 and typical computation time was about 1 day per run.

C. A formalism for calculating inhomogeneity correction

The tissue heterogeneity factors are more easily incorporated into conventional dose calculation computer programs if expressed in the form of analytical equations. With this goal in mind, we developed a formalism for calculating the tissue inhomogeneity correction using data for homogeneous media as input. Following the Interstitial Collaborative Working Group (ICWG)[13] formalism, dose rate at a point along the transverse axis is given by

$$\dot{D}_{medium}(r) = (\Lambda_{medium} S/r^2) g_{medium}(r), \qquad (1)$$

where Λ_{medium} is the dose rate constant (dose rate measured at 1 cm along the transverse axis of the source with unit air kerma strength), $g_{medium}(r)$ is the radial dose function for homogeneous medium, and S is the strength of the source in terms of air kerma strength. For the heterogeneous phantom shown in Fig. 2, the dose rate at a point between the source and the front surface of the heterogeneity is anticipated to be nearly the same as the dose rate in homogeneous medium 1 and is modeled by the following expression that is similar to Eq. (1):

$$\dot{D}(r) = (\Lambda_{medium\ 1} S/r^2) g_{medium\ 1}(r), \quad \text{for } r < r_1. \quad (2)$$

Dose rate in the inhomogeneity between r_1 and r_2, will also depend upon the radial dose function and dose rate constant for the homogeneous medium 2 and can be expressed by

$$\dot{D}(r) = (\Lambda_{medium\ 2} S/r^2) g_{medium\ 2}(r) \cdot \alpha, \quad \text{for } r_1 < r < r_2, \qquad (3)$$

where α is a correction factor introduced to take into account the change in radiation field in the region $r < r_1$. This correction factor, α, can be easily calculated knowing

that at $r = r_1$ the dose rate in the two media coincide (ignoring the interface effects at $r = r_1$, which are important only at microscopic dimensions[14]). Thus

$$\frac{\Lambda_{medium\ 1} S}{r_1^2} g_{medium\ 1}(r_1) = \frac{\Lambda_{medium\ 2} S}{r_1^2} g_{medium\ 2}(r_1) \alpha \qquad (4)$$

hence,

$$\alpha = [g_{medium\ 1}(r_1) \cdot \Lambda_{medium\ 1}]/[g_{medium\ 2}(r_1) \cdot \Lambda_{medium\ 2}]. \qquad (5)$$

Replacing α in Eq. (3) by Eq. (5) gives

$$\dot{D}(r) = \frac{\Lambda_{medium\ 1} S}{r^2} \cdot \frac{g_{medium\ 2}(r) g_{medium\ 1}(r_1)}{g_{medium\ 2}(r_1)}. \qquad (6)$$

Similarly, for the regions $r > r_2$, it is reasonable to assume that the distance dependence of the dose rate would be similar to the radial dose function of medium 1. Corrected for the entrance irradiation, the dose rate in this region is modeled as follows:

$$\dot{D}(r) = (\Lambda_{medium\ 1} S/r^2) g_{medium\ 1}(r) \cdot \beta, \qquad (7)$$

where β can be calculated by matching the dose rates at $r = r_2$ (again ignoring interface effects). This results in the following expression for β:

$$\beta = g_{medium\ 2}(r_2) g_{medium\ 1}(r_1)/g_{medium\ 2}(r_1) g_{medium\ 1}(r_2). \qquad (8)$$

Substituting β from Eq. (8) in Eq. (7), we obtain:

$$\dot{D}(r) = \frac{\Lambda_{medium\ 1} S}{r^2}$$

$$\times \frac{g_{medium\ 1}(r) \cdot g_{medium\ 2}(r_2) \cdot g_{medium\ 1}(r_1)}{g_{medium\ 2}(r_1) g_{medium\ 1}(r_2)},$$

$$\text{for } r > r_2. \qquad (9)$$

Putting Eqs. (2), (6), and (9) together, one can express the dose rates at any point in the heterogeneous medium as

$$\dot{D}(r) = (\Lambda_{medium\ 1} S/r^2) g(r), \qquad (10)$$

where

$$g(r) = \begin{cases} g_{medium\ 1}(r), & r < r_1, \\ g_{medium\ 2}(r) \cdot \dfrac{g_{medium\ 1}(r_1)}{g_{medium\ 2}(r_1)}, & r_1 < r < r_2, \\ g_{medium\ 1}(r) \cdot \dfrac{g_{medium\ 2}(r_2) \cdot g_{medium\ 1}(r_1)}{g_{medium\ 2}(r_1) \cdot g_{medium\ 1}(r_2)}, & r > r_2. \end{cases}$$

$$(11)$$

The radial dose function data for ^{125}I, ^{103}Pd, ^{241}Am, and ^{192}Ir in Solid Water and polystyrene are shown in Table I.

III. RESULTS

Figure 3(a)–(c) shows the measured and Monte Carlo calculated dose rates at distances of 1 to 8 cm along the transverse axis of ^{241}Am, ^{125}I, and ^{103}Pd sources in the heterogeneous phantom (with a 2-cm-thick polystyrene cy-

TABLE I. Radial dose function $g(r)$ for [103]Pd, ^{125}I, [241]Am, and ^{192}Ir sources.

Depth (cm)	[103]Pd		[125]I		[241]Am		[192]Ir	
	Solid[a] Water	Polystyrene[d]	Solid[b] Water	Polystyrene[c]	Solid[d] Water	Polystyrene[d]	Solid[b] Water	Polystyrene[d]
1	1.00	1.00	1.00	1.00	1.00	1.00	1.00	1.00
2	0.499	0.830	0.932	1.079	1.41	1.28	1.15	1.16
3	0.280	0.623	0.694	0.996	1.48	1.43	1.10	1.14
4	0.152	0.489	0.520	0.936	1.51	1.59	1.08	1.15
5	0.0797	0.388	0.401	0.891	1.53	1.75	1.10	1.19
6	0.0433	0.296	0.312	0.829	1.54	1.87	1.13	1.21
7	0.0225	0.218	0.246	0.735	1.50	1.92	1.14	1.20
8	...	0.159	0.199	0.634	1.42	1.93	1.11	1.14
9	...	0.126	0.172	0.548	1.31	1.95	1.04	1.06
10	...	...	0.168	0.515	1.21	...	0.98	1.01

[a]Interpolated from Meigooni, Sabnis, and Nath.[16]
[b]Interpolated from Nath, Meigooni, and Meli.[17]
[c]Interpolated from Meigooni, Meli, and Nath.[8]
[d]Present work.

lindrical shell replacing the Solid Water as shown in Fig. 1) relative to the dose rates in the homogeneous Solid Water phantom. These results indicate an increase in relative dose rates (relative to that in Solid Water) in all cases right after the heterogeneity by about 130%, 55%, and 10% for [103]Pd, ^{125}I, and [241]Am, respectively. For points before the heterogeneity (toward the source), a negligible effect is observed. The inhomogeneity correction factor increased from 1.00 before the heterogeneity to a maximum of about 1.10, 1.55, and 2.30 at a point just beyond (within 0.5 cm) the heterogeneity for [241]Am, ^{125}I, and [103]Pd sources, respectively. As distance beyond the heterogeneity increased, the inhomogeneity effect was still quite large for ^{125}I and [103]Pd; about 1.40 and 1.90, respectively, at 4 cm beyond the heterogeneity [Fig. 3(b) and (c)]. For [241]Am sources, the inhomogeneity effect decreased to a negligible amount at about 3 cm beyond the heterogeneity [Fig. 3(a)]. A comparison of the inhomogeneity effects for [103]Pd, ^{125}I, and [241]Am is shown in Fig. 4.

Effects of two different heterogeneity thicknesses were also investigated theoretically using the Monte Carlo calculation technique, and experimentally using TLDs. For ^{125}I our studies indicate that the inhomogeneity effects increase considerably when the thickness of the inhomogeneity is increased from 1-cm-thick polystyrene to 2 cm (Fig. 5). For the smaller (1 cm thick) heterogeneity, the correction factor reached a maximum value of 1.25 just beyond the heterogeneity; and then decreased to a negligible value at points about 3 cm beyond the heterogeneity. The maximum inhomogeneity effect for 2.1-cm-thick heterogeneity was 1.55. Thus for ^{125}I the inhomogeneity effect increases by about 24% as the thickness of the heterogeneity increases from 1 to 2 cm. This experimental observation agrees with the prediction of the dose calculation formalism with an accuracy of better than 1%. Having tested the validity of our dose calculation formalism, it is predicted that the inhomogeneity correction factors increase by 34% and 6% for [103]Pd and [241]Am, respectively, as the thickness of inhomogeneity increases from 1 to 2 cm.

The results of our Monte Carlo simulations are in agree-

ment with measured data, within about 8% (Table II). To analyze the differences between measured data and Monte Carlo simulated data, average values of the ratios of measured and Monte Carlo data were calculated in three different regions; before the heterogeneity, inside the heterogeneity, and beyond the heterogeneity.

The formalism described in Sec. III C was used to calculate the dose rates of ^{192}Ir, [241]Am, ^{125}I, and [103]Pd sources in the heterogeneous medium. These calculations were performed using the radial dose functions shown in Table I. As an example, predicted absolute dose rates for [103]Pd in the heterogeneous medium are shown in Fig. 6. Overall, they are in good agreement with measured data (Table II). For comparison, absolute dose rates as a function of distance from a [103]Pd source in homogeneous phantoms of Solid Water and polystyrene are also shown. To investigate the accuracy of the dose calculation formalism, the ratios of dose rate in heterogeneous medium at a given point to that in homogeneous Solid Water medium were determined as a function of distance from [241]Am, ^{125}I, and [103]Pd sources and the results were compared to the ratios of measured data, as shown in Fig. 3(a)–(c). A quantitative comparison of predictions of the dose calculation formalism with measured and Monte Carlo data are shown in Table II. The maximum deviations are −12% and +8%. The overall agreement in the entire range for all isotopes is within ±2%.

IV. DISCUSSION AND CONCLUSIONS

It has been shown earlier by us that there are significant differences in the penetrating ability of photons from ^{125}I sources in homogeneous phantoms of Solid Water, PMMA, and polystyrene.[8] In this previous study, the penetration of radiation was higher in polystyrene than in PMMA and that in PMMA was higher than that in Solid Water. It was also noted that the differences between polystyrene, PMMA, and Solid Water are not proportional to the density of the material because polystyrene with a density of 1.044 g/cm^3 exhibits a larger difference relative to
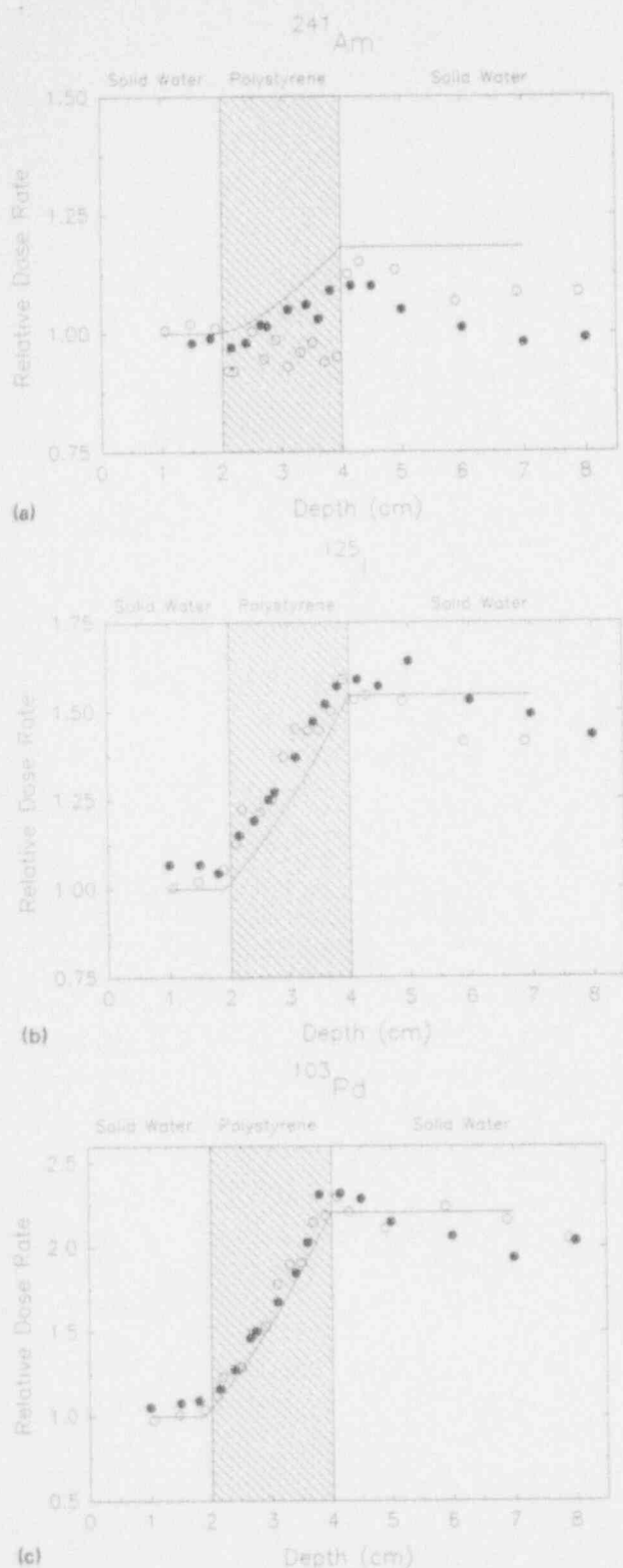
(a)

(b)

(c)

FIG. 3. (a) Dose rates of ^{241}Am in a heterogeneous Solid Water phantom with a 2.1-cm-thick polystyrene shell, relative to that in a homogeneous Solid Water phantom. Filled circles represent measured data, open circles Monte Carlo results and the solid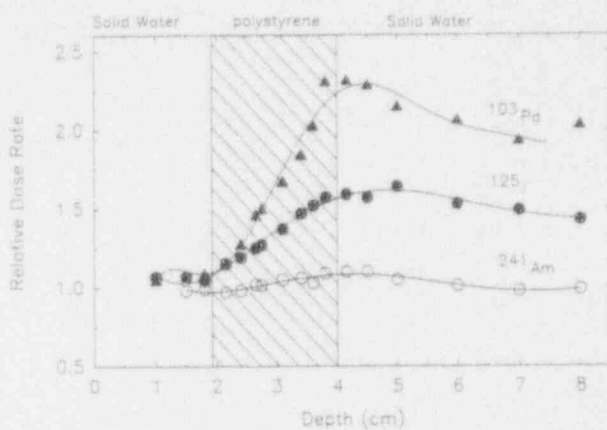 curve the predictions of our dose calculation formalism. (b) Dose rates of ^{125}I in a heterogeneous Solid Water phantom with a 2.1-cm-thick polystyrene shell, relative to that in a homogeneous Solid Water phantom. Filled circles represent measured data, open circles Monte Carlo results and the solid curve the predictions of our dose calculation formalism. (c) Dose rates of ^{103}Pd in a heterogeneous Solid Water phantom with a 2.1-cm-thick polystyrene shell, relative to that in a homogeneous Solid Water phantom. Filled circles represent measured data, open circles Monte Carlo results and the solid curve the predictions of our dose calculation formalism.

FIG. 4. Dose rates from ^{241}Am, ^{125}I, and ^{103}Pd sources measured in a heterogeneous phantom with a 2.1-cm-thick polystyrene shell, relative to that in a homogeneous Solid Water phantom at the same source-to-detector distance. The solid curves representing least-square fit to the measured data using a polynomial function is just to guide the eye.

Solid Water than PMMA with a density of 1.18 g/cm^3. It was noted that the penetrating ability of low-energy photons is much more sensitive to the atomic number of the medium than the density. Because the atomic number of Solid Water, PMMA, and polystyrene are 7.4, 6.5, and 5.7, respectively, one would expect a smaller relative probability of photoelectric absorption in polystyrene than in PMMA, and also smaller in PMMA than in Solid Water. These data led us to expect a larger effect with a polystyrene inhomogeneity in Solid Water than with a PMMA inhomogeneity in Solid Water; therefore, we elected to conduct the present study with a polystyrene inhomogeneity.

This project was limited to a cylindrical geometry that allows multiple TLD measurements at a given radial distance in a single experiment. Also, the cylindrical geometry is highly efficient for Monte Carlo simulation of photon–
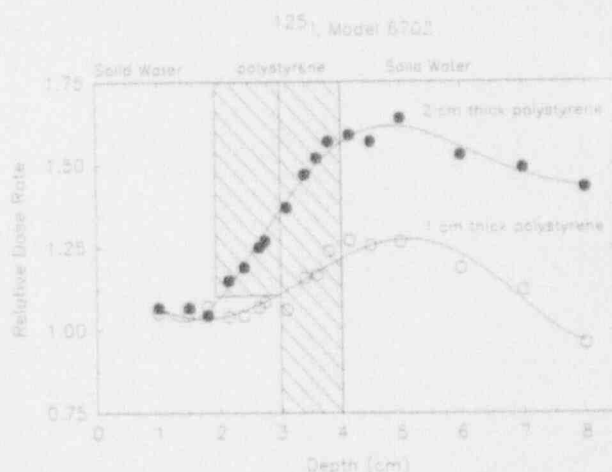

FIG. 5. Monte Carlo calculated dose rates from ^{125}I in a heterogeneous phantom with a 1.0- or 2.1-cm thick polystyrene shell, relative to that in a homogeneous Solid Water phantom, at the same source-to-detector distance, for two different sizes (thickness) of inhomogeneity. The solid curves represent least-square fit to the data to guide the eye.

TABLE II. Comparisons of data from measurements, Monte Carlo simulations and the dose calculation formalism.

| Isotope | Mean value of the ratios of doses | | | |
	Before poly inhomogeneity	Inside poly inhomogeneity	Beyond poly inhomogeneity	Entire range
Measured versus				
Monte Carlo: ^{241}Am	0.968	1.075	0.939	1.005
^{125}I	1.024	0.992	1.054	1.019
^{103}Pd	1.067	0.927	0.981	0.981
Measured versus				
Formalism: ^{241}Am	0.98	0.957	0.879	0.932
^{125}I	1.052	1.078	0.997	1.040
^{103}Pd	1.074	0.983	0.966	0.984
Monte Carlo versus				
Formalism: ^{241}Am	1.012	0.890	0.936	0.927
^{125}I	1.027	1.087	0.946	1.021
^{103}Pd	1.007	1.060	0.985	1.020

electron transport. The spherical geometry is more efficient than the cylindrical geometry, but the spherical phantoms for experiments are very difficult and expensive to fabricate. In this project, our intention was to develop benchmark data that can be used to evaluate the accuracy of theoretical models and Monte Carlo simulations of inhomogeneity effects in brachytherapy.

As expected by the higher energy of photons emitted by ^{192}Ir compared to ^{125}I, ^{103}Pd, and ^{241}Am, our formalism predicts no inhomogeneity effect for the ^{192}Ir sources in the geometry described in Sec. II A. This theoretical expectation is also supported by previous experimental data with a high activity ^{192}Ir source from a high dose rate remote afterloader in a water tank.[15] In this experiment it was observed that introducing a 6.1-cm slab of polystyrene in water phantom in between the source and detector changed the dose rate only by about 0.8% relative to the dose rate in a homogeneous water phantom. Thus we are fairly confident that the lack of inhomogeneity effect for ^{192}Ir, as predicted by our formalism, is real.

In conclusion, we have measured inhomogeneity corrections for dose in a cylindrical Solid Water phantom containing a polystyrene inhomogeneity. As expected, this inhomogeneity correction is observed to be larger for lower energy photon emitters and for thicker inhomogeneity. The inhomogeneity correction is not directly related to the density of the materials, but is dependent upon the atomic composition of the materials. A dose calculation formalism that can be easily implemented in commercially available treatment planning computer codes, has been developed. Accuracy of the dose calculation formalism has been tested only for points along the transverse axis in a cylindrical geometry. Although it is reasonable to expect that it will perform adequately for planar or spherical geometry, its accuracy in the presence of small heterogeneities in complex geometries is totally unknown. For more accurate dose calculations in a complex heterogeneous medium such as a patient, further work is required.
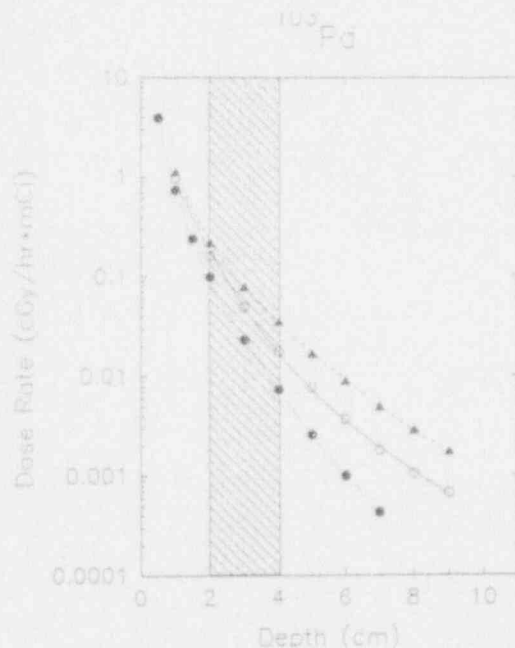
ACKNOWLEDGMENTS

FIG. 6. Comparison of measured dose rates (open circles) and calculated values using our dose calculation formalism (solid line), along the transverse axis of the ^{103}Pd source in a Solid Water phantom with a 2-cm-thick cylindrical shell of polystyrene as inhomogeneity. Also shown in this figure are the measured dose rate in a homogeneous Solid Water (solid circles) and homogeneous polystyrene phantom (solid triangles), respectively. The lines through the homogeneous phantom data (the broken and dotted lines) are polynomial fits through the data, just to guide the eye.

[1] R. Nath, "New radioactive sources for brachytherapy," Phys. Today 42, S50–51 (1989).

[2] H. E. Johns and J. R. Cunningham, The Physics of Radiology (Charles Thomas, Springfield, IL, 1983), 4th ed.

[3] R. G. Dale, "A Monte Carlo derivation of parameters for use in the tissue dosimetry of medium and low energy nuclides," Br. J. Radiol. 55, 748–757 (1982).

[4] S. C. Prasad, D. A. Bassano, and S. S. Kubsad, "Buildup factors and dose around a ^{137}Cs source in the presence of inhomogeneities," Med. Phys. 10, 705–707 (1983).

[5] S. C. Prasad and D. A. Bassano, "Lung density effect on ^{125}I distribution," Med. Phys. 12, 99–100 (1985).

[6]AAPM Task Group No. 32, "Specification of brachytherapy source strengths," AAPM Rep. No. 21 (American Institute of Physics, New York, 1987).

[7]R. Nath, L. Gray, and C. H. Park, "Dose distributions around cylindrical ^{241}Am sources for a clinical intracavitary applicator," Med. Phys. 14, 809–817 (1987).

[8]A. S. Meigooni, J. A. Meli, and R. Nath, "A comparison of solid phantoms with water for dosimetry of ^{125}I brachytherapy sources," Med. Phys. 15, 695–701 (1988).

[9]J. A. Halbleib, T. A. Mehlhoun, and R. P. Kensek, The Integrated Tiger Series (ITS) of coupled electron photon Monte Carlo transport code system, version 2.1, Sandia National Laboratories. CCC-467 Radiation Shielding Information Center, Computer Code Collection, Oak Ridge National Laboratory, 1987.

[10]M. J. Berger and S. M. Seltzer, ETRAN Monte Carlo Code system for electron and photon transport through extended media, CCC-107, Radiation Shielding Information Center, Computer Code Collection, Oak Ridge National Laboratory, May 1973.

[11]F. Biggs and R. Lighthill, "Analytical approximations for x-ray cross sections II," SC-RR-71 0507, Sandia National Laboratories (December, 1971).

[12]F. Biggs and R. Lighthill, "Analytical approximations for total pair-production cross sections," SC-RR-68-619, Sandia National Laboratories (September, 1968).

[13]Interstitial Collaborative Working Group, Interstitial Brachytherapy, edited by L. L. Anderson, R. Nath, K. A. Weaver et al. (Raven, New York, 1990).

[14]F. W. Spiers, "Transition-zone dosimetry," in Radiation Dosimetry, edited by F. H. Attix and E. Tochilin (Academic, New York, 1969), Vol. III.

[15]J. A. Meli, A. S. Meigooni, and R. Nath, "On the choice of phantom material for the dosimetry of ^{192}Ir sources," Int. J. Radiat. Oncol. Biol. Phys. 14, 587–594 (1988).

[16]A. S. Meigooni, S. Sabnis, and R. Nath, "Dosimetry of palladium-103 brachytherapy sources for permanent implant," Endo. Hypertherm. Oncol. 6, 107–117 (1990).

[17]R. Nath, A. S. Meigooni, and J. A. Meli, "Dosimetry on transverse axes of ^{125}I and ^{192}Ir interstitial brachytherapy source," Med. Phys. 17, 1032–1040 (1990).

Medical Physics

Dosimetry on transverse axes of ^{125}I and ^{192}Ir interstitial brachytherapy sources

Ravinder Nath, Ali S. Meigooni, and Jerome A. Meli
Department of Therapeutic Radiology, Yale University School of Medicine, New Haven, Connecticut 06510

pp. 1032–1040

Medical Physics

Dosimetry on transverse axes of ^{125}I and ^{192}Ir interstitial brachytherapy sources

Ravinder Nath, Ali S. Meigooni, and Jerome A. Meli
Department of Therapeutic Radiology, Yale University School of Medicine, New Haven, Connecticut 06510

Dosimetry on transverse axes of ^{125}I and ^{192}Ir interstitial brachytherapy sources

Ravinder Nath, Ali S. Meigooni, and Jerome A. Meli
Department of Therapeutic Radiology, Yale University School of Medicine, New Haven, Connecticut 06510

Dose rates along the transverse axes of ^{125}I model 6702, ^{125}I model 6711 and ^{192}Ir 0.2-mm steel sources for interstitial brachytherapy have been measured in a solid-water phantom for distances up to 10 cm using LiF thermoluminescent dosimeters (TLDs). Specific dose rate constants, the dose rates in water per unit source strength 1 cm along the perpendicular bisector of the source, are determined to be 0.90 ± 0.03, 0.85 ± 0.03, and 1.09 ± 0.03 cGy h^{-1} U^{-1} for ^{125}I model 6702, ^{125}I model 6711 and ^{192}Ir 0.2-mm steel sources, respectively (1 U = unit of air kerma strength $= 1 \mu$Gy m^2 h$^{-1} = 1$ cGy cm^2 h^{-1}). In older and obsolete units of source strength (i.e., mCi apparent), these are 1.14 ± 0.03, 1.08 ± 0.03, and 4.59 ± 0.15 cGy h^{-1} mCi^{-1} (apparent). Currently accepted values of specific dose rate constant for ^{125}I sources are up to 20% higher than our measured values which are in good agreement with the results of our Monte Carlo simulations. But for ^{192}Ir there is good agreement between our measured value of the specific dose rate constant and currently accepted values. The radial dose function for ^{125}I model 6702 is found to be consistently larger than that for ^{125}I model 6711, with an increasing difference as the distance from the source increases. Our measured values for the radial dose function for ^{125}I sources are in good agreement with the results of our Monte Carlo simulation as well as the measured values of Schell *et al.* [Int. J. Radiat. Oncol. Biol. Phys. **13**, 795–799 (1987)] for model 6702 and Ling *et al.* [Int. J. Radiat. Oncol. Biol. Phys. **9**, 1747–1752 (1983)] for model 6711. However, some of the recently reported Monte Carlo values of the radial dose function for ^{125}I sources are significantly larger than measured values; up to 18% at a distance of 5 cm. Our measured radial dose function for the ^{192}Ir seed is in good agreement with our Monte Carlo calculated values, and with both our earlier data for the high activity ^{192}Ir source of a remote afterloader and recommended values by Meisberger *et al.* [Radiol. **90**, 953–957 (1968)].

Key words: ^{125}I, ^{192}Ir, brachytherapy, dosimetry, radial dose function, specific dose rate constant

I. INTRODUCTION

Despite the availability of extensive literature on the dosimetry of interstitial brachytherapy sources, measured data on dose rates around ^{125}I and ^{192}Ir sources in a tissue equivalent medium are extremely sparse. To the best of our knowledge, there are no previous reports in the peer-reviewed scientific literature which present direct measurements of dose rates in a medium from interstitial brachytherapy sources in current use, i.e., ^{125}I model 6711 source (silver wire iodine-125 seed), ^{125}I model 6702 source (no marker iodine-125 seed) and ^{192}Ir (0.2-mm steel encapsulation iridium-192 seed). Generally, dose rates in tissue are determined using the exposure rate constant, the exposure-to-dose conversion factor (f factor) and the tissue attenuation correction factors.[1] However, newer protocols recommend the use of air kerma strength for source strength, specific dose rate constants and radial dose functions for dose calculations.[5,7] The exposure rate constants for point and filtered sources of ^{125}I and ^{192}Ir have been determined theoretically[2-4] and experimentally[5-8] by a number of investigators. The correction factors for tissue attenuation also have been determined both experimentally and theoretically for a variety of brachytherapy nuclides.[9-31] The calculations have used either Berger's method[10-14] of point-isotropic source buildup factors[15] or

Monte Carlo simulation techniques.[16-30] Also, specific dose rate constants and radial dose functions have been calculated by several investigators using Monte Carlo simulations.[16-25] The only direct measurement of dose rates in a medium are those from Kubo and Anderson[32] in 1979, who used a hemispherical ionization chamber in a tissue equivalent phantom, Krishnaswamy[12] in 1975 who used LiF thermoluminescent dosimeters (TLDs) in an acrylic phantom and Hartmann *et al.*[13] in 1983 who used LiF TLDs in a mix-D phantom. All three of these measurement were for the now discontinued model 6701 ^{125}I source. Even for measurements of relative doses such as the radial dose function or the angular distribution around sources in current use only one or two sets of measurements have been reported for the ^{125}I model 6702 source,[33] the ^{125}I model 6711 source,[34] the ^{192}Ir 0.2-mm steel source[30] and the ^{192}Ir 0.1-mm Pt source.[31] On the other hand, several Monte Carlo simulations investigating the radial dependence of depth dose in various tissues and two dimensional dose distributions have been reported.[16-30]

To rectify the paucity of measured dosimetry data for ^{125}I and ^{192}Ir sources, the National Cancer Institute (NCI) organized in 1985 an Interstitial Collaborative Working Group (ICWG). One of the objectives of the ICWG was to evaluate the accuracy of the dosimetry data of ^{125}I and ^{192}Ir. The

ICWG comprised three independent research teams from Memorial Sloan Kettering Institute, the University of California at San Francisco, and Yale University, who conducted a thorough analysis of the dosimetry of 125I and 192Ir sources. This paper presents a part of the dosimetry data generated by one of the participating institutions during the course of this three year effort.

II. MATERIALS AND METHODS

A. Definitions and basic equations

It has been common practice to express the strength of brachytherapy sources in terms of equivalent mass of radium (mg) or apparent activity (mCi). Equivalent mass of radium is that amount of radium in 0.5-mm Pt encapsulation which produces the same exposure rate in air at a large distance from the source center along the transverse axis. Similarly, apparent activity is the activity of a point hypothetical bare source which produces the same exposure rate in air as the actual source. In 1974, the National Council on Radiation Protection and Measurement[35] (NCRP) recommended that "the specification of gamma-ray brachytherapy sources *should* be in terms of the exposure rate at one meter from, and perpendicular to, the long axis of the source at its center." Following the recommendations by the NCRP, other national and international groups have made similar recommendations, except that exposure rate has been replaced by air kerma rate. For brachytherapy sources, the air kerma is related to exposure by[36]

$$K = (W/e)X, \tag{1}$$

where W/e is the average energy required to produce an ion pair in dry air and has a value of $33.97 \text{ J C}^{-1} = 0.876$ cGy R^{-1}. In agreement with these recommendations, the AAPM[36] has also recommended the use of air kerma strength for specification of brachytherapy sources. Air kerma strength S_K is defined as the product of air kerma rate in air at a large distance ℓ from the source center along the transverse axis and the distance ℓ squared,

$$S_K = \dot{K}_\ell \ell^2. \tag{2}$$

The recommended unit of air kerma strength is μGy m^2 h^{-1} which is numerically equal to cGy cm^2 h^{-1}. In this paper, we shall denote this unit by the symbol U; i.e.,

$$1U = 1\mu\text{Gy m}^2 \text{ h}^{-1} = 1\text{cGy cm}^2 \text{ h}^{-1}. \tag{3}$$

An apparent activity of 1 mCi is equivalent to 1.27 U and 4.20 U for 125I and 192Ir sources, respectively and 1 mg Ra Eq of 192Ir is equivalent to 7.53 U. These conversion factors are based on an exposure rate constant of 1.45 and 4.60 R cm^2 mCi^{-1} h^{-1} for 125I and 192Ir, respectively.[3,37] The ICWG in its final report has also recommended the adoption of air kerma strength for the specification of brachytherapy sources.[37] Furthermore, the ICWG has developed a formalism for the dose calculation of interstitial brachytherapy sources which is briefly described in the Appendix. As shown in the Appendix, the dose rate from 125I and 192Ir sources at distances greater than 1 cm along the
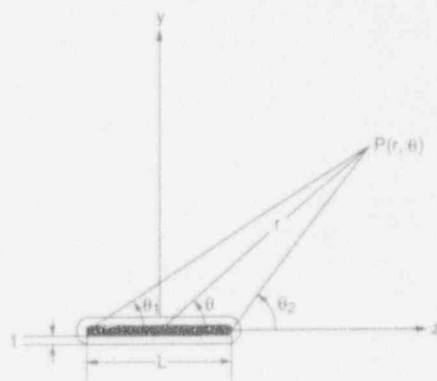

FIG. 1. Schematic diagram illustrating the geometry of a dose calculation formalism for a linear radioactive source.

transverse axis can be expressed by

$$D(r) = \Lambda S_K \frac{g(r)}{r^2}, \tag{4}$$

where r is the radial distance from the source center, Λ is the specific dose rate constant defined as the dose rate per unit air kerma strength at 1 cm along the transverse axis of the seed, and $g(r)$ is the radial dose function that accounts for radial dependence of photon absorption and scatter in the medium.

For the point source approximation, the isotropic dose distribution around interstitial sources can be obtained using the anisotropy factor ϕ_{an}, as follows

$$\dot{D}_{point}(r) = \Lambda S_K \frac{g(r)}{r^2} \phi_{an}, \tag{5}$$

where the anisotropy factor is the ratio of 4π-averaged dose rate, at a distance of r, to the dose rate at the same distance along the transverse axis and has values of 0.96, 0.94 and 1.00 for 125I model 6702, 125I model 6711 and 192Ir sources, respectively.[37]

B. Radioactive sources

Measurements, reported here, were performed using the 125I seeds manufactured by 3M (Medical Products Division/3M, St. Paul, MN), which are available in two different models. Low-activity seeds, model 6711, can contain up to 555 MBq (15 mCi) 125I adsorbed onto a silver wire, while high-activity seeds, model 6702, contain up to 1480 MBq (40.0 mCi) 125I adsorbed on three ion exchange resin spheres (0.6-mm diameter). The outside dimensions of these sources are 4.5 mm long ×0.8-mm diameter. Each type of seed emits the spectrum of 125I ranging from 27.4 to 35.5 keV. Model 6711 also emits characteristic x rays of silver between 22.1 and 25.2 keV. The average photon energies for the model 6702 and model 6711 sources are 28.5 and 27.4 keV, respectively. Details of the source have been described previously by Ling et al.[38] and Schell et al.[33] for the model 6702 source and by Ling et al.[39] for the model 6711 source.

The 192Ir source contains a 30% 192Ir–70% Pt alloy wire encapsulated in a 0.2-mm-thick stainless-steel tube (Best Industries). The outside dimensions are 3.0 mm long ×0.5-mm diameter the source emits a wide spectrum of energies

mostly in the range of 201 to 884 keV with an average value of 360 keV.[30]

Source strengths were measured with a re-entrant well-type ionization chamber calibrated by the Radiological Physics Center (RPC), Houston, Texas, for several brachytherapy sources, including the ^{192}Ir and ^{125}I sources used in this work. The constancy of the well-type chamber was checked using an NIST-calibrated 10.04 mg ^{226}Ra source. The overall precision of the calibration of the brachytherapy source has been estimated to $\pm 1\%$. During the course of these calibrations, the source strengths were in the range of 10–40, 5–18 and 18–46 U for the ^{125}I model 6702, ^{125}I model 6711 and ^{192}Ir sources, respectively.

To verify the accuracy of strength determination, a specially ordered seed of each type with a precise and individual calibration was obtained from the manufacturer. Strengths of these three seeds were then measured using the well-type chamber described above, and then the sources were sent to the other two participants in the ICWG. The agreement among the three ICWG participants and the manufacturer's values for the source strengths was within $\pm 2\%$.

C. Dose measurement techniques

Dose measurements were in a $20 \times 20 \times 20$ cm solid-water phantom (Radiation Measurements Inc., model 451) using LiF TLDs. In previous Monte Carlo studies, it has been shown that solid water [composition H (8.09%), C(67.22%), N(2.40%), O(19.84%), Ca(2.32%), and Cl(0.13%)] is equivalent to water for ^{125}I and ^{192}Ir dose measurements within 5%.[21,29] In each measurement, LiF chips were distributed in precisely drilled holes along four lines diverging from the seed. Chip centers were located at 1-cm intervals along each line ranging from 1 to 10 cm from the seed. With this arrangement, up to four measurements were simultaneously obtained at each distance. A diagram of the setup is shown in Fig. 2. Additional slabs of solid water were placed on the side of the phantom near the source to ensure the presence of at least 10 cm of medium in all directions around the source. The TLD chips at distances of 8–10 cm from the source along the two outer radial lines (Fig. 2) were closer than 10 cm from the phantom edge. However, no measurable difference between the results from inner and outer radial lines was observed. TLD chips were arranged in a pattern that minimized interchip effect; i.e., perturbation of the radiation field by the presence of other chips in the phantom.[21] In each measurement all chips received approximately the same dose by varying the irradiation time; the chips nearest the source being removed first from the jig. So as not to alter the irradiation conditions, other chips were placed in the vacated positions.

Details of our protocol for TLD measurements have been described previously[21] and are described here briefly. Three batches with 100 each LiF TLD chips with dimensions of $3.1 \times 3.1 \times 0.89$ mm (TLD-100, Teflon chips, Harshaw Co.) were used in this work. Before each experiment, TLDs were annealed in an aged aluminum tray at 400 °C for one hour and then kept at room temperature for 45 min followed by 80 °C heating for 24 h. After irradiation and a waiting period of at least 24 h, the responses of the TLD chips were mea-
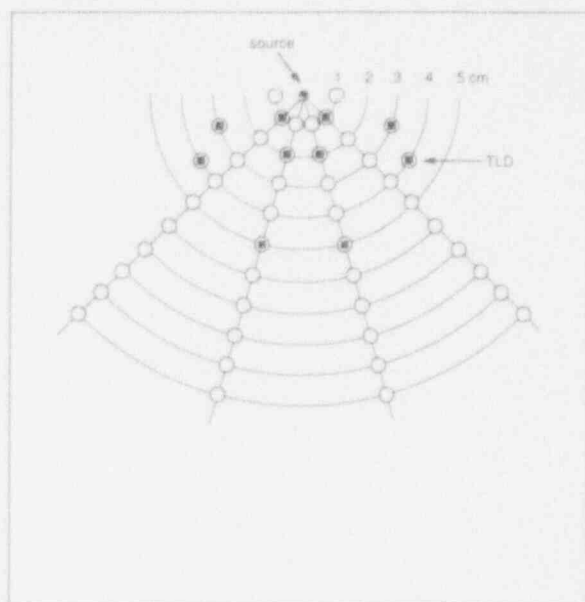

FIG. 2. Schematic diagram of the experimental setup for dose measurements along the transverse axis of the source. The source axis is perpendicular to the plane of the figure.

sured with a Harshaw TLD reader (models 2000A and 2000B). The response of individual chips was corrected for differences in their physical properties such as mass, size, etc., using a chip factor.

Since the shape of the TLD chips (a flat square) allows three different orientations relative to the source, the effect of chip orientation was investigated. As described in our earlier work, chip orientation has a negligible effect on our measurements.[21]

Also a small correction factor was applied for the finite size of the TLD chip.[21] While this factor was significantly different from unity for distances less than 1 cm, its values in this work were 1.013, 1.003 and 1.001 for distances of 1, 2, and 5 cm, respectively.

The sensitivity of LiF TLD, defined as the TLD response per unit dose to water, varies considerably with photon energy. As previously described,[21] the sensitivity of LiF chips was determined for 60-, 80-, 100-, and 250-kV and 4-MV x-ray beams and a high-activity (370 GBq) ^{192}Ir source. For the orthovoltage energies and the ^{192}Ir source, the chips were irradiated in air simultaneously with the NIST (formerly NBS)—calibrated Spokas chamber whose ionization charge was converted to dose to water in air following the ICRU (1973) protocol.[40] For the 4-MV x-ray beam, the chips were irradiated at d_{max} in phantom, and dose was calculated according to the AAPM (1983) protocol from the charge collected with an NIST-calibrated thimble chamber. Responses of the LiF as a function of dose-to-water were used to determine the sensitivity of LiF for each photon beam. The sensitivities were then related to the monoenergetic equivalent of each x-ray beam. For the ^{125}I sources, the TLD sensitivity relative to 4-MV x-ray beams (Varian Clinac 4) was 1.41. In the case of ^{192}Ir, a depth dependent energy correction, as described by Meigooni et al.,[16] was used to take into account the degradation of ^{192}Ir photon spectrum with increasing

depth; the values of relative TLD sensitivities used in the ^{192}Ir measurements were 1.00, 1.02, 1.05, 1.06, and 1.08 for source-to-detector distances of 1, 3, 5, 7, and 10 cm, respectively.

D. Monte Carlo calculations

Monte Carlo calculations were performed using the integrated tiger series (ITS) codes which are expansions of the ETRAN code of Berger and Seltzer[41] allowing multidimensional and multimedia phantoms. The ITS series is mainly a combination of three codes: (i) TIGER, for one-dimensional calculations; (ii) CYLTRAN, for calculations in cylindrical geometry; and (iii) ACCEPT, for any complex geometry. These codes incorporate photon and electron transport in the energy range of 1.0 keV to 1.0 GeV. In this work, calculations were performed in a spherical phantom using the ACCEPT section of the ITS code. Multiple scattering steplengths were obtained using the logarithmic grid spacing option which results in energy loss by a factor of $2^{-1/8}$ in the path increment. This path length was further subdivided by the code into 1–10 step lengths, depending upon atomic number and density of the medium. For solid water and titanium, the number of steps in the path increment were 3 and 6, respectively. All the calculations were done on a MicroVax II computer operating under the Micro VMS operating system, version 4.3. Typical calculations employed 1–2 million photon histories which resulted in a statistical uncertainty of up to ± 3%.

Depth doses in solid water were calculated for an isotropic point source emitting the photon spectrum for ^{125}I sources encapsulated by a spherical titanium shell of 0.05 mm thickness. The effect of 0.2-mm-thick steel encapsulation on the photon spectrum emitted by ^{192}Ir sources was found to be negligible, which is in agreement with the earlier observations of Boyer and Cobb.[3] The phantom was divided into concentric spherical shells of 2 mm thickness with the encapsulated source at the center of a 30-cm-diam sphere. The ITS code computes the average energy deposited to the spherical shells by the secondary electrons for each emitted photon in units of MeV photon^{-1}. Dividing by the mass of the shell gives the dose to the medium in units of MeV g^{-1} photon^{-1}. The photon spectra used in these calculation for ^{125}I sources

are given in Table I. The photon spectrum for ^{192}Ir has already been described.[30] ^{125}I, model 6702, emits an average of 1.47 x-ray photons per disintegration. ^{125}I, model 6711, emits an average of 1.85 photons per disintegration and the ^{192}Ir 0.2-mm steel source emits 2.17 photons per disintegration. Using these data and attenuation factors of 0.879 and 0.859 by the 0.05-mm-thick titanium wall for the photon spectra emitted by ^{125}I models 6702 and 6711, respectively, we converted the Monte Carlo calculated dose rates per unit photon fluence to dose rates per unit air kerma strength.

In this work, the Monte Carlo simulations described above are used only for the determination of relative depth dose, because our Monte Carlo simulations assume a point source encapsulated in a spherical shell of titanium which may not result in exactly the same radiation field as the actual seed configuration. For this reason, we do not recommend the use of our Monte Carlo simulations for absolute dose determinations.

III. RESULTS

A. ^{125}I sources

Measured values of the specific dose rate constant, i.e., the dose rate at 1 cm from a unit strength source along transverse axis in water, were 0.90 ± 0.03 and 0.85 ± 0.03 cGy h^{-1} U^{-1} for ^{125}I models 6702 and 6711, respectively. These are the averages of about 12 measurements for each determination. In terms of the now obsolete unit of apparent activity these constants are 1.14 ± 0.03 and 1.08 ± 0.03 cGy h^{-1} mCi^{-1}, respectively (Table II).

Dose rates in solid water at distances of 1 to 8 cm along the transverse axis of the sources are shown, per unit air kerma strength, in Fig. 3. The agreement between our measured (data points) and calculated (solid line) dose rates is excellent.

Measured dose rates in solid water were converted to radial dose function, $g(r)$, using Eq. (8), and the results are shown in Fig. 4. The $g(r)$ for the ^{125}I model 6702 source is consistently larger than that for model 6711 (Table III). The difference between the two models increases with increasing distance, reaching a value of up to 15% at a distance of 8 cm. The reason for this difference in $g(r)$ is that model 6702 emits photons with an average energy of 28.5 keV which is larger than the 27.4 keV average photon energy of model 6711. This small difference in photon energy produces a measurable change in $g(r)$ for ^{125}I because of steep

TABLE I. Spectrum of photons emitted by encapsulated ^{125}I sources.

	Photons/Disintegration	
	Model 6702[a]	Model 6711[b]
0.0354	0.0666	0.0666
0.0318	0.0426	0.0426
0.0309	0.2056	0.2056
0.0274	0.7615	0.7615
0.0272	0.3906	0.3906
0.0252		0.085
0.0221		0.300
TOTAL	1.467	1.852

[a] Reference 45.
[b] Reference 46.

TABLE II. Dose rates at 1 cm along the transverse axis of ^{125}I model 6702, ^{125}I model 6711, and ^{192}Ir 0.2-mm steel sources in terms of unit air kerma strength (1 U = 1 μGy m^2 h^{-1} = 1 cGy cm^2 h^{-1}) and unit apparent activity [mCi (app)].

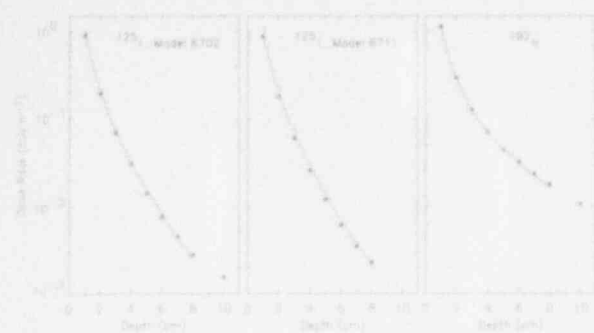|	Dose rate constant, Λ	
Source	(cGy h^{-1} U^{-1})	(cGy h^{-1} mCi^{-1})
^{125}I model 6702	0.90 ± 0.03	1.14 ± 0.03
^{125}I model 6711	0.85 ± 0.03	1.08 ± 0.03
^{192}Ir 0.2-mm steel	1.09 ± 0.03	4.59 ± 0.14

FIG. 3. Dose rate per unit air kerma strength as a function of distance along the transverse axes of ^{125}I model 6702 source (left panel), ^{125}I model 6711 source (middle panel) and [192]Ir 0.2-mm steel encapsulation source (right panel). The measured data are shown by filled circles and the Monte Carlo calculated values are illustrated by the bar graphs.

TABLE III. Measured radial dose functions, $g(r)$, for ^{125}I model 6702, ^{125}I model 6711 and ^{192}Ir sources.

Distance along the transverse axis (cm)	Radial dose function		
	[192]Ir	[125]I Model 6702	[125]I Model 6711
0.5	1.01	0.86	0.84
1.0	1.00	1.00	1.00
2.0	1.03	0.86	0.84
3.0	1.00	0.68	0.63
4.0	0.97	0.53	0.47
5.0	0.97	0.38	0.34
6.0	0.97	0.29	0.26
7.0	0.95	...	...
8.0	0.94	0.196	0.165
10.0	0.87	...	...

dependence of photoelectric attenuation at low energies.

To facilitate interpolation, we fitted the data for $g(r)$ to a fifth-order polynomial function of r, as given by the following expression

$$g(r) = \sum_{i=0}^{5} a_i r^i \qquad (6)$$

The values of the parameters a_i for a fit to the data from $r = 1$ to 8 cm are given in Table IV. The fitted curves, shown as the lines through the data points in Fig. 4, illustrate the good quality of the fit.

B. [192]Ir sources

Measured values of the specific dose rate constant for ^{192}Ir was 1.09 ± 0.03 cGy h^{-1} U^{-1} which is equivalent to 4.59 ± 0.14 cGy h^{-1} mCi^{-1}. Dose rates in solid water at distances of 1 to 10 cm along the transverse axis are shown, per unit air kerma strength, in Fig. 3. The agreement be-

tween our measured (data points) and calculated (solid line) dose rates is excellent.

The radial dose function, $g(r)$, was calculated from the measured dose rates and the results are shown in Fig. 4. Because of the relatively high photon energy, the $g(r)$ at large distances (> 2 cm) for ^{192}Ir is much larger than that for ^{125}I sources (Table III). At 8 cm the $g(r)$ for ^{192}Ir drops to only 0.94 in comparison to low values of 0.20 and 0.17 for ^{125}I models 6702 and 6711 sources, respectively. Also shown in Fig. 4 is earlier data[29] for $g(r)$ obtained using the high activity (nominally 370 GBq) [192]Ir source of a remote afterloading system (GammaMed IIi). As shown in Fig. 4, the radial dose function for the conventional ^{192}Ir brachytherapy source with 0.2-mm-thick steel encapsulation is the same as for the high-activity source (5.5 mm long × 0.5-mm diameter with steel encapsulation of 0.25 mm thickness).

For ^{192}Ir, the data was fit by a third-order polynomial, the coefficients of which are listed in Table IV. This fit is shown as the line through the data points in Fig. 4. The polynomial fits to the ^{192}Ir data presented here are valid for the range of distances 1 to 10 cm from the source and should not be extrapolated to other points outside this range.

IV. DISCUSSION AND CONCLUSION

Specific gamma-ray constant and exposure rate constant for a point ^{192}Ir source have been calculated by many investigators in the past. For a bare point source, Glasgow[2] calculated values of 4.62 and 4.69 R cm^2 h^{-1} mCi^{-1} for the specific gamma ray constant and exposure rate constant, respectively. In the same year, Boyer and Cobb[3] calculated the exposure rate constant to be 4.64, 4.60 and 4.39 R cm^2 h^{-1} mCi^{-1} for a bare source, 0.2-mm steel encapsulated source and 0.1-mm Pt encapsulated source, respectively. In 1981 Glasgow[4] also reported similar values, 4.45 ± 0.10 and 4.30 ± 0.10 for exposure rate constant of 0.2-mm steel and 0.1-mm Pt encapsulated ^{192}Ir source, respectively. Calculated values of the specific dose rate constant in water were reported by Dale[16] in 1982, which were corrected later by Mayles and Turner[27] to be 4.46 ± 0.05 cGy h^{-1} mCi^{-1} for [192]Ir. Except for the measurements by the ICWG[37] which
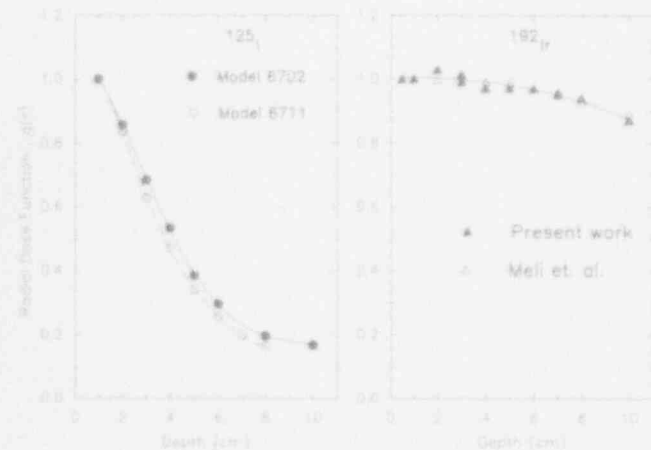

FIG. 4. Radial dose function for ^{125}I model 6702 and ^{125}I model 6711 (left panel) and [192]Ir 0.2-mm steel encapsulation source (right panel). The lines through the data points are the polynomial fits to the measured data.

TABLE IV. Coefficients for the fifth-order polynomial fit to the radial dose function, $g(r)$, for ^{125}I model 6702, ^{125}I model 6711 and coefficients for the third-order polyomial fit for ^{192}Ir 0.2-mm steel source. The polynomials are accurate from 1 to 10 cm for ^{192}Ir and 1 to 8 cm for ^{125}I, and should not be used outside this range.

Coefficient	^{125}I Model 6702	^{125}I Model 6711	^{192}Ir 0.2-mm steel
a_0	1.0815×10^0	1.00780×10^0	1.0068×10^0
a_1 (cm^{-1})	-3.25830×10^{-2}	1.37020×10^{-1}	3.2336×10^{-4}
a_2 (cm^{-2})	-5.84030×10^{-2}	-1.84310×10^{-1}	-9.0861×10^{-4}
a_3 (cm^{-3})	1.01940×10^{-2}	4.45030×10^{-2}	-4.4500×10^{-5}
a_4 (cm^{-4})	-5.94180×10^{-4}	-4.57420×10^{-3}	0.0
a_5 (cm^{-5})	1.00060×10^{-5}	1.77240×10^{-4}	0.0

are in the process of being reported, there are no measured data to verify these calculated dose rate constants for ^{192}Ir. In this paper, we report a measured value of 4.59 ± 0.14 cGy h^{-1} mCi^{-1} which is in good agreement with the measured values determined by the other participants in the ICWG.

Considerable literature exists on measured and calculated exposure rate constants for the now obsolete ^{125}I model 6701 source.[6,32,38] These data, as well as the Monte Carlo calculation by Dale[18,19] for a bare point source of ^{125}I, do not apply directly to the currently used ^{125}I sources. It has been common practice to use 1.30 cGy h^{-1} mCi^{-1} for the specific dose rate constant for both models 6702 and 6711 ^{125}I sources.[42] This value is derived from the product of the exposure rate constant of 1.45 R cm^2 h^{-1} mCi^{-1} and the f factor of 0.90. This derivation assumes that the tissue attenuation correction at 1 cm in water and the effects of source distribution of radioactivity in the sources, are negligible. The value of 1.30 cGy h^{-1} mCi, however, is in good agreement with Krishnaswamy's[12] measured value of 1.35 cGy h^{-1} mCi^{-1} and his calculated value of 1.32 cGy h^{-1} mCi^{-1} for the obsolete ^{125}I model 6701. In this work, measured values of the specific dose rate constant are 1.14 and 1.08 cGy a^{-1} mCi^{-1} for ^{125}I model 6702 and 6711 sources, respectively. These are in good agreement with the results from other participants of the ICWG, indicating that the currently used specific dose rate constants need to be revised downward by 14% and 20% for ^{125}I models 6702 and 6711 sources, respectively.

Recently, Williamson[23] has performed Monte Carlo simulations of ^{125}I models 6701, 6702 and 6711 sources, and Burns and Raeside[22,24] have done the same for ^{125}I models 6702 and 6711 sources. For model 6702, Burns and Raeside[22] reported a specific dose rate constant of 1.32 cGy h^{-1} mCi^{-1}; for model 6711, Burns and Raeside[24] reported a value of 1.29 cGy h^{-1} mCi^{-1}. Burns and Raeside calculated dose rate per contained millicurie about model 6711 seeds. Their reported value of 1.29 was obtained by normalizing with respect to a bare point source in water. The accuracy of this method for absolute dose determination is somewhat questionable. Williamson[23] reported specific dose rate constants of 1.16, 1.22 and 1.23 cGy h^{-1} mCi^{-1} for ^{125}I models 6711, 6701 and 6702, respectively. In his work Williamson also demonstrated that much of this discrepancy may be due to inclusion of very low-energy x rays in the

NIST ^{125}I exposure standardization experiments. Some of these Monte Carlo calculated values are up to 20% higher than the measured and Monte Carlo calculated values of this work.

For the ^{125}I model 6702 source, our measured and calculated values of $g(r)$ are in excellent agreement with the measured values from Schell et al.[13] and Monte Carlo values of Burns and Raeside[22]. The agreement with Monte Carlo calculations of Williamson and Quintero[20] is not as good (Fig. 5). For example, calculated values for $g(r)$ at 5 cm from Burns and Raeside[22] and Williamson and Quintero[20] are 0.43 and 0.46, respectively, which are about 10% and 18% larger than our measured value of 0.39. Our Monte Carlo calculated values of $g(r)$ for ^{125}I model 6702 source are in good agreement with our measured data with a mean deviation of 4% for radial distance in the range of 1–8 cm.

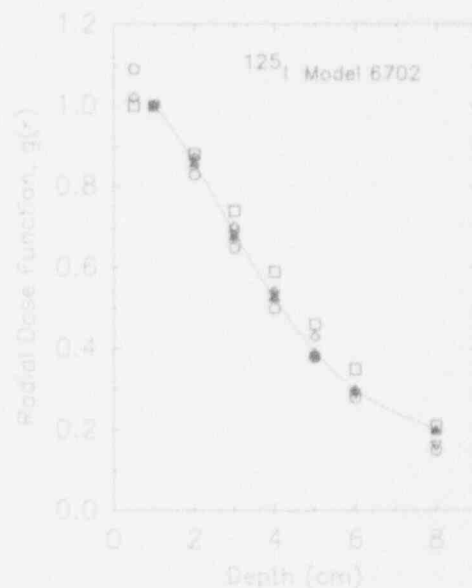The reasons for the discrepancy among the various Monte Carlo calculations for both dose rate constant and $g(r)$ are

FIG. 5. Radial dose function for the ^{125}I model 6702 sources measured (▲) and calculated (▽) during the present work as compared with the measured data by Schell et al. (○), calculated values by Burns and Raeside (◇), and Williamson and Quintero (□). The solid line is the polynomial fit to our measured data.
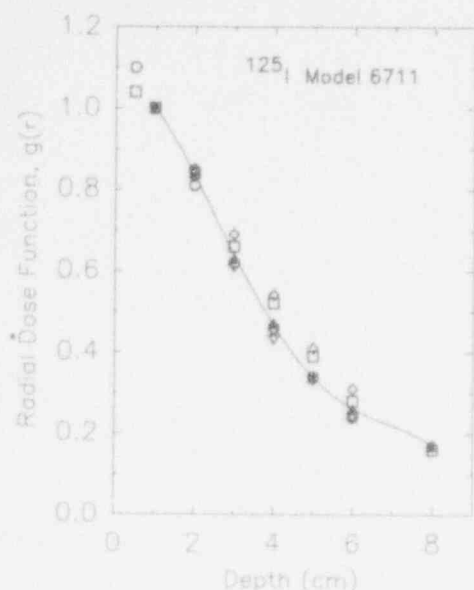
FIG. 6. Radial dose function for the ^{125}I model 671 1 sources measured (▲) and calculated (▽) during the present work as compared with the measured data by Ling *et al.* (○), calculated values by Burns and Raeside (◇), and Williamson and Quintero (□). The solid line is the polynomial fit to our measured data.

FIG. 7. Comparison of radial dose function of ^{192}Ir sources measured (●) and calculated (○) during the present work with the measured data by Meli *et al.* (△) and Meisberger *et al.* (□), and calculated data by Dale (▲). The solid line is the polynomial fit to our measured data.

unclear. One possible reason may be the use of a different definition of apparent activity. Burns and Raeside[22,24] define the apparent activity to be that activity of a hypothetical bare point source which would produce the same dose rate in water at 1 cm as the actual source. In contrast, the conventional definition of apparent activity is in terms of equal exposure rate in air. Further work is needed to resolve the discrepancies in these Monte Carlo simulations.

For the ^{125}I model 6711 source, our measured values of $g(r)$ are in excellent agreement with our Monte Carlo calculated values with mean deviation of 4%; calculated values being consistently lower than measured values. Also, our measured $g(r)$ is in excellent agreement with that measured by Ling *et al.*[39] However, the Monte Carlo calculated $g(r)$ by Burns and Raeside[24] and Williamson and Quintero[20] are about 18% larger than our measurements and Monte Carlo calculations and also Ling's measurements. For example, the values of $g(r)$ at 5 cm are 0.34, 0.33, 0.34, 0.41, and 0.39 from our measurements, our calculations, Ling's measurements,[39] Burn and Raeside's calculations[24] and Williamson and Quintero's calculation,[20] respectively (Fig. 6). As stated above, further work is needed to investigate the reasons for this discrepancy.

For ^{192}Ir 0.2-mm steel source, our measured values of $g(r)$ are in good agreement with our Monte Carlo calculated values with a mean deviation of about 1%. Our measured values are also in excellent agreement with those measured by Meli *et al.*[29] for a high-activity remote afterloading system; and with those reported by Meisberger *et al.*[9] (Fig. 7). There is, however, a significant discrepancy between our values for $g(r)$ and Dale's.[16] His values are Monte Carlo calculated and are consistently higher than the other data by about 10% at a distance of 10 cm.

In a recent article Thomason and Higgins[31] present LiF-TLD measurement of dose along the transverse axis of ^{192}Ir
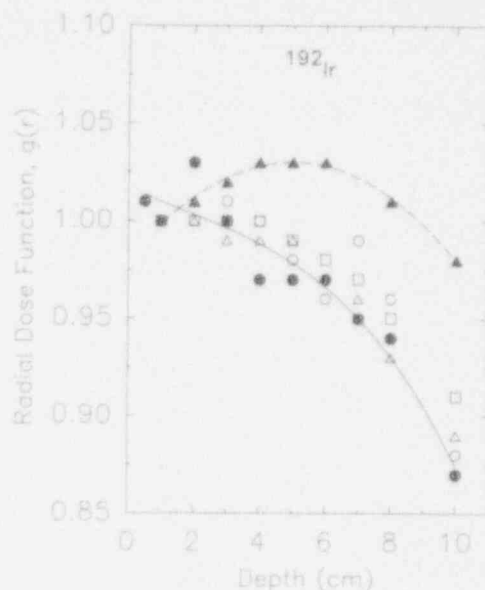
brachytherapy seeds. However, they define the radial dose function using an equation different from the original definition of Dale's[16] and then compare their radial dose function to that given by Dale[16] even though the latter author defined it differently. A direct comparison of the two differently defined radial dose functions is not valid as pointed out by Meli *et al.*[44] The connection between these two is, in the terminology of Meisberger *et al.*,[9] the tissue attenuation factor at 1 cm which is the ratio of the dose to water in a water medium to the dose to water in air. Moreover, Thomason and Higgins[31] say that they "looked at" the effect of the changing energy spectrum of ^{192}Ir with distance in phantom on the response of LiF and found it to be of negligible consequence. They do not supply enough details to allow an analysis of their conclusion. However, this conclusion is contrary to the one drawn by Meigooni *et al.*[30] who showed by measurement and by Monte Carlo calculation that the sensitivity of LiF to ^{192}Ir increases with distance in phantom from the source. This is due to the increase in the relative number of low-energy photons with increasing distance. For these reasons, we conclude that the radial dose function reported by Thomason and Higgins[31] is erroneous, and cannot be compared directly with our measurements or Dale's calculations.

In conclusion, there is a need to revise the dosimetry data which is being used for the determination of dose rates produced by ^{125}I and ^{192}Ir interstitial brachytherapy sources. Specifically, we conclude that (i) the values of specific dose rate constants for ^{125}I models 6702 and 6711 sources need to be revised downward by up to 20%, (ii) the value of the specific dose rate constant for ^{192}Ir 0.2-mm steel source does not need a revision, and (iii) the values of the radial dose functions do not need any revision from the measured values of Ling *et al.*[32] for the ^{125}I model 6711 source, the measured values of Schell *et al.*[32] for the ^{125}I model 6702 source and the measured values of Meisberger *et al.*[9] for ^{192}Ir sources. However, some recent calculations of radial dose function by

Monte Carlo simulations[16,20,22,24] do not agree with measurement and therefore need further investigation.

ACKNOWLEDGMENTS

APPENDIX

According to the ICWG,[37] dose rate in a patient is best calculated from quantities measured solely in a tissue equivalent phantom. Following the ICWG formalism, the dose rate at a point with coordinates (r,θ) from the center of a source (Fig. 1) can be expressed as

$$D(r,\theta) = \Lambda S_K \frac{G(r,\theta)}{G(1,\pi/2)} F(r,\theta) g(r), \qquad (A1)$$

where r is the radial distance from the source center in the plane containing the source axis (cm), θ is the polar angle, Λ is the specific dose rate constant (cGy h^{-1} U^{-1}) and is described in more detail below, $G(r,\theta)$ is the geometry factor (cm^{-2}) that accounts for the distribution of the radioactive material and is described in the following paragraphs, $F(r,\theta)$ is the anisotropy factor that accounts for the angular dependence of photon absorption and scatter in the encapsulation and the medium (dimensionless) and is described in the following paragraphs, $g(r)$ is the radial dose function that accounts for radial dependence of photon absorption and scatter in the medium (dimensionless) and has been described by Dale.[16]

The quantity Λ, referred to as the specific dose rate constant, is the dose rate per unit air kerma strength at 1 cm along the transverse axis of the seed and has units of cGy h^{-1} U^{-1}; i.e.,

$$\Lambda = D(1,\pi/2) S_K. \qquad (A2)$$

Unlike the exposure rate constant, the specific dose rate constant is defined for a real physical source rather than a hypothetical bare point source of the particular isotope. Any change in the distribution of the isotope or in thickness, length or material of the encapsulation will result in a different dose rate at 1 cm for the same air kerma strength and hence a different value of Λ.

For a point source and a uniformly distributed line source, the geometry factors, $G(r,\theta)$ are given by

$$G(r,\theta) = \begin{cases} r^{-2} & \text{for a point source} \qquad (A3) \\ \dfrac{\theta_2 - \theta_1}{Ly} & \text{for a line source of active length } L, \end{cases}$$

$$\qquad (A4)$$

with distances and angles for the line sources as defined in Fig. 1. For points along the transverse axis, the geometry factor for a line source reduces to

$$G(r,\pi/2) = \frac{2 \tan^{-1}(L/2y)}{Ly}. \qquad (A5)$$

Along the transverse axis, the values of $G(r,\pi/2)$ for a line source of active length 3.0 mm (approximately the active length of ^{125}I and ^{192}Ir seeds) are 3.885, 0.993, and 0.250 at distances of 0.5, 1, and 2 cm, respectively. In comparison, these values for a point source would be 4.00, 1.00, and 0.250. Thus, for distances equal to and greater than 1 cm, the point source geometry factor is within 0.7% of the value for the 3-mm-long (active length) line sources of ^{125}I or ^{192}Ir sources. However, for a distance of 0.5 cm, the point source approximation for $G(r,\theta)$ can result in up to a 3% error.

The radial dose function $g(r)$ accounts for photon absorption and scatter in the medium along the transverse axis ($\theta = \pi/2$) and, by definition, is unity at 1 cm. $g(r)$ can be determined from a depth dose curve along the transverse axis, as follows

$$g(r) = \frac{D(r,\pi/2) G(1,\pi/2)}{D(1,\pi/2) G(r,\pi/2)}. \qquad (A6)$$

The angular anisotropy factor $F(r,\theta)$ accounts for absorption and scatter of the photons in the medium and encapsulation at any polar angle relative to that for $\theta = \pi/2$ and the same radial distance. This function is also obtained from relative dose measurements, using the following expression

$$F(r,\theta) = \frac{D(r,\theta) G(r,\pi/2)}{D(r,\pi/2) G(r,\theta)}. \qquad (A7)$$

For points along the transverse axis, Eq. (A1) reduces to

$$D(r) = \Lambda S_K \frac{G(r,\pi/2)}{G(1,\pi/2)} g(r), \qquad (A8)$$

which, for r greater than or equal to 1 cm, further simplifies to

$$D(r) = \Lambda S_K \frac{g(r)}{r}. \qquad (A9)$$

For the point source approximation, the specific dose rate constant, Λ, in Eq. (A9) should be multiplied by anisotropy factors of the seed as follows:

$$D_{point}(r) = \Lambda S_K \frac{g(r)}{r^2} \phi_{an}, \qquad (A10)$$

where ϕ_{an} is the anisotropy factor which is defined as the ratio of 4π-averaged dose rate at a given radial distance divided by the dose rate at the same distance along the transverse axis.

[1] R. J. Shalek and M. Stovall, "Dosimetry in Implant Therapy," in *Radiation Dosimetry*, Vol. III, edited by F. A. Hix and E. Tochilin (Academic Press, New York, 1969), pp. 743–807.

[2] G. P. Glasgow and L. T. Dillman, "Specific gamma-ray constant and exposure rate constant of ^{192}Ir," Med. Phys. 6, 49–52 (1979).

[3] A. L. Boyer and P. D. Cobb, "^{192}Ir Hospital calibration procedures," in *Recent Advances in Brachytherapy Physics*, edited by D. R. Shearer, AAPM Medical Physics Monograph No. 7, (American Institute of Physics, New York, 1979), pp. 82–103.

[4] G. P. Glasgow, "Exposure rate constants for filtered ^{192}Ir sources," Med. Phys. 8, 502–503 (1981).

[5] T. P. Loftus, "Standardization of iridium-192 gamma ray sources in terms of exposure," J. Res. Natl. Bur. Stand. (U.S.) 85, 19–25 (1979).

[6] R. J. Schulz, P. Chandra, and R. Nath, "Determination of the exposure rate constant for ^{125}I using a scintillation detector," Med. Phys. 7, 355–361 (1980).

[7] T. P. Loftus, "Exposure standardization of iodine-125 seeds used in brachytherapy," J. Res. Natl. Bur. Stand. (U.S.) 89, 295–303 (1984).

[8] A. M. Hashemi, M. D. Mills, K. R. Hogstrom, and P. R. Almond, "The

exposure rate constant for a silver wire ^{125}I seed," Med. Phys. **15**, 228–234 (1988).

L. L. Meisberger, R. J. Keller, and R. J. Shalek, "The effective attenuation in water of the gamma rays of gold-198, iridium-192, cesium-137, radium-226 and cobalt-60," Radiol. **90**, 953–957 (1968).

L. L. Anderson, "Dosimetry for Interstitial Radiation Therapy," in *Handbook of Interstitial Brachytherapy*, edited by B.S. Hilaris (Publishing Science Group, Acton, MA, 1975), pp. 87–115.

L. L. Anderson and I. Y. Ding, "Dosimetry consideration for ^{125}I," in *Afterloading: 20 Years of Experience 1955-75*, edited by B. S. Hilaris (Robert Gold & Assoc., New York, 1975), pp. 63–72.

V. Krishnaswamy, "Dose distributions around an ^{125}I seed source in tissue," Radiol. **126**, 489–491 (1978).

G. H. Hartmann, W. Schlegel, and H. Scharfenberg, "The three-dimensional dose distribution of ^{125}I seeds in tissue," Phys. Med. Biol. **28**, 693–699 (1983).

G. P. Glasgow, "The ratio of the dose in water and exposure in air for a point source of ^{192}Ir: A Review in Recent Advances in Brachytherapy Physics," edited by D.R. Shearer, Medical Physics Monograph. No. 7 (AAPM, NY, 1987), pp. 104–110.

M. J. Berger, "Energy deposition in water by photons from point isotropic sources," J. Nucl. Med. Suppl. **1**, 17–21 (1968).

R. G. Dale, "A Monte Carlo derivation of parameters for use in the tissue dosimetry of medium and low energy nuclides," Brit. J. Radiol. **55**, 748–757 (1982).

G. S. Burns and R. E. Raeside, "Monte Carlo estimates of specific absorbed fractions for an I-125 point source in water," Med. Phys. **10**, 197–198 (1983).

R. G. Dale, "Some theoretical derivations relating to the tissue dosimetry of brachytherapy nuclides, with particular reference to iodine-125," Med. Phys. **10**, 176–183 (1983).

R. G. Dale, "Revisions to radial dose function data for ^{125}I and ^{137}Cs," Med. Phys. **13**, 963–964 (1986).

J. F. Williamson and F. J. Quintero, "Theoretical evaluation of dose distributions in water about models 6711 and 6702 ^{125}I seeds," Med. Phys. **15**, 891–897 (1988).

A. S. Meigooni, J. A. Meli, and R. Nath, "A comparison of solid phantoms with water for dosimetry of ^{125}I brachytherapy sources," Med. Phys. **15**, 695–701 (1988).

G. S. Burns and D. E. Raeside, "Monte Carlo simulation of the dose distribution around ^{125}I seeds," Med. Phys. **14**, 420–424 (1987).

J. F. Williamson, "Monte Carlo evaluation of specific dose constants in water for ^{125}I seeds," Med. Phys. **15**, 686–694 (1988).

G. S. Burns and D. E. Raeside, "Two-dimensional dose distribution around a commercial ^{125}I seed," Med. Phys. **15**, 56–60 (1988).

S. Webb and R. A. Fox, "The dose in water surrounding point isotropic gamma-ray emitters," Brit. J. Radiol. **52**, 482–484 (1979).

R. O. Kornelsen and M. E. J. Young, "Brachytherapy build-up factors," Brit. J. Radiol. **54**, 136 (1981).

W. P. M. Mayles and P. C. R. Turner, "The calculation of ^{192}Ir parameters for use in tissue dosimetry," Brit. J. Radiol. **56**, 606 (1983).

J. F. Williamson, "The accuracy of the line and point source approximations in ^{192}Ir dosimetry," Int. J. Radiat. Oncol. Biol. Phys. **12**, 409–414 (1986).

J. A. Meli, A. S. Meigooni, and R. Nath, "On the choice of phantom material for the dosimetry of ^{192}Ir sources," In. J. Radiat. Oncol. Biol. Phys. **14**, 587–594 (1988).

A. S. Meigooni, J. A. Meli, and R. Nath, "Influence of the variation of energy spectra with depth in the dosimetry of ^{192}Ir using LiF TLD," Phys. Med. Biol. **33**, 1159–1170 (1988).

C. Thomason and P. Higgins, "Radial dose distribution of ^{192}Ir and ^{137}Cs seed sources," Med. Phys. **16**, 254–257 (1989).

H. Kubo and L. L. Anderson, "Specific dose rate factor for ^{125}I seeds," Med. Phys. **6**, 347 (1979) (Abstract).

M. C. Schell, C. C. Ling, Z. C. Gromadzki, and K. R. Working, "Dose distributions of model 6702 I-125 seeds in water," Int. J. Radiat. Oncol. Biol. Phys. **13**, 795–799 (1987).

C. C. Ling, M. C. Schell, E. D. Yorke, B. B. Palos, and D. O. Kubiatowicz, "Two-dimensional dose distribution of ^{125}I seeds," Med. Phys. **12**, 652–655 (1985).

National Council of Radiation Protection and Measurements, "Specification of Gamma-Ray Brachytherapy Sources," NCRP Report No. 41 (NCRP, Washington, DC, 1974).

AAPM Report No. 21, *Specification of Brachytherapy Source Strength* (Amer. Assoc. of Physicists in Medicine, New York, NY, 1987).

Interstitial Collaborative Working Groups, Interstitial Brachytherapy: Physical, Biological and Clinical Considerations, edited by L. L. Anderson, R. Nath, and K. A. Weaver *et al.* (Raven Press, New York, 1990).

C. C. Ling, L. L. Anderson, and W. U. Shipley, "Dose inhomogeneity in interstitial implants using ^{125}I seeds," Int. J. Radiat. Oncol. Biol. Phys. **5**, 419–425, (1979).

C. C. Ling, E. O. Yorke, J. T. Spiro, D. Kubiatowicz, and D. Bennett, "Physical dosimetry of ^{125}I seeds of a new design for interstitial implant," Int. J. Radiat. Oncol. Biol. Phys. **9**, 1747–1752 (1983).

International Commission on Radiation Units, Measurement of Absorbed Dose in a Phantom Irradiated by a Single Beam of X or Gamma Rays, ICRU Report No. 23, Washington, DC, 1973.

M. G. Berger and S. M. Seltzer, CCC-107, Radiation Shielding Information Center, computer code collection, Oak Ridge National Laboratory (1968).

C. C. Ling, E. D. Yorke, I. Spiro, D. Kubiatowicz, and D. Bennett, "Physical dosimetry of ^{125}I seeds for interstitial implant," in *Advances in Radiation Therapy Treatment Planning*, edited by A. E. Wright and A. L. Boyer, Medical Physics Monograph No. 9, AAPM (American Institute of Physics, New York, 1982), pp. 560–574.

J. A. Meli, A. S. Meigooni, and R. Nath, "Rebuttal to the Letter-to-the editor of R. G. Dale," Int. J. Radiat. Oncol. Biol. Phys. **16**, 1654–1655 (1989).

J. A. Meli, A. S. Meigooni, and R. Nath, "Comments on 'Radial dose distribution of ^{192}Ir and ^{137}Cs seed sources,' by C. Thomason and P. Higgins, letter to Medical Physics, 1989.

L. T. Dillman and F. C. Von der Lage, Medical Internal Radiation Dosimetry of the Society of Nuclear Medicine (MIRD), Supplement No. 10, (1975).

H. Kubo, "Comparison of two independent exposure measurement techniques for clinical I-125 seeds," Med. Phys. **12**, 221–224 (1985).

J. F. Williamson and R. Nath, "Clinical implementation of AAPM Task Group 32 recommendations on brachytherapy source strength specification," Med. Phys. (to be published).

Interseed effects on dose for ^{125}I brachytherapy implants

Ali S. Meigooni, Jerome A. Meli, and Ravinder Nath
*Yale University School of Medicine, Department of Therapeutic Radiology, 333 Cedar St.,
New Haven, Connecticut 06510*

Dose calculations in multiseed brachytherapy implants are done by adding the contribution of each individual seed and by assuming that radiation from each seed is unaffected by the presence of the other seeds. To test the validity of this assumption, dose measurements with various configurations of multiseed implants of ^{125}I model 6702 and ^{125}I model 6711 sources were performed. For a linear configuration of three ^{125}I model 6702 seeds at 1-cm separation, with their transverse axes coincident, doses at distances of 3.05 and 5.09 cm from the center along the transverse axis were found to be about 8% lower than the sum of doses from the three individual seeds. However, for three seeds at 1-cm intervals with their longitudinal axes coincident, doses at 3.05 and 5.09 cm distances from the center along the longitudinal axis were found to be about equal to the dose sums from individual seeds. These initial experiments indicated that the magnitude of the interseed effect depends upon the orientation of the seed relative to each other in an implant. To evaluate the importance of this interseed effect for multiseed configurations of ^{125}I model 6702 and ^{125}I model 6711 seeds, dose rates at various distances from a two-plane implant (each plane containing a 3×3 array of sources in a 1-cm spacing square grid) were measured in a Solid Water phantom with LiF TLDs. These measurements were carried out in two different planes at different orientations relative to the implant. The average values of the interseed effect at distances ranging from 1 to 7 cm outside the implant were observed to be about the same for ^{125}I model 6702 and model 6711 sources. The mean value of the interseed effect was 6% and the maximum was 12%. On the whole, the interseed effect reduces the dose at the periphery of the iodine implant by 6%.

Key words: iodine-125, brachytherapy, source-to-source shielding, dosimetry, TLD

I. INTRODUCTION

Interstitial brachytherapy continues to play an important role in the management of various sites of cancer, such as head and neck, brain, and prostate. A quantitative evaluation of the outcome of interstitial brachytherapy depends on an accurate determination of the dose distribution throughout the irradiated volume. Presently, dose at any point of a multiseed implant is calculated simply by adding the doses from each seed, assuming that the presence of the other seeds does not affect the radiation field. However, in a typical multiseed implant there may be many seeds in close proximity to each other which may cause seed-to-seed interference. Because encapsulation materials (titanium, platinum, or stainless steel) in interstitial sources have a much higher atomic number and density than tissue, a large number of seeds in tissue can theoretically affect the dose by altering the radiation field.

Using Monte Carlo simulations, Burns and Raeside[1] studied perturbations of the single seed dose distribution created by the presence of one and three neighboring seeds (models 6702 and 6711) for seed spacings of 0.5 and 0.75 cm. Their results are tabulated in terms of the ratio of dose rate in the presence of the neighboring dummy seeds to the dose rate without them. Also, they have calculated the dose perturbation in single- and two-plane implants of ^{125}I seeds with 16 seeds (array of 4×4) on each plane. Seeds and planes were spaced by 0.5 and 0.75 cm. Their calculations indicate that dose perturbation is highly dependent

on the size and geometry of the implant. They estimated a maximum perturbation of 9.8% for two-plane implants of ^{125}I seeds, with 0.5-cm separation between the planes. Moreover, they suggested that the perturbation effect for a two-plane implant would be smaller for seed separations greater than 0.5 cm. From these Monte Carlo calculations, Burns and Raeside[1] conclude that, "The clinical significance of the perturbation effect depends on the location of the dose calculation point and on the details of implant construction. The largest dosimetry errors, both in terms of absolute dose and as a percentage of the reference dose, occur within the seed array. It should be understood, however, that the perturbation corrected dose at these central points exceeds the reference dose. Therefore, the interior regions of the implant are not underdosed. In fact, the shadowing effect may actually serve to reduce local hot spots within the interior of the implant. Perturbation effects may be clinically important at the periphery of the implant where shadowing will cause the peripheral isodose lines to bow inward, so that the margin around the tumor volume will be less than that indicated by calculations based on simple superposition of single seed dosimetry data." Thus Burns and Raeside have already shown that the interior regions of the implants are not underdosed due to interseed effects, but there may be clinically significant effects near the periphery. Therefore, in this paper we concentrated on the region outside the implant volume to investigate the perturbation of dose at the periphery of the

implant and to adjacent normal tissues at risk.

In this paper we demonstrate experimentally the presence of such an interseed effect, defined as the ratio of the measured dose rate from the implant to the sum of dose rates from the individual seeds, for some simple source configurations and for a selected multiseed implant.

II. MATERIALS AND METHODS

A. [125]I sources

The measurements reported here were performed using ^{125}I seeds (manufactured by 3M Medical Products Division, St. Paul, MN) which are available in two models. Low activity model 6711 seeds of up to 555 MBq (15 mCi) contain ^{125}I adsorbed onto a silver wire, while high activity model 6702 seeds of up to 1480 MBq (40.0 mCi) contain ^{125}I absorbed on three or more ion exchange resin spheres. Each type of seed emits a spectrum ranging from 27.4 to 35.5 keV. Model 6711 also emits characteristic x rays of silver between 22.1 and 25.2 keV. The average photon energies emitted by ^{125}I models 6702 and 6711 seeds are 28.5 and 27.4 keV, respectively.

The strength of these seeds was measured by using a re-entrant, well-type ionization chamber[2] calibrated by the Radiological Physics Center (M.D. Anderson Tumor Institute, Houston, TX) for a multitude of brachytherapy sources, including [125]I. The constancy of the well-type chamber was checked using a 10.4 mg [226]Ra source. The overall precision of the brachytherapy source calibration was about ±1%. The strengths of ^{125}I models 6702 and 6711 sources employed in this were 3.68 and 1.09 U which are equivalent to 2.91 and 0.855 mCi (apparent), respectively. Air kerma strength is the recommended method of specifying the strength of brachytherapy sources in the U.S., as described in AAPM Report 21[3] (1 U = unit of air kerma strength = $1\ \mu G\ m^2 h^{-1} = 1\ cGy\ cm^2 h^{-1}$). For ^{125}I, 1 mCi apparent is equivalent to 1.270 U.

B. Phantom material

In comparison to a water phantom, the dosimetry of brachytherapy implants can be performed more accurately in solid phantoms because a precise positioning of detectors and sources can be more easily accomplished. The measurements presented in this work were performed in a Solid Water (model 420, manufactured by RMI, Middleton, WI) phantom. Several 20×20-cm slabs of Solid Water were carefully machined to accommodate up to nine ^{125}I seeds [Fig. 1(a)] with 1-cm separations (center-to-center) and thermoluminescent dosimeter (TLD) chips [Fig. 1(a) and (b)] at distances of 1.02, 2.03, 3.05, 4.07, 5.09, and 7.13 from the center of the seed array. In the seed plane shown in Fig. 1(a), the smallest distance of the TLD chips from the center of seed array was 2.03 cm. These phantom slabs holding the seeds and TLDs were surrounded with other slabs of 0.5, 1.0, or 2.0 cm thicknesses to construct a cube of 20×20×20 cm with the seeds placed approximately in the middle of the cube.

The phantom sheet shown in Fig. 1(a) was also used in the experiments shown in Figs. 2 and 3. In these exper-

FIG. 1. TLD and source arrangement for multiseed two-plane implant experiment. The open circles are the position of TLD, carefully machined on slabs of Solid Water phantom. The phantom size is $20 \times 20 \times 20$ cm³.

iments, three seeds were arranged in the phantom sheet with their longitudinal axes parallel for experiment 1 (Fig. 2) and coincident for experiment 2 (Fig. 3). The seed arrangement for the two-plane implant (array of 3×3 seeds in each plane) is shown in Fig. 4, together with the planes (shaded) that contained the TLDs. Center-to-cen-
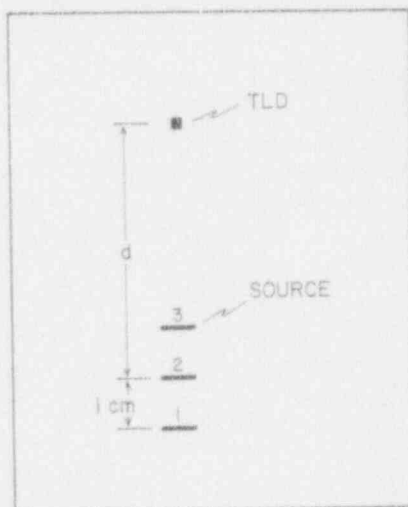

FIG. 2. Arrangement of TLD and three seeds located parallel to each other for experiment #1. The transverse axes of the three seeds in this experiment were coincident to each other.
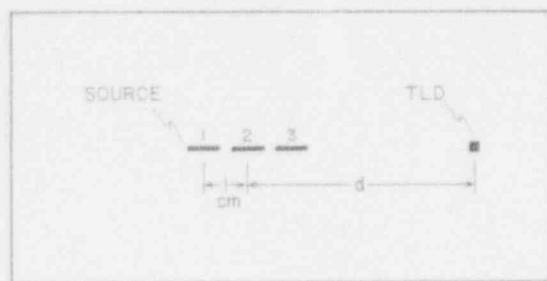
THREE SEED IMPLANT
Experiment #2

ter seed separations of 1.0 cm were used in all experiments. The empty holes were filled with Solid Water plugs or liquid water. For protection of personnel from the radiation field, the above phantom was placed in the center of a lead enclosure with outside dimensions of 70-cm width ×70-cm length×50-cm height. The floor and vertical walls of the lead enclosure were made with 5-cm-thick lead bricks and the top was covered by a clear leaded acrylic sheet (4-mm lead equivalent). The lead enclosure did not affect the dose measurements inside the phantom by more than 1%.
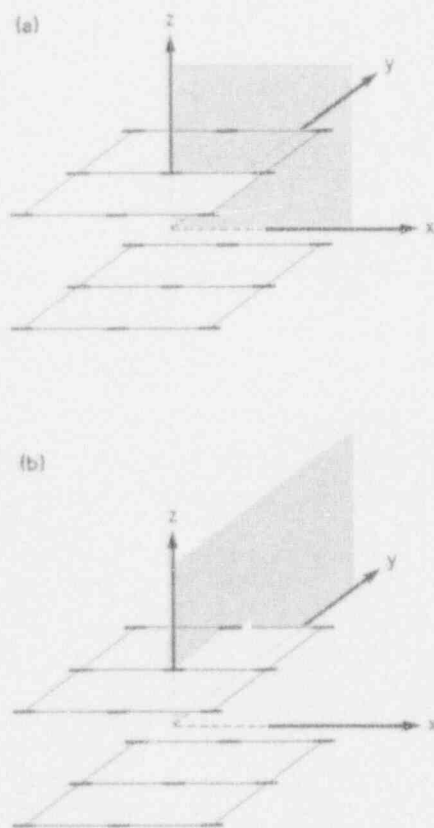
TABLE I. Measured dose rates for three seeds parallel to each other in three-seed implant experiment 1 as shown in Fig. 2.

			Dose rate from		
	Seed #1	Seed #2	Seed #3	All 3 seeds	
d	$\dot{D}_1$	$\dot{D}_2$	$\dot{D}_3$	$\dot{D}_{1+2+3}$	$\dfrac{\dot{D}_{1+2+3}}{\dot{D}_1 + \dot{D}_2 + \dot{D}_3}$
(cm)	(cGy h^{-1})	(cGy h^{-1})	(cGy h^{-1})	(cGy h^{-1})	
3.05	0.038	0.087	0.246	0.344	0.928
5.09	0.009	0.0179	0.038	0.060	0.924

C. Thermoluminescent dosimetry methods

Measurements were performed using LiF thermoluminescent dosimetry (TLD) chips with dimensions of 3.1 ×3.1×0.89 mm (Harshaw TLD-100 chips). The protocol used for the measurements has been described previously.[4] Briefly, the TLDs were annealed in an aged aluminum tray at 400 °C for 1 h, then kept at room temperature for 45 min and then heated to 80 °C for 24 h. The TLDs were read 24 h after irradiation using Harshaw Company, Atlas 2000A and 2000B model TLD readers. TLD response was converted to absorbed dose by calibrating the chips in a 4-MV x-ray beam and correcting for energy dependence at ^{125}I photon energies based upon previously published results.[4–6]

Each experiment was repeated several times to improve the statistical quality of the data. To ensure reproducibility of the setup all phantom slabs were labeled and assembled in a rigid positioning frame. The overall accuracy of dose measurement at a given point was estimated to be ±3%.

III. RESULTS

The presence and magnitude of the interseed effect was investigated by comparing measured and calculated doses around a two-plane multiseed implants containing ^{125}I models 6702 and 6711 sources, respectively. For a better understanding of the interseed effect we also measured dose rates for two linear configurations of ^{125}I model 6702 seeds, as discussed below.

A. Three seed implant #1

Figure 2 shows the arrangement of three ^{125}I model 6702 seeds with their transverse axes coincident. The seeds were parallel to each other with 1-cm spacing between them in the Solid Water phantom described above. Dose rates were measured for one seed at a time and for all three seeds together at two points along the common transverse axis. The sum of the dose rates obtained for the three individual seeds were 7.8% and 8.2% greater than the dose rates of the three seeds together, at 3.05 and 5.09 cm from the center seed, respectively. If it is assumed that shielding one seed by another reduces the dose rates by a factor of a, then the result may be expressed in the following form:

$$\dot{D}_{1+2+3} = a^2 \dot{D}_1 + a \dot{D}_2 + \dot{D}_3, \qquad (1)$$

where $\dot{D}_{1+2+3}$ and $\dot{D}_i$ for $i = 1,2,3$ are the dose rates from all three seeds and ith seed, respectively. Using the mea-

TABLE II. Measured dose rates for three seeds along a straight line in three-seed implant experiment 2 as shown in Fig. 3.

d (cm)	Dose rate from				
	Seed #1 D_1 (cGy h^{-1})	Seed #2 D_2 (cGy h^{-1})	Seed #3 D_3 (cGy h^{-1})	All 3 seeds D_{1+2+3} (cGy h^{-1})	$\dfrac{D_{1+2+3}}{D_1 + D_2 + D_3}$
3.05	0.024	0.0494	0.153	0.226	1.0
5.09	0.0067	0.0116	0.0238	0.042	1.0

sured values of dose rates shown in Table I, Eq. (1) gives $a = 0.83$.

B. Three seed implant #2

Figure 3 shows the arrangement of three ^{125}I model 6702 seeds with longitudinal axes coincident, and a 1-cm center-to-center distance in the Solid Water phantom described above. Dose rates were measured 3.05 and 5.09 cm from the center of the middle seed, along the common longitudinal axis. The sum of dose rates from the three individual seeds was about the same (within 1%) as the dose rate for all three seeds (Table II). Therefore, the value of a in Eq. (1) would be 1.0 for this configuration. For an explanation of this surprising result, the reader is referred to the discussion section.

C. Two-plane implant

The above experiments show the existence of an interseed effect and that its magnitude is dependent on the configuration of the implant. The interseed effect was investigated for two-plane implants using 6702 and 6711 sources. The planes were separated by 1 cm and each plane contained nine seeds [Fig. 1(a)] in a 3×3 array with a 1-cm center-to-center separation. Figure 4(a) and (b) show the schematic diagram of seed arrangement. The shaded areas in Fig. 4 represent the two planes in which dosimetry measurements were performed. Dose rates were measured around the two-plane implant by placing the TLD planes [Fig. 1(b)] parallel to, and at distances of 0.5, 1.5, 2.5, 3.5, and 4.5 cm from a plane halfway between the two seed planes. Only one TLD plane was used in each measurement to prevent any dose perturbation caused by the presence of the other TLD planes. Moreover, dose rates at the center of each plane [Fig. 4(b)] were measured with Solid Water plugs replacing the surrounding TLD chips and a negligible effect (less than 1%) was found. In the plane of the seeds the TLD chips were staggered around the implant to minimize dose perturbation by other chips. The measured dose rates on each plane were averaged to one quadrant, at distances of 0.0, 1.02, and 3.05 cm along the x and y axes, as shown in Figs. 5 and 6. In the seed plane, the smallest distance was 2.03 cm for both x and y directions.

Measurements of the dose rates contributed by each seed of the two-plane implant, without the presence of the other seeds, would be very time consuming. They were instead calculated with a treatment planning system (Theraplan VO4AB, from Theratronix, Inc.). Two-dimen-
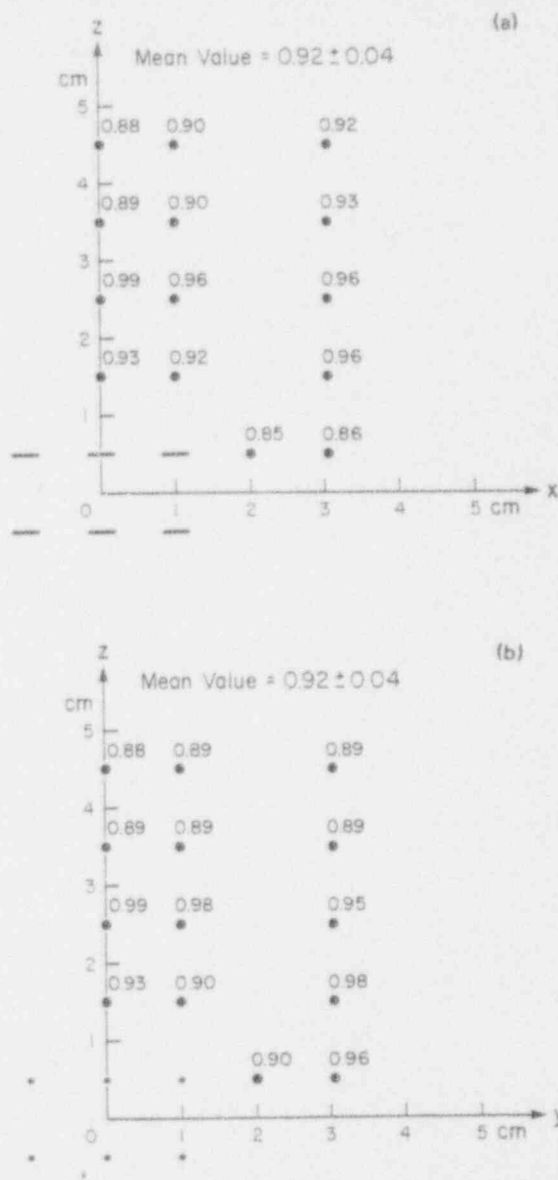
FIG. 5. Ratios of measured to calculated dose rates of ^{125}I model 6702 in the (a) xz plane, (b) yz plane, as shown in Fig. 4(a) and (b).

sional dose distribution data recommended by the Interstitial Collaborative Working Group[7] of the NCI, was entered as input to the treatment planning system. The accuracy of the algorithm was verified by comparing measured and calculated values to some selected points around a single source. Good agreement was observed at all distances equal to or greater than 0.5 cm. At shorter distances, experimental error and accuracy of the calculated values obtained from extrapolation of single seed data introduces some discrepancies which need to be investigated further. In this work, we restrict ourselves to distances greater than or equal to 0.5 cm.

Figures 5 and 6 show the maps and average interseed effect, expressed as a ratio of measured dose rate from the whole implant to the calculated sum of the dose rates from individual seeds on the xz and yz planes, for two-plane implants of ^{125}I models 6702 and 6711 sources, respectively. These figures show average interseed effects of 0.92 ± 0.04 and 0.95 ± 0.04 around the 6702 and 6711 implants,
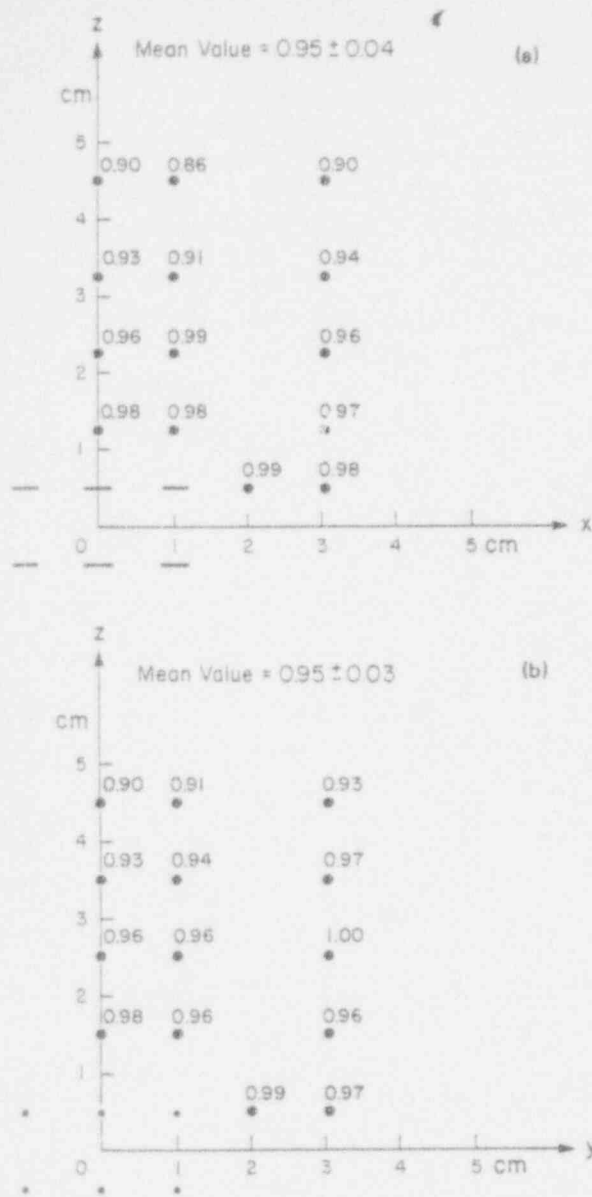
FIG. 6. Ratios of measured to calculated dose rates of ^{125}I model 6711 in the (a) xz plane, (b) yz plane, as shown in Fig. 4(a) and (b).

respectively. Thus simple superposition of single seed dosimetry data overestimates dose by an average of 8% and 5% at these measurement points for the 6702 and 6711 seeds, respectively.

IV. DISCUSSION AND CONCLUSION

In this paper, experimental results are presented which demonstrate for the first time the existence of interseed effects in intersitital brachytherapy implants using ^{125}I models 6702 and 6711 seeds. The region of most interest in interstitial brachytherapy is the implanted volume and its vicinity. Burns and Raeside[1] have already shown that points within the implant did not receive doses lower than the prescribed dose (which was specified at the implant periphery). However, they observed large differences between dose estimates based on simple superposition and perturbation corrected dose estimates. In the present work

we concentrated our efforts on the points outside the implant volume and its periphery. We observed that at the periphery of the implant, the interseed effect lowers the actual dose rate from that obtained by adding the contribution from individual seeds by about 6%. The magnitude of the effect depends upon seed, number of seeds, and seed configuration, but is about the same within our measurement uncertainty of ±4%, for the two models of ^{125}I. Even for an implant with as few as 18 seeds, the interseed effect has an average magnitude of 6% for ^{125}I seeds. These findings suggest that for implants using low energy photon emitters such as ^{125}I or ^{103}Pd, the interseed effect should be taken into account for an accurate determination of dose at the periphery of the implanted volume. Also, we observe a larger interseed effect when the sources are parallel to each other with their transverse axes coincident (experiment #1) compared to a source configuration in which longitudinal axes of sources are coincident (experiment #2).

Theoretical studies by Burns and Raeside indicate that interseed effect should be larger for the ^{125}I model 6711 source than for model 6702. Our data indicate an $8\% \pm 4\%$ effect for model 6702 and a $5\% \pm 4\%$ effect for model 6711. The uncertainties for measurements at individual points were ±3% and the uncertainty (the standard error of the mean) in the average value for all points of measurements was ±4%. Considering the uncertainty of ±4% in our measurement, we conclude that the interseed effect in our measurements is about the same for both models 6702 and 6711, and has an average value of 6%. Thus our results are in qualitative agreement with the Burns and Raeside Monte Carlo calculations which also indicate an effect of about the same magnitude (their Table XI, criterion 1 about 4% for model 6702 and 7% for model 6711). Furthermore, Burns and Raeside's data show that the interseed effect decreases as one moves away from the implant. Using this information, we can conclude that our measured data outside the implant represents a lower limit to the magnitude of the interseed effect near the periphery of the implant, i.e., a minimum of 6% reduction in peripheral dose due to interseed effect.

We expressed the interseed effect as a fraction (or percentage), i.e., of the dose at a given point divided by the calculated dose at the same point, assuming simple superposition of single source data. It should be noted that clinical significance of this effect can be appreciated more readily if we express this difference as a percentage of a reference dose, e.g., peripheral dose. As indicated above, our data indicates on average, a 6% effect at points 1 to 5 cm outside the implant. Within our measurement uncertainty of ±4%, this effect is about the same at all the points in the range of distances studied in this work. Thus we conclude that at the periphery of the implant, one would expect an interseed effect of at least $6\% \pm 4\%$. Since doses for brachytherapy are usually prescribed at the periphery, this means an underdosage of about 6% of the dose at the periphery.

The dose perturbation effect in a simple geometry was expressed using the parameter a and Eq. (1). In general, one would expect that a would depend upon seed separa-

tion, and the distance between the shadowing seed and the measurement point, since these factors will affect the relative importance of primary and scattered radiation. Also, a for seed #1 (Fig. 2), which is shielded by *two* seeds, would not equal a for seed #2, which is shielded by *one* seed. To investigate the validity of such a simplification, using our measured value of a ($=0.83$), we calculated the interseed effect for the pair of 6702 seeds in the Burns and Raeside study. The farthest distance studied by them is 2 cm and the largest spacing is 0.75 cm, conditions closest to our measurements in experiments #1 (spacing of 1 cm and distance of 3 cm). We calculate an interseed effect of 0.83 while Burns and Raeside calculate a value of 0.85 (Table VI in Burns and Raeside). Considering the approximate nature of Eq. (1), the large measurement uncertainty and differences in experimental conditions between the two studies, the above agreement is very good.

An interesting and surprising observation from our work is that no net attenuation is detected for seeds aligned longitudinally. The lack of interseed effect when seeds are aligned longitudinally (experiment 2 in the manuscript) can be explained as follows: At points along the longitudinal axis of the source, the contribution from primary photons is very small because only a small area of the active source is facing the point of interest. Also, the transmission of 30-keV photons through the end wells of an iodine seed is only about 20%. The measurement points along the seed axis in experiment 2 are 2 and 4 cm from the end of the closest seed and this amount of medium attenuates the 20% transmission down to about 10% and 5%, respectively. Thus the closest seed contributes very little primary radiation to the measurement points and the seeds "behind" it contribute virtually no primary radiation. The dose along the long axis at these distances, which is approximately 50% of that at the same distance transverse to the seed[7] is therefore overwhelmingly due to the scatter radiation. For these reasons, the interseed effect at points along the seed axis will be smaller than at points which are not along the source axis.

Further work is needed to extend these experiments to points inside the implant and to ^{103}Pd seeds. There is need to evaluate the interseed effect in implants of different sizes and seed densities as well as for multiseed implants with randomly distributed seed orientations. Also, further studies of interseed effects using Monte Carlo simulations of brachytherapy implants[1,8] are warranted. Only after a detailed analysis of the interseed effect in multiseed implants is done, can the impact of this effect on clinical dosimetry and subsequent clinical outcome by adequately evaluated.

ACKNOWLEDGMENTS

[1] G. S. Burns and D. E. Raeside, "The accuracy of single-seed dose superposition for I-125 implants," Med. Phys. **16**, 627–631 (1989).

[2] L. W. Berkley, W. F. Hanson, and R. J. Shalek, "Discussion of the characteristics and results of measurements with a portable well-type ionization chamber for brachytherapy sources," American Association of Physicists in Medicine, Medical Physics Monograph No. 7, *Recent Advances in Brachytherapy Physics*, edited by D. R. Shearer (American Institute of Physics, New York, 1981), pp. 38–48.

[3] R. Nath, L. Anderson, D. Jones, C. Ling, R. Loevinger, J. Williamson, and W. Hanson, *Specification of Brachytherapy Source Strength*, AAPM Report #21 (American Institute of Physics, New York, 1987).

[4] A. S. Meigooni, J. A. Meli, and R. Nath, "A comparison of solid phantoms with water for dosimetry of ^{125}I brachytherapy sources," Med. Phys. **15**, 695–701 (1988).

[5] G. H. Hartmann, W. Schlegel, and H. Scharfenberg, "The three-dimensional dose distribution of ^{125}I seeds in tissue," Phys. Med. Biol. **28**, 693–699 (1983).

[6] K. A. Weaver, "Response of LiF powder to ^{125}I photons," Med. Phys. **11**, 850–854 (1984).

[7] Interstitial Collaborative Working Group, *Interstitial Brachytherapy*, edited by L. L. Anderson *et al.* (Raven, New York, 1990).

[8] J. F. Williamson and F. J. Quintero, "Theoretical evaluation of dose distributions in water about models 6711 and 6702 ^{125}I seeds," Med. Phys. **15**, 891–897 (1988).